การเปรียบเทียบสมรรถนะของเครื่องปฏิกรณ์จุลภาคแบบเยื่อเลือกผ่านแบบต่างๆสำหรับการผลิตเมทานอลจากแก๊สชีวภาพและไฮโดรเจน

นายคุณวัฒน์ อุนทักษิณกุล

จุฬาลงกรณ์มหาวิทยาลัย
Chulalongkorn University

บทคัดย่อและแฟ้มข้อมูลฉบับเต็มของวิทยานิพนธ์ตั้งแต่ปีการศึกษา 2554 ที่ให้บริการในคลังปัญญาจุฬาฯ (CUIR)
เป็นแฟ้มข้อมูลของนิสิตเจ้าของวิทยานิพนธ์ ที่ส่งผ่านทางบัณฑิตวิทยาลัย
The abstract and full text of theses from the academic year 2011 in Chulalongkorn University Intellectual Repository (CUIR)
are the thesis authors' files submitted through the University Graduate School.

วิทยานิพนธ์นี้เป็นส่วนหนึ่งของการศึกษาตามหลักสูตรปริญญาวิศวกรรมศาสตรมหาบัณฑิต
สาขาวิชาวิศวกรรมเคมี ภาควิชาวิศวกรรมเคมี
คณะวิศวกรรมศาสตร์ จุฬาลงกรณ์มหาวิทยาลัย
ปีการศึกษา 2560
ลิขสิทธิ์ของจุฬาลงกรณ์มหาวิทยาลัย

Performance comparison of different membrane micro-channel reactors for methanol production from biogas and hydrogen

Mr. Khunnawat Ountaksinkul

จุฬาลงกรณ์มหาวิทยาลัย
Chulalongkorn University

A Thesis Submitted in Partial Fulfillment of the Requirements
for the Degree of Master of Engineering Program in Chemical Engineering
Department of Chemical Engineering
Faculty of Engineering
Chulalongkorn University
Academic Year 2017

Copyright of Chulalongkorn University

Thesis Title	Performance comparison of different membrane micro-channel reactors for methanol production from biogas and hydrogen
By	Mr. Khunnawat Ountaksinkul
Field of Study	Chemical Engineering
Thesis Advisor	Professor Suttichai Assabumrungrat, Ph.D.
Thesis Co-Advisor	Paravee Vas-Umnuay, Ph.D.

Accepted by the Faculty of Engineering, Chulalongkorn University in Partial Fulfillment of the Requirements for the Master's Degree

.....Dean of the Faculty of Engineering

(Associate Professor Supot Teachavorasinskun, D.Eng.)

THESIS COMMITTEE

.....Chairman

(Professor Bunjerd Jongsomjit, Ph.D.)

.....Thesis Advisor

(Professor Suttichai Assabumrungrat, Ph.D.)

.....Thesis Co-Advisor

(Paravee Vas-Umnuay, Ph.D.)

.....Examiner

(Palang Bumroongsakulsawat, Ph.D.)

.....External Examiner

(Suwimol Wongsakulphasatch, Ph.D.)

จุฬาลงกรณ์มหาวิทยาลัย
Chulalongkorn University

คุณวัฒน์ อุนทักษิณกุล : การเปรียบเทียบสมรรถนะของเครื่องปฏิกรณ์จุลภาคแบบเยื่อเลือกผ่านแบบต่างๆสำหรับการผลิตเมทานอลจากแก๊สชีวภาพและไฮโดรเจน (Performance comparison of different membrane micro-channel reactors for methanol production from biogas and hydrogen) อ.ที่ปรึกษาวิทยานิพนธ์หลัก: ศ. ดร. สุทธิชัย อัสสะบำรุงรัตน์, อ.ที่ปรึกษาวิทยานิพนธ์ร่วม: ดร. ปารวี วาศน์อำนวย, 79 หน้า.

เพื่อที่จะบูรณาการการผลิตเมทานอลพร้อมกับการปรับปรุงสมถรรนะของแก๊สชีวภาพภายในหนึ่งหน่วยดำเนินการ แบบจำลองพลศาสตร์ของไหลเชิงคำนวณของเครื่องปฏิกรณ์แบบเยื่อเลือกผ่านลักษณะท่อสามชั้น (TMR) และเครื่องปฏิกรณ์จุลภาคแบบเยื่อเลือกผ่านลักษณะแผ่น (MMR) ถูกจำลองผ่านโปรแกรม คอมโซล มัลติฟิสิกส์ 5.3เอ และเปรียบเทียบสมถรรนะของเครื่องปฏิกรณ์ภายใต้สภาวะที่กำหนดไว้ สำหรับการออกแบบแนวคิดของเครื่องปฏิกรณ์เหล่านี้ ช่องภายในเครื่องปฏิกรณ์สามารถแบ่งออกเป็น 3 ส่วนคือ ช่องแก๊สชีวภาพ, ช่องเกิดปฏิกิริยา และช่องแก๊สกวาด แก๊สคาร์บอนไดออกไซด์ในแก๊สชีวภาพซึ่งเข้าสู่ช่องแก๊สชีวภาพนั้นจะถูกแยกผ่านเยื่อเลือกผ่านเพื่อไปผลิตเมทานอลภายในช่องเกิดปฏิกิริยา หลังจากนั้นน้ำที่เกิดขึ้นจากปฏิกิริยาต่างๆในช่องเกิดปฏิกิริยาจะแพร่ผ่านเยื่อเลือกผ่านไปยังช่องแก๊สกวาดเพื่อที่จะทำให้ปฏิกิริยาเลื่อนไปข้างหน้าและเพิ่มอัตราการผลิตของเมทานอล ผลได้ของเมทานอลและปัจจัยการแพร่ของแก๊สคาร์บอนไดออกไซด์และน้ำของ MMR มีค่าเท่ากับ 28.88, 99.24 และ 89.64% ซึ่งมีค่าสูงกว่า TMR 18.92, 65.79 และ 77.16 % ตามลำดับ ในส่วนเพิ่มเติม อัตราส่วนของพื้นที่ผิวต่อปริมาตรของ MMR ซึ่งทำให้อัตราการถ่ายเทความร้อนและมวลสูงนั้น เป็นปัจจัยสำคัญที่ส่งผลต่อสมรรถนะของเครื่องปฏิกรณ์ สำหรับกรณีของ MMR พารามิเตอร์สำหรับการดำเนินงานและการออกแบบยังคงศึกษาเช่นกัน อัตราส่วนของอัตราการไหลเชิงมวลของช่องแก๊สชีวภาพต่อช่องเกิดปฏิกิริยา (อัตราการไหลของแก๊สในช่องชีวภาพ) และ WHSV ในช่องเกิดปฏิกิริยาส่งผลอย่างมีนัยสำคัญต่อสมรรถนะของเครื่องปฏิกรณ์ จากช่วงในการศึกษา สภาวะที่เหมาะสมคือ อุณหภูมิขาเข้าที่ 508.15 เคลวิน, ความดันที่ 50 บาร์, WHSV ที่ 20 ชม.$^{-1}$, อัตราส่วนของอัตราการไหลเชิงมวลของช่องแก๊สชีวภาพต่อช่องเกิดปฏิกิริยาที่ 0.5 ,อัตราส่วนช่องแก๊สกวาดต่อช่องเกิดปฏิกิริยาที่ 4 ความยาวของเครื่องปฏิกรณ์ที่ 75 มิลลิเมตร และ ความกว้างของเครื่องปฏิกรณีที่ 0.5 มิลลิเมตร

จุฬาลงกรณ์มหาวิทยาลัย
Chulalongkorn University

ภาควิชา	วิศวกรรมเคมี	ลายมือชื่อนิสิต	.....
สาขาวิชา	วิศวกรรมเคมี	ลายมือชื่อ อ.ที่ปรึกษาหลัก	.....
ปีการศึกษา	2560	ลายมือชื่อ อ.ที่ปรึกษาร่วม	.....

5970118121 : MAJOR CHEMICAL ENGINEERING

KEYWORDS: METHANOL PRODUCTION / MEMBRANE MICRO-CHANNEL REACTOR / BIOGAS / COMSOL MULTIPHYSICS

KHUNNAWAT OUNTAKSINKUL: Performance comparison of different membrane micro-channel reactors for methanol production from biogas and hydrogen. ADVISOR: PROF. SUTTICHAI ASSABUMRUNGRAT, Ph.D., CO-ADVISOR: PARAVEE VAS-UMNUAY, Ph.D., 79 pp.

In order to integrate simultaneous methanol production with biogas upgrading in a single unit, the computational fluid dynamics (CFD) models of a triple pipe tubular membrane reactor (TMR) and a planar membrane micro-structured reactor (MMR) were established via COMSOL Multiphysics 5.3a and compared their effect on reactor performance under predetermined condition. For the conceptual design of these reactors, the channel inside the reactors can be divided into three parts; biogas channel (BC), reaction channel (RC) and sweep gas channel (SC). The CO_2 in biogas entering into BC is separated through CO_2 selective membrane to produce methanol inside RC. Afterwards, water occurred from the reactions in RC diffuses through water selective membrane to SC in order to shift the reactions to move forward as well as improve methanol production rate. The methanol yield, factor of CO_2 and water permeation of MMR provides 28.88, 99.24 and 89.64% which are higher than TMR 18.92, 65.79 and 77.16 %, respectively. In addition, the surface to volume ratio of MMR providing high both heat and mass transfer rate is a key factor affecting to the performance of reactor. For MMR, the operating and design parameters were also investigated. The mass flow ratio of BC to RC (gas flow rate in biogas channel) and WHSV in reaction channel are able to significantly influence to the reactor performance. From the studied ranges, the optimal condition includes inlet temperature of 508.15 K, pressure of 50 bar, WHSV of 20 h^{-1}, BC:RC ratio of 0.5, SC:RC ratio of 4, reactor length of 75 mm and width of 0.5 mm.

จุฬาลงกรณ์มหาวิทยาลัย
Chulalongkorn University

Department:	Chemical Engineering	Student's Signature .....
Field of Study:	Chemical Engineering	Advisor's Signature .....
Academic Year:	2017	Co-Advisor's Signature .....

ACKNOWLEDGEMENTS

First of all, I would like to express my sincere thanks to my thesis advisor, Prof. Dr. Suttichai Assabumrungrat and my co-advisor, Dr. Paravee Vas-Umnuay for their invaluable recommendation, educational equipment as well as constant encouragement throughout the course of this research. I am most grateful for their teaching and suggestions, not only the research methodologies but also many other methodologies in life. I would not have achieved this far and this thesis would not have been completed without all the support that I have always received from them.

Furthermore, I gratefully thank Dr. Tara Jiwanuruk and Dr.Nattapong Kasempremchit for teaching simulation techniques in COMSOL Multiphysics program and all suggestions improving this investigation. The various problems in simulation could be solved by their guidance.

I would also like to express thanks Prof. Dr. Bunjerd Jongsomjit as the chairman, Dr. Palang Bumroongsakulsawat and Dr. Suwimol Wongsakulphasatch as the members of thesis committee for their valuable suggestion in improvement of my research.

จุฬาลงกรณ์มหาวิทยาลัย
CHULALONGKORN UNIVERSITY

Moreover, I gratefully express thank the financial supports from the Thailand Research Fund and NSTDA Chair Professor Grant. as well as Department of Chemical Engineering, Faculty of Engineering, Chulalongkorn University.

Finally, I most gratefully acknowledge with thanks to my family, especially my father as well as my friends for constant encouragement, inspiration, precious recommendations and financial supports throughout the period of this research.

CONTENTS

Page

จุฬาลงกรณ์มหาวิทยาลัย
Chulalongkorn University

Page

จุฬาลงกรณ์มหาวิทยาลัย
Chulalongkorn University

จุฬาลงกรณ์มหาวิทยาลัย
CHULALONGKORN UNIVERSITY

LIST OF FIGURES

จุฬาลงกรณ์มหาวิทยาลัย
Chulalongkorn University

จุฬาลงกรณ์มหาวิทยาลัย
Chulalongkorn University

Chulalongkorn University

จุฬาลงกรณ์มหาวิทยาลัย
Chulalongkorn University

จุฬาลงกรณ์มหาวิทยาลัย
CHULALONGKORN UNIVERSITY

LIST OF TABLES

จุฬาลงกรณ์มหาวิทยาลัย
Chulalongkorn University

CHAPTER 1: INTRODUCTION

1.1 Rationale

Currently, the growth of energy demand in Thailand has become one of the crucial issues, as shown by the record in Fig. 1.1, thus leading to the development of alternative energy utilization. The biodiesel fuel which is one of those is a current essential alternative energy. In biodiesel production, methanol plays an important role as one of the raw materials. Not only does it is directly used via transesterification process [1-3], but it can also indirectly be used to produce sodium methoxide which has also been widely used as a catalyst in biodiesel process [4]. In order to compensate the methanol used in these processes, the source of raw materials such as hydrogen and carbon dioxide need to be supplied. Fortunately, hydrogen is available from sodium methoxide process which is a by-product from the reaction between methanol and metallic sodium [5, 6]. For carbon dioxide, biogas (CO_2 and CH_4 are main components) occurring from biological transformation of organic matter wastes [7, 8] such as oil palm meal in palm oil industries is one of important carbon dioxide sources [9].

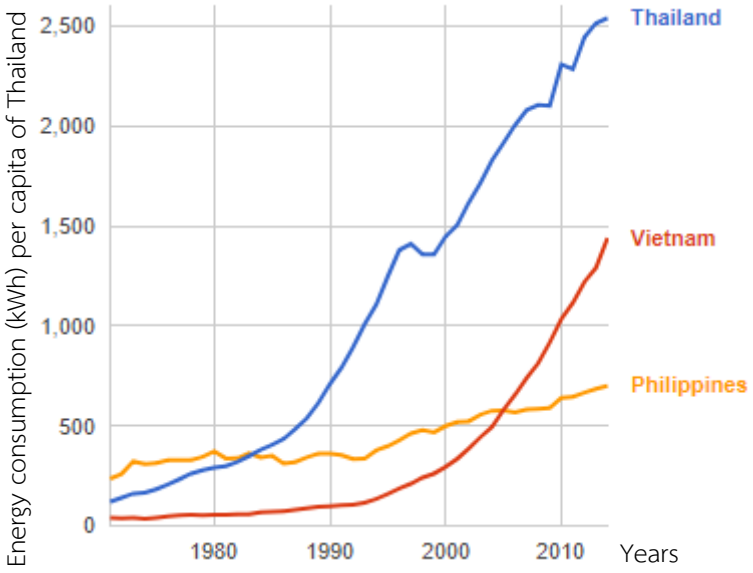

Fig. 1.1: Energy consumption (kWh) per capita of Thailand in each year (Data from World bank/ Last updated: Sep 18 2017)

In general, biogas has been widely used for three applications: heat and steam, generation/cogeneration of electricity and vehicle fuel [7]. However, biogas needs to be purified by removing contaminant substances such as carbon-dioxide (CO_2), hydrogen sulfide (H_2S), water (H_2O) and ammonia (NH_3) before use. Moreover, the upgraded biogas is required to have CH_4 content of 95% (v/v) for a high calorific value and engine safety in transport vehicle engines [7]. As a consequence, the purification process emits a lot of carbon-dioxide waste. For this reason, this investigation studied about methanol production from carbon dioxide waste separated from biogas and hydrogen waste occurred in sodium methoxide process presented in dash line box below (Fig. 1.2)

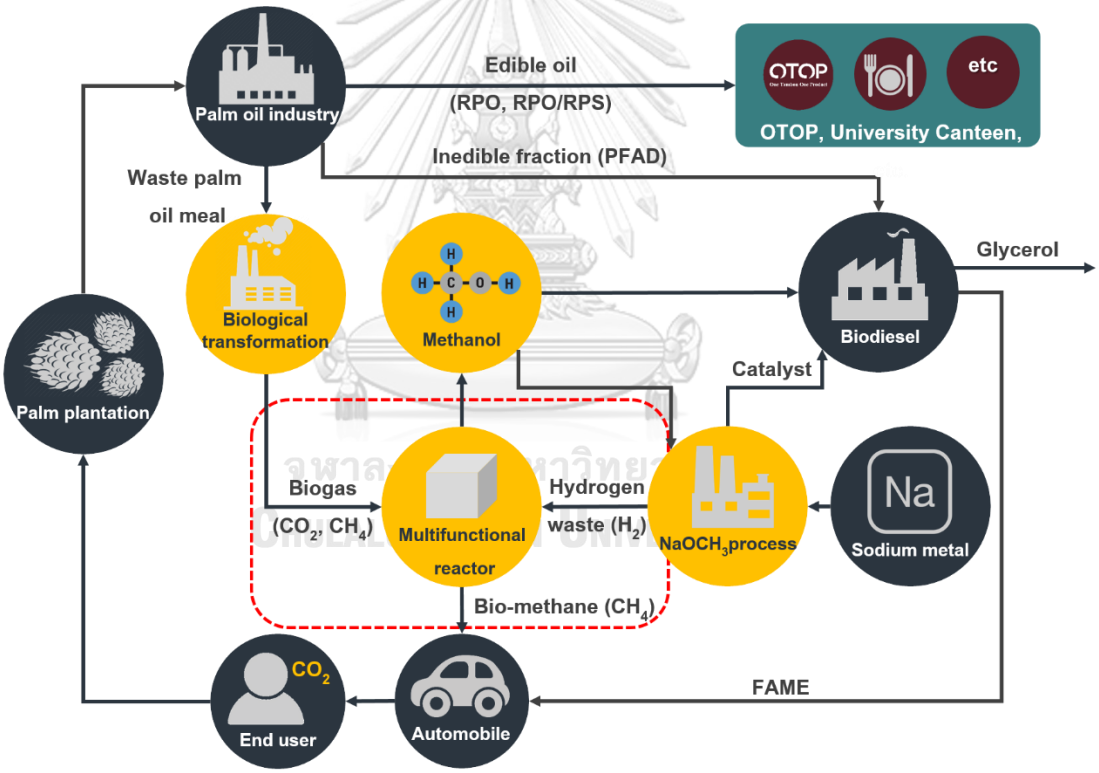

Fig. 1.2: The conceptual framework of methanol process from biogas and hydrogen.

Generally, most of the reactors used for the commercial methanol synthesis plants are a vertical shell & tube heat exchanger reactor with packed catalyst pellets in tubes and cooling water circulated in the shell side [10]. In this process, handling run-away reaction is very essential due to a possible highly exothermic reaction that could occur in the methanol synthesis. What is worse is that the utilization of CO_2 for

the production of fine chemicals is severely limited by the reaction equilibrium in most cases which have been widely reported elsewhere [11]. Hence, controlling temperature and enhancing CO_2 conversion in reactor play an important role in choosing reactor types. In recent years, the membrane microchannel reactors have become a new technology for many catalytic processes. The microchannel provides a high surface/volume ratio and an enhanced mass and heat transfer rate [12]. Additionally, the reactions can be moved forward from disturbance of chemical equilibrium according to Le Chatelier's principle by using a membrane. From all of these reasons, the membrane microchannel reactor is one of the suitable alternatives which has a better performance than any other conventional reactors.

Over the years, the microchannel reactor has been investigated in many catalytic processes such as Fischer Tropsch [13, 14], methane steam reforming [15], carbon-dioxide methanation [16] and dehydrogenation processes [17, 18] *etc*. Besides, methanol synthesis via the microchannel reactor has also been studied for several years ago. H.Bakhtiary-Davijany et al. (a) [19] studied methanol synthesis in a micro fixed bed cross-flow heat-exchanger by using CuO/ZnO catalyst supported alumina. CO conversion could be achieved approximately 50% at temperature of 270 °C and pressure of 80 bar, which was close to the thermodynamic equilibrium. Then, F.Hayer et al. [12] studied dimethyl ether synthesis in the same reactor mentioned above. They found that the temperature profiles of both researches in microchannel reactors provide isothermal behavior due to high heat transfer from the high surface/volume ratios. In addition, Karim et al. [20] compared the performance packed bed and wall-coated microchannel reactor in methanol steam reforming on $CuO/ZnO/Al_2O_3$. They found the temperature gradients were up to 40°C in packed bed micro channel reactor. In other words, this reactor was heat transfer limiting. On the other hand, the wall-coated microchannel reactor was free from heat and mass transfer limitations. Furthermore, they also found that the production rate in wall-coated type could be enhanced by increasing the thickness of the coated wall.

The membrane reactor has been investigated in various research studies, which focus on water removal membrane reactor for methanol synthesis. Farsi et al. [10, 21],

จุฬาลงกรณ์มหาวิทยาลัย
Chulalongkorn University

Barbieri et al.[22], Struis et al.[23, 24] and Gallucci & Basile [25] simulated one dimensional model of membrane tubular reactor but used the different membranes for permeating water from reaction side. The results appeared that the membrane reactor in these research studies could overcome the equilibrium limitation according to Le Chatelier's principle: "When any system at equilibrium is subjected to change in concentration, temperature, volume, or pressure, then the system readjusts itself to counteract (partially) the effect of the applied change and a new equilibrium is established." In these cases, the reduction of water in the system by using membrane could shift the equilibrium to the forward side. In other words, the rate of reaction, extent and yield of methanol could be enhanced significantly. Farsi et al. (a) [10] proved that the membrane reactor could provide the production rate of methanol more than that of the conventional reactor of about 4.06% by simulating an unsteady state one-dimensional heterogeneous mathematical model at temperature of 503 K and pressure of 76.98 bar. Furthermore, they found that the membrane reactor also improved the lifetime of catalysts from deactivation model in the simulation.

According to the reasons mentioned above, the different membrane wall-coated micro-channel reactor (MMR) and triple pipe tubular membrane reactor (TMR) for methanol and bio-methane production are developed. In this work, the feeds for the system include biogas and hydrogen which could be derived from palm oil and biodiesel industries. Biogas is a major product from biological transformation under anaerobic condition of oil palm meal from mill processing whereas hydrogen is a by-product from production of sodium methoxide, a catalyst for biodiesel process, from sodium and methanol. The channels of these reactors can be divided into three parts; biogas channel (BC), reaction channel (RC) and sweep gas channel (SC). Biogas and hydrogen are fed into multifunctional reactors combining reaction and membrane separation in a single unit. CO_2 in biogas is separated through membrane to react with hydrogen in the reaction channel to form methanol and bio-methane is obtained in the retentate side or biogas channel. The water in reaction channel is separated via water selective membrane to sweep gas channel in order to overcome the limitation of reaction equilibrium. The models in this research are divided into two characteristics:

จุฬาลงกรณ์มหาวิทยาลัย
Chulalongkorn University

the planar membrane microchannel reactor (MMR) and the triple pipe tubular membrane reactor (TMR). Therefore, the goal of this study is to investigate the effect of the different characteristics of reactor on the reactor performance and to determine a suitable design. For the suitable design, the effects of its operating and design parameters on reactor performance including inlet temperature, pressure, WHSV, mass flow ratio of BC to RC and SC to RC, reactor length and width were also investigated.

1.2 Research Objectives

The aim of this research is to develop the multifunctional reactor for simultaneous methanol production with biogas upgrading in a single unit. The specific objectives to achieve this goal are as follows:

- To investigate the effect of the different characteristics of reactor (planar membrane microchannel reactor, tubular membrane reactor) on reactor performance and find a suitable design for simultaneous methanol production with biogas upgrading.
- To study the effect of operating and design parameters on reactor performance and to find a proper condition and the dimensions of the reactor.

จุฬาลงกรณ์มหาวิทยาลัย
CHULALONGKORN UNIVERSITY

1.3 Scope of work

In this research, the reactor models for simultaneous methanol production with biogas upgrading are developed. The scope of this work can be divided into three steps:

1. Validate kinetic model for methanol synthesis involving CO hydrogenation, CO_2 hydrogenation and reverse water gas shift with Van-dal and Chakib Bouallou [26] and find proper membranes for water removal from reaction channel and carbon-dioxide separation from biogas.

2. Simulate the two-dimensional steady state pseudo homogeneous mathematical models by COMSOL Multiphysics 5.3a program. The models in this research have been divided into two configurations: 1.The planar membrane wall-coated microchannel reactor (MMR) and 2.The triple pipe tubular membrane reactor (TMR). Moreover, this research compares the performance of reactor in each case to find the suitable design for methanol synthesis from biogas and hydrogen.

3. Investigate the effect of operating parameters (involving inlet temperature, pressure, WHSV, mass flow ratio of BC to RC and mass flow ratio of SC to RC) and design parameters (involving channel width and reactor length) on reactor performance by sensitivity analysis to determine the proper condition and the dimensions of reactor for our system.

1.4 Expected Outputs

Find the suitable design for simultaneous methanol production with biogas upgrading from the models proposed earlier and find the proper condition and the dimensions of the reactor in order to achieve the highest performance.

จุฬาลงกรณ์มหาวิทยาลัย
Chulalongkorn University

1.5 Research plan

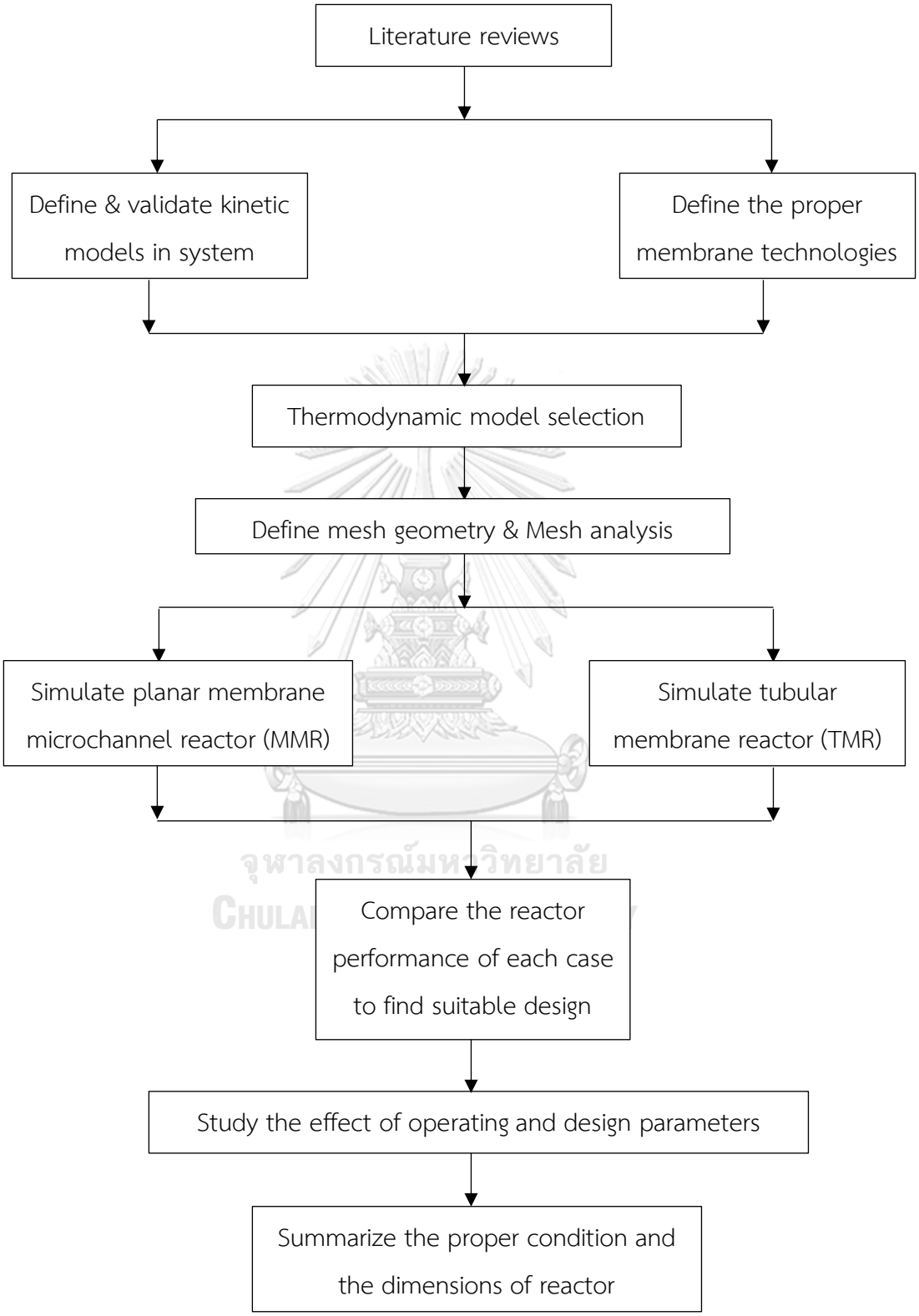

Fig. 1.3: Research plan

CHAPTER 2: THEORY

In this chapter, we perform the necessary theories for this research, which include methanol production, biogas upgrading, membrane separation technologies and computational fluid dynamics simulation.

2.1 Methanol Production

Methanol (MeOH) or methyl alcohol is perhaps called wood alcohol because it was once produced mainly as a by-product in the destructive distillation of wood. Methanol, being a methyl group linked to a hydroxyl group, is the simplest alcohol and has physical properties as followed:

Table 2.1: physical properties of methanol [27]

Properties of methanol (methyl alcohol)	
Molecular formula	CH_3OH
CAS.No.	67-56-1
Molecular weight	32.04 [kg/kmol]
Physical state and appearance	Colourless liquid
Odour	Distinctive odour
Specific gravity	$0.792^{20/4}$
Melting point	-97-8 [°C]
Boiling point	64.7 [°C]
Solubility of 100 parts of water	available
Solubility of 100 parts of alcohol	available
Solubility of 100 parts of ether	available

The molecular weights are based on the atomic weight values in "Atomic weights of the Elements 2001," *PURE Appl. Chem.*, **75,** 1107, 2003. **The densities** are given for the temperature indicated and are usually referred to water at 4°C, *e.g.,* $1.028^{95/4}$ a density of 1.028 at 95° C referred to water at 4° C, the 4 being omitted when it is not clear whether the reference is to water at 4°C or at the temperature indicated by the upper figure. **The melting and boiling points** given have been selected from available data as probably the most accurate. **The solubility** is given in grams of the substance in 100 of the solvent.

จุฬาลงกรณ์มหาวิทยาลัย
Chulalongkorn University

Methanol is essential in various industrial processes and useful in the production of fuels, pesticides and drug etc. [28]. Additionally, Milani et al. [29] performed numerous routes of carbon-dioxide and methanol utilizations, as shown in Fig. 2.1. Methanol has been widely used in chemical processes by using as fuel, fuel additive by blending with different grades of gasoline for vehicles and antifreeze agents. Moreover, it could be used as feedstocks in acetic acid, methyl formate and formaldehyde productions etc.

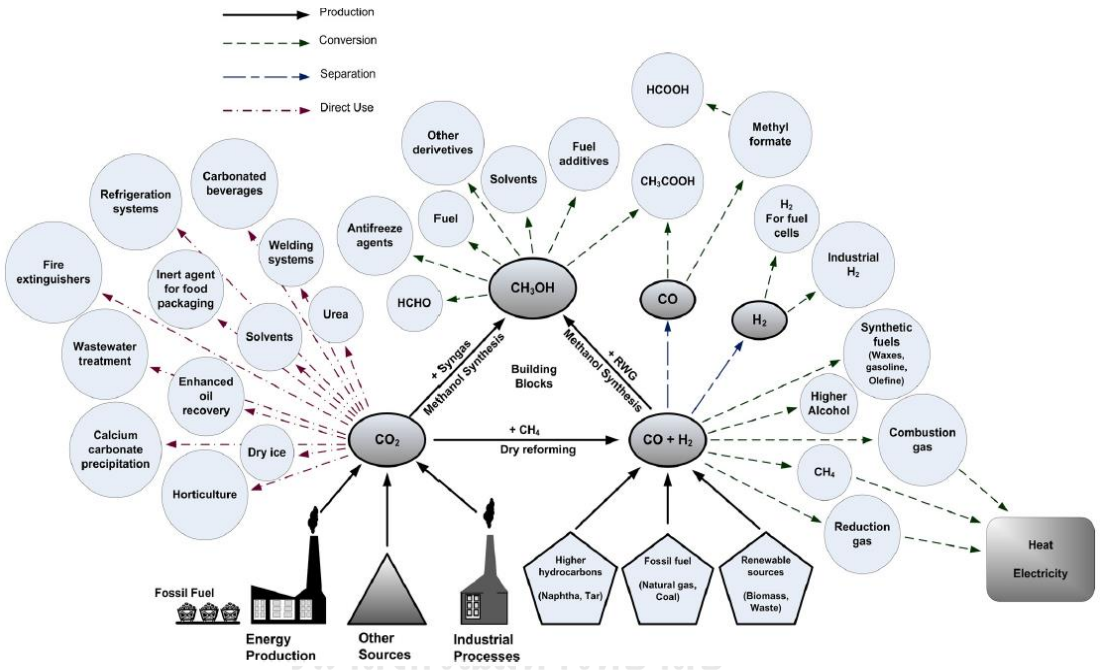

Fig. 2.1: Possible CO_2 utilization trends in various products and procedures [29]

Chulalongkorn University

Furthermore, industrial methanol has been mostly produced form carbon-monoxide, carbon-dioxide and hydrogen in a catalytic processes but there are many researches, which study about methanol production from carbon-dioxide gases. The production of methanol from CO_2 can be divided into two different ways: in one step and in two steps. The one step conversion is a direct CO_2 hydrogenation to methanol. On the other hand, in the two steps conversion, CO_2 is first converted into CO via reverse water gas shift reaction and then hydrogenated into methanol.*[26]* These routes are performed as followed:

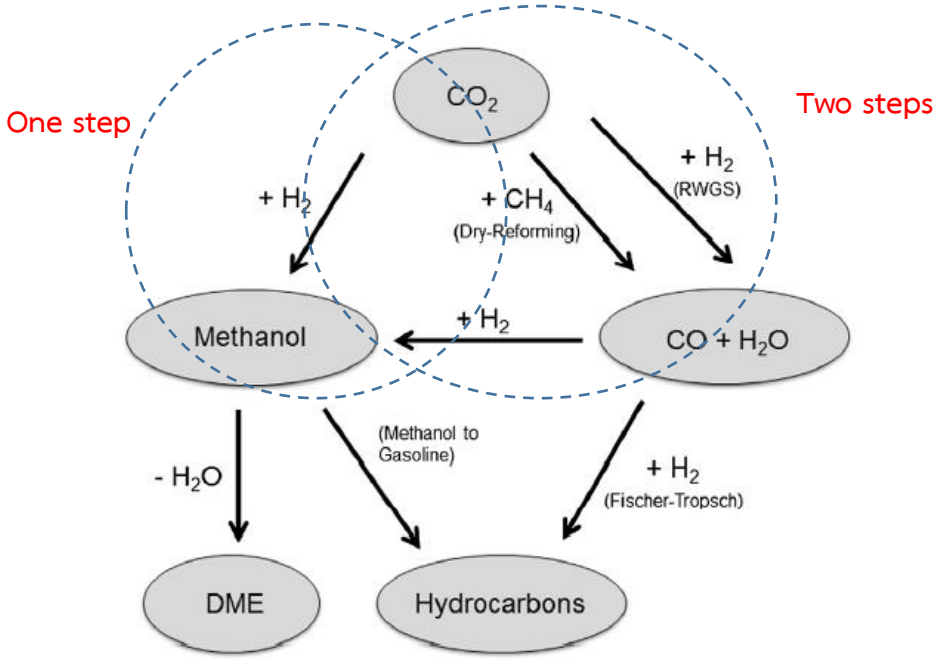

Fig. 2.2: one step and two steps conversion for methanol production from CO_2 [26]

2.1.1 Commercial processes

In commercial scale of methanol production, there are different designs of methanol synthesis reactors as following: [30]

- Quench reactor
- Adiabatic reactors in series
- Boiling water reactors (BWR)

จุฬาลงกรณ์มหาวิทยาลัย
Chulalongkorn University

The quench reactor consists of a series of adiabatic catalyst beds in a single shell, which has one pressure. The feedstocks are divided into various fractions to feed in each catalyst bed. Normally, the catalyst beds have been used up to 5 beds.

While the adiabatic reactors in series are adiabatic reactors or fixed bed reactors in a synthesis loop. The synthesis loop has approximately 2-4 fixed bed reactors. In between the reactors, the coolers are installed to adjust the temperature and prepare as an input for the next reactor.

The boiling water reactor (BWR) or shell and tube heat exchanger reactor is packed with catalyst beds in the tube side in principle. The cooling takes place on the

shell side. BWR provides nearly isothermal behavior and gives a high conversion compared with the other types with the same amount of catalyst. In general, the operating temperature in this reactor for methanol synthesis is between 240°C - 260°C, which leads to a high reaction rate. Additionally, the generated steam can be used to drive the compressors and subsequently as a distillation steam.

For commercial plants of methanol synthesis, there are many processes such as Lurgi low-pressure methanol synthesis process, ICI low-pressure methanol process, Haldor Topsøe methanol process and the MGC low-pressure process. These processes mostly use natural gas as a feedstock and combine with steam reformer to form syngas. The details of each process is explained as followed:

Lurgi low-pressure methanol synthesis process

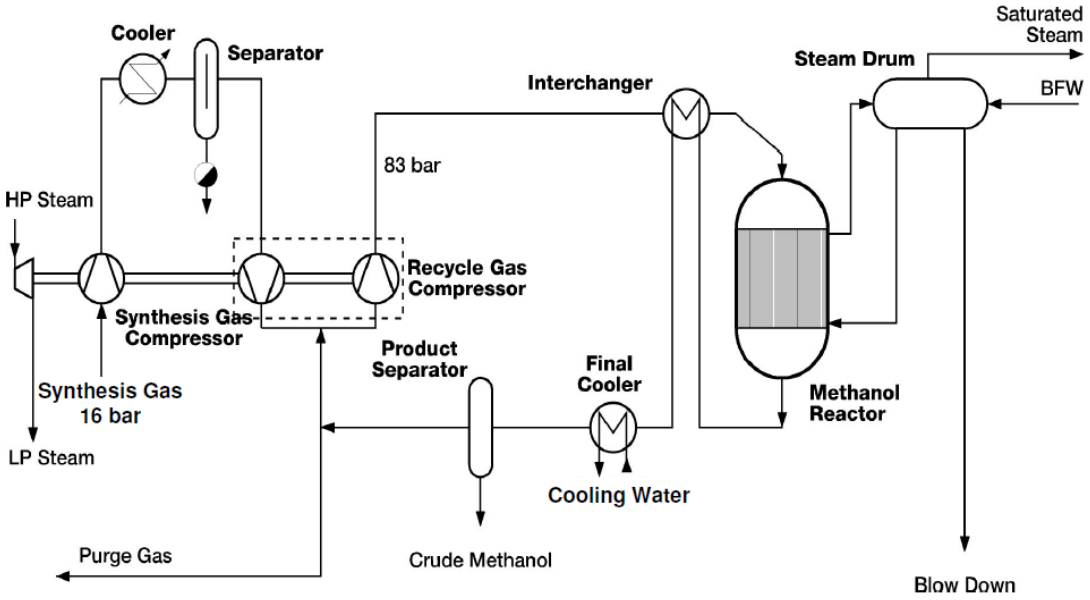

Fig. 2. 3: Lurgi low-pressure methanol process [31]

The syngas, which is the feedstock for methanol synthesis, can be produced via two routes namely steam reforming and partial oxidation and feedstock for the production of syngas includes gaseous hydrocarbons such as methane as well as liquid hydrocarbons like naphtha. Steam reforming is carried out at temperatures of 850 - 860°C. Desulphurized naphtha is contacted with steam at this temperature to produce hydrogen and carbon oxides. And then the produced syngas is compressed to 50 – 80

bar from 16 bar before it is fed into the methanol reactor. This reactor is a shell and tube type with the catalysts filled in the tubes, which operates at temperature of 250 – 260 °C and pressure of 50 – 60 bar. The heat of reaction is removed by circulating cold water on the shell side and this generates high pressure steam for other usages.[30]

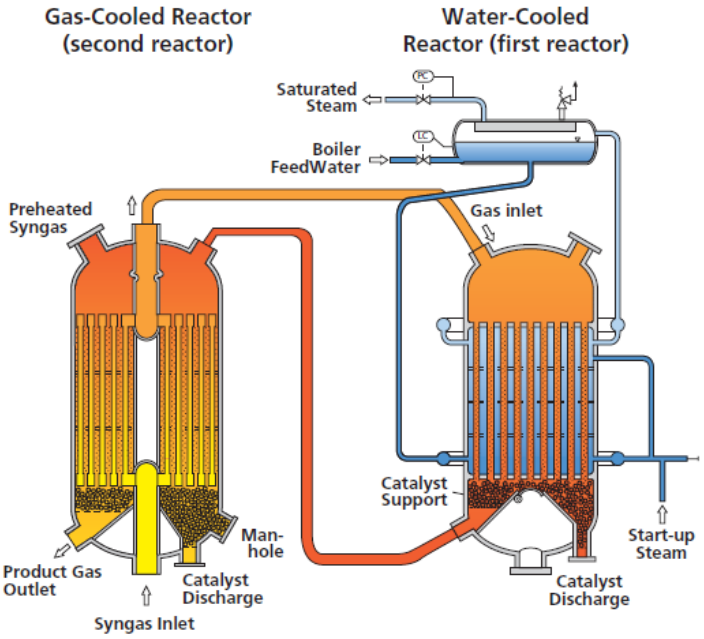

Fig. 2.4: Gas-cooled reactor and water-cooled reactor in Lurgi process [31]

Lurgi has recently developed a dual reactor system following Fig. 2.3 by combining with gas-cooled reactor in series for providing isothermal condition and high efficiency. The first reactor (water-cooled reactor) has a higher space velocities and higher temperatures compared with a single-stage synthesis reactor. This system leads to significant size reduction of water-cooled reactor compared with conventional processes. The methanol-containing gas or reacting gas leaving the water-cooled reactor is fed to gas-cooled reactor for preheating cold feed-gas. Hence, the reaction temperature is continuously reduced in the gas-cooled reactor but the equilibrium driving force for methanol synthesis is maintained.

จุฬาลงกรณ์มหาวิทยาลัย
Chulalongkorn University

ICI low-pressure methanol process

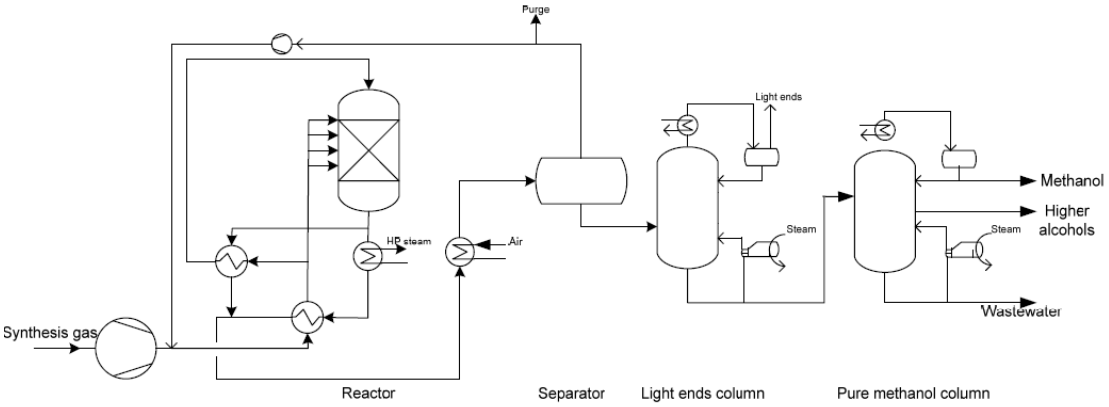

Fig. 2.5: ICI low-pressure methanol process [30]

In the ICI low-pressure methanol process, the syngas, which is compressed and mixed with recycled stream, is heated by heat exchanger with the reactor effluent. And then this stream is divided into 2:3 ratios. 40% of the stream is fed into the reactor after preheating with reactor effluent again. In this process, the reactor is an adiabatic reactor and a single catalyst bed and this is quenched by cold reactants in different height of catalyst beds. The product stream will be cooled by exchanging heat both the fresh synthesis gas and water for generating high pressure steam. Moreover, it is also cooled with an air-cool heat exchanger in which methanol and water are condensed. Then, the gas and liquid in product stream will be separated in a flash drum under pressure. The separated gas from flash drum will be recycled and mixed with fresh feed and purged in some part. On the other hand, the methanol-containing stream will be purified in two different columns: light ends column and pure methanol column. In the first column, the gases and other light impurities will be removed, as methanol is separated from other heavy alcohols in the second column. [30]

จุฬาลงกรณ์มหาวิทยาลัย
Chulalongkorn University

Haldor Topsøe methanol process

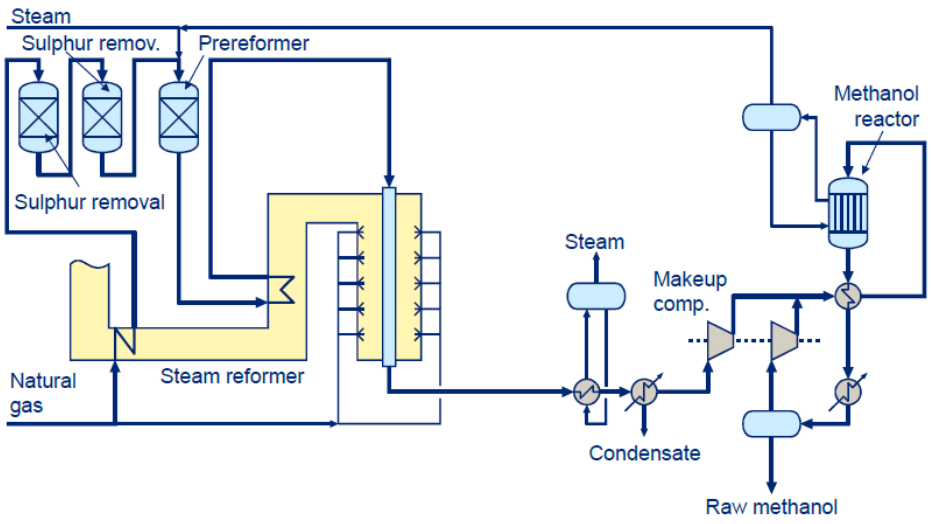

Fig. 2.6: Haldor Topsøe methanol production by one step reforming [32]

In Haldor Topsøe methanol process, the natural gas will be preheated and purified by removal of sulphur in the first step. Then, the purified stream is fed into the reformer together with steam in order to occur steam reforming reaction to form syngas. The syngas, which is cooled and compressed, is mixed with the recycled stream and is heated by heat exchanger. The product stream from methanol reactor will be cooled with feed gas by the same heat exchanger and separated into recycled stream and raw methanol.

จุฬาลงกรณ์มหาวิทยาลัย
Chulalongkorn University

MGC low-pressure process

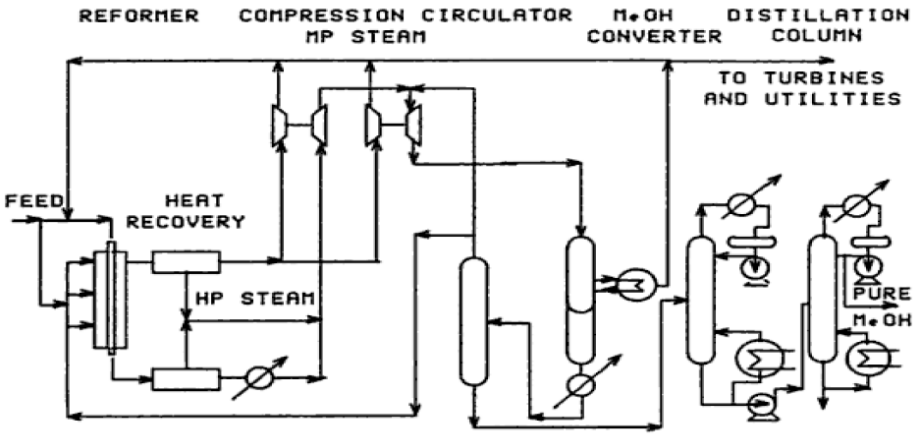

Fig. 2.7: MGC-low pressure process [30]

MGC process or Mitsubishi Gas Chemical low-pressure methanol synthesis process uses copper-based methanol synthesis catalyst and operates at temperature ranging from 200–280ºC and a pressure range of 50 – 150 atm. In this process, hydrocarbon is used as feedstock and desulphurized before entering into a steam reformer at temperature of 500 ºC. As the result, the exit stream from the reformer contains hydrogen, carbon monoxide and carbon dioxide at 800 - 850ºC. The gases are compressed in a centrifugal compressor and mixed with the recycle stream before being fed into the quench reactor.[30]

2.1.2 Reactions and mechanisms involving methanol synthesis

The reactions for methanol synthesis involve three main equilibrium reactions: carbon-monoxide hydrogenation (2.1), carbon-dioxide hydrogenation (2.2) and reverse water-gas shift (2.3). Additionally, there is methanation (2.4) as a side reaction in methanol synthesis and all reactions are indicated as following:

CO hydrogenation:

$CO + 2H_2 \leftrightarrow CH_3OH$ ΔH_{298}= -90.4 kJ/mol (2.1)

CO_2 hydrogenation:

$CO_2 + 3H_2 \leftrightarrow CH_3OH + H_2O$ ΔH_{298}= -49.4 kJ/mol (2.2)

Reverse water-gas shift:

$CO_2 + H_2 \leftrightarrow CO + H_2O$ ΔH_{298}=+41.0 kJ/mol (2.3)

Methanation:

$CO + 3H_2 \leftrightarrow CH_4 + H_2O$ ΔH_{298}= -247 kJ/mol (2.4)

For methanol synthesis, it requires a catalytic process for acceleration of the reactions. Hence, there are various researches studying about the appropriate catalyst for hydrogenation of CO_2. The commercial catalysts based on Cu/Zn formulations are mostly available from many catalytic manufacturers such as Katalko from Johnson-Matthey and MegaMax from Clariant *etc.* [33] Bayat et al. [28] performed the mechanistic details of the hydrogenation of CO_2 into methanol on a Cu surface. It can be summarized as the elementary reaction steps as following: [28]

จุฬาลงกรณ์มหาวิทยาลัย
Chulalongkorn University

$H_2(g) \rightarrow 2H(a)$ (2.5)

$CO_2(g) \rightarrow CO_2(a)$ (2.6)

$CO_2(a) + 2H(a) \rightarrow HCOO(a) + H(a)$ (2.7)

$HCOO(a) + H(a) \rightarrow H_2COO(a)$ (2.8)

$H_2COO(a) + H(a) \rightarrow H_2CO(a) + OH(a)$ (2.9)

$H_2CO(a) + H(a) \rightarrow H_3CO(a)$ (2.10)

$H_3CO(a) + H(a) \rightarrow CH_3OH$ (2.11)

$OH(a) + H(a) \rightarrow H_2O$ (2.12)

*Remark: H (a): adsorbed hydrogen

From these elementary reactions mentioned above, steps (2.7)–(2.11) are considered as the major steps for methanol synthesis. Furthermore, Bayat et al. [28] illustrated the proposed mechanism by depicted in Fig. 2.8. The results showed that chemisorbed CO_2-, formate, dioxomethylene, formaldehyde, and methoxy are the main intermediates in methanol synthesis [28].

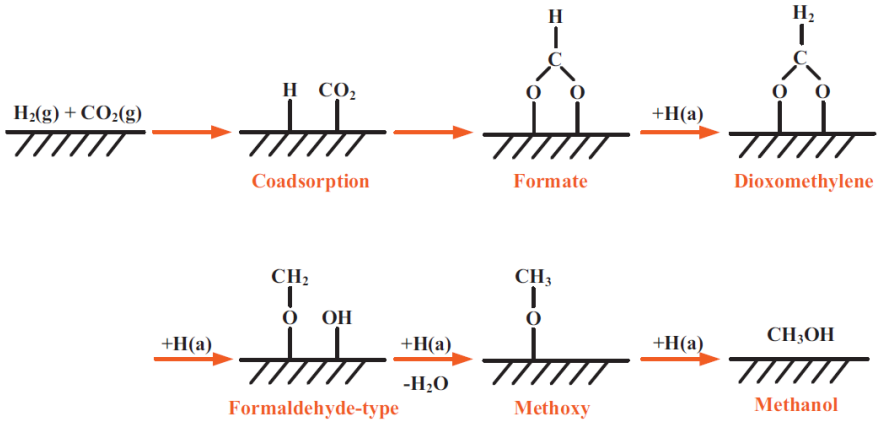

Fig. 2.8: Summary of methanol synthesis mechanisms [28]

For kinetic models of the commercial catalysts (copper oxide mixed with zinc oxide supported on alumina; $CuO/ZnO/Al_2O_3$) in methanol synthesis, there are many researches developing the kinetic models for this catalyst. Generally, the kinetic models proposed by Vanden Bussche and Froment [34] and Graaf et al. [35] have been

widely known and used in predicting behavior of hydrogenation of CO_2 in various research studies. Yet, the kinetic models of Van-Dal et al. [26] rearranged from Vanden Bussche and Froment [34] are used for this research. These kinetic models are expressed as followed:

Methanol synthesis:

$$r_{CH_3OH} = \frac{k_1 P_{CO_2} P_{H_2} - k_6 P_{H_2O} P_{CH_3OH} P_{H_2}^{-2}}{\left(1 + k_2 P_{H_2O} P_{H_2}^{-1} + k_3 P_{H_2}^{0.5} + k_4 P_{H_2O}\right)^3} \quad (2.13)$$

Reverse water-gas shift:

$$r_{RWGS} = \frac{k_5 P_{CO_2} - k_7 P_{H_2O} P_{CO} P_{H_2}^{-1}}{1 + k_2 P_{H_2O} P_{H_2}^{-1} + k_3 P_{H_2}^{0.5} + k_4 P_{H_2O}} \quad (2.14)$$

$$lnk_i = A_i + \frac{B_i}{T} \quad (2.15)$$

where pressure of each species (P_i) is given in Pa, temperature (T) in K and reaction rate (r) in kmol $kg_{cat}^{-1}s^{-1}$. In addition, the k parameters in reaction rate equations mentioned above are presented in Table 2.2 as following:

Table 2.2: Parameters of the rearranged kinetic model.

k_i	A_i and B_i	values	k_i	A_i and B_i	values
k_1	A_1	-29.87	k_4	B_4	14,928.9
	B_1	4,811.2	k_5	A_5	4.804
k_2	A_2	8.147		B_5	-11,797.5
	B_2	0	k_6	A_6	17.55
k_3	A_3	-6.452		B_6	-2,249.8
	B_3	2,068.4	k_7	A_7	0.131
k_4	A_4	-34.95		B_7	-7,023.5

จุฬาลงกรณ์มหาวิทยาลัย
Chulalongkorn University

2.2 Biogas upgrading

Typically, biogas contains mainly two substances: CH_4 and CO_2. However, this gas also comprises different common gases (H_2S, NH_3, H_2, N_2, O_2, CO, H_2O), saturated

or halogenated carbohydrates, solid particles and siloxanes. For biogas generation, The biogas occurs from the biological transformation of organic matters under anaerobic conditions or anaerobic digestion process presented in Fig. 2.9 [8], which this process involves hydrolysis of complex organic matters, fermentation and methanogenesis.

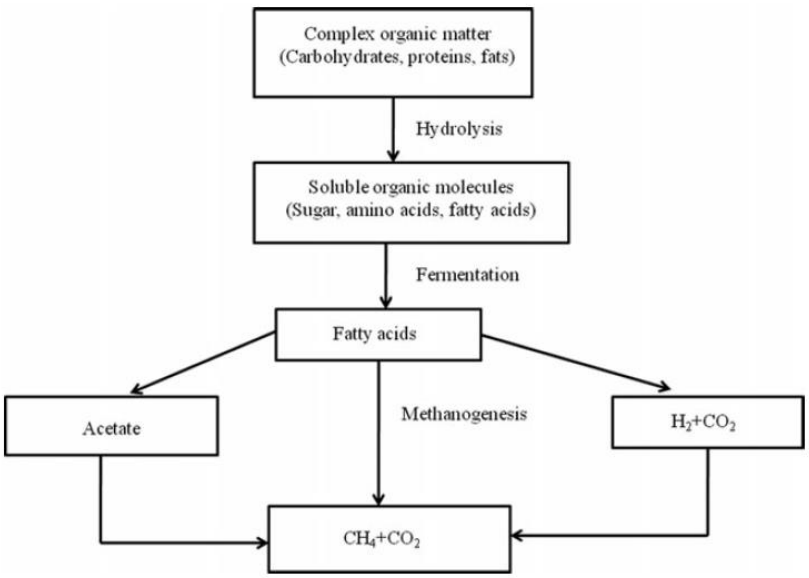

Fig. 2.9: Schematic representation of the anaerobic digestion process for biogas generation [8]

Most of organic matters present in agricultural waste (manures, sewage, sludge, green wastes), landfills or municipal wastes. Furthermore, the industrial wastes are also the sources of biogas such as wastewater from agri-food industry, alcohol distilleries, beverage industry, pulp and paper industry [7]. Absolutely, the composition of biogas varies with the biomass digested. In table 2.3, the typical composition of biogas in three different sources is presented.

จุฬาลงกรณ์มหาวิทยาลัย
Chulalongkorn University

Table 2.3: typical composition (%) of biogas [7]

Component	**Agricultural waste**	**Landfills**	**Industrial waste**
Methane, CH_4	50-80	50-80	50-70
Carbon-dioxide, CO_2	30-50	20-50	30-50
Hydrogen sulphide, H_2S	0.70	0.10	0.80
Hydrogen, H_2	0-2	0-5	0-2
Nitrogen, N_2	0-1	0-3	0-1

Component	Agricultural waste	Landfills	Industrial waste
Oxygen, O_2	0-1	0-1	0-1
Carbon monoxide, CO	0-1	0-1	0-1
Ammonia, NH_3	Traces	Traces	Traces
Siloxanes	Traces	Traces	Traces
Water, H_2O	Saturation	Saturation	Saturation

In term of utilization, biogas should be cleaned up initially and the composition of biogas should be adjusted to suit with the different quality requirement in each application. For example, the quality requirements for vehicle fuel utilization according to Czech Standard CSN 65 6514 are expressed in table 2.4 [36]. In purification processes, many technologies have been used for upgrading biogas to bio-methane: adsorption, chemical and physical absorption, cryogenic separation and membrane separation. In adsorption process, the contaminants (CO_2, higher C_xH_y, H_2S, Si-, F-, Cl-compounds and odorous compounds) will be removed via activated carbon/ carbon molecular sieves. For chemical and physical absorption, CO_2 and H_2S are absorbed in the scrubbing medium such as water, amine and glycols etc. CO_2 is liquefied due to high pressure and low temperature in cryogenic separation. And for membrane separation, CO_2 separation applies the principle of different compound permeability through the membrane. In addition, Vrbova and Ciahotny [36] compared the advantages and the disadvantages of each technology presented in Table 2.5

จุฬาลงกรณ์มหาวิทยาลัย
CHULALONGKORN UNIVERSITY

Table 2.4: Bio-methane quality requirements for vehicle fuel utilization [36]

requirement	Required value
Methane	Min 95.0 mol%
Hydrogen sulfide	<= 10 mg m^{-3}
CO_2+N_2+O_2 content	Max 5 mol%
CO_2 content	Max 2.5 mol%
H_2O content	Max 32 mg m^{-3}

Table 2.5: Comparison of technologies for biogas upgrading [36]

processes	advantages	disadvantages
adsorption	•High quality gas •Dry process •No chemicals •No wastewater •Partial N_2 and O_2 removal •no bacterial contamination in waste gas •certified technology	•needs H_2S removal •3–4 adsorption columns • CH_4 quality is not stable • complicated process • higher investment costs • high energy demands • large equipment
absorption	•high-quality gas • suitable investment costs • no need for gas purification prior to the process • compact process • certified/tested technology • it is possible to reuse CO_2	• wastewater liquidation • high water consumption • higher investment costs • high energy demands • large equipment
cryogenic separation	• high-quality gas • no chemicals • no water • compact process • it is possible to reuse CO_2	• gas pre-purification needed • very high energy consumption • high investment cost • complicated process • it is possible to reuse CO_2
membrane separation	• dry process • no chemicals • low mechanical deterioration • compact process	• gas pre-purification needed • higher methane losses • unstable long-term behaviour

จุฬาลงกรณ์มหาวิทยาลัย
Chulalongkorn University

Chen et al. [7] revealed various advantages of membrane separation. For example, it had low demand of electric energy, low investment and operating costs as well as the methane recovery could be enhanced up to 99.5% by using multiple membrane steps and multi compressors or suitable membrane configurations. Moreover, the significant point was the possibility in adjusting the plant layout to local particularities. Hence, membrane separation is suitable alternative for applying in this research from all mentioned above.

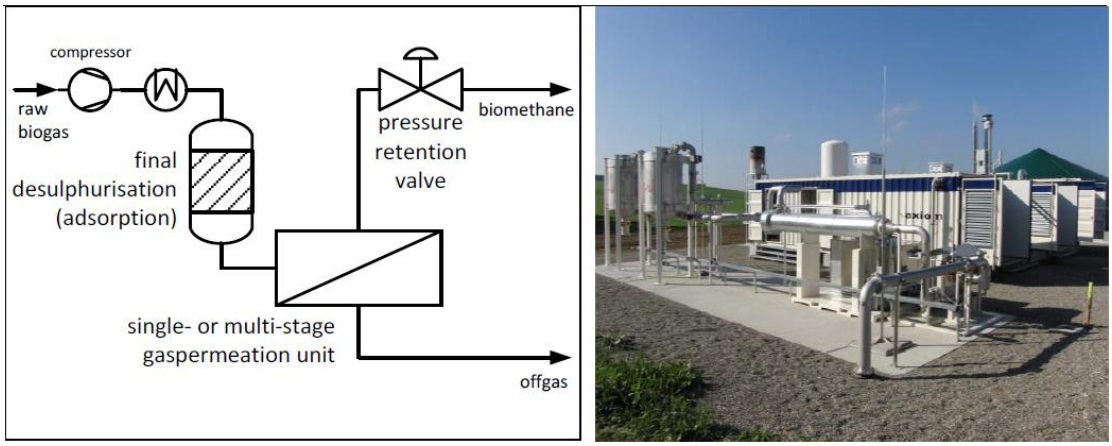

Fig. 2.10: Flowsheet of a typical biogas upgrading unit applying the membrane technology gas permeation; picture of the upgrading plant Kisslegg, Germany with a raw biogas capacity of 500m³/h (Source: AXIOM Angewandte Prozesstechnik) [37]

The typical process of biogas upgrading applying membrane technology is shown in Fig 2.10. The raw biogas, which is compressed to operating pressure is cooled for eliminating ammonia. Then, the remaining raw biogas is desulphurized by adsorption on zinc oxide or iron in adsorption column. Finally, the single or multi-stage gas permeation unit is used for separating the other remaining gases and each design of gas permeation unit affects to the desired bio-methane quality. Furthermore, both the desired quality and quantity of bio-methane can be controlled by operating pressure or compressor speed. For this research, this step also emits a lot of carbon dioxide waste. Therefore, integrating this step with methanol production by using CO_2 from biogas as a feedstock to react with H_2 is an interesting idea and is investigated.

2.3 Membrane separation technologies

For membrane separation technologies, Chen et al. [7] depicted the equation of permeation for pure gas based on steady state empirical observation as following:

$$N = P\left(\frac{\Delta p}{l}\right) \qquad (2.16)$$

where N is the permeation flux, P is permeability coefficient or proportionality coefficient, Δp is the pressure difference across the membrane and l is thickness of

the membrane. The permeability coefficient (*P*) can be determined from two parts: (1) thermodynamic part or solubility coefficient (*S*) considered by the number of gas molecules that absorbed into and onto membrane, (2) a kinetic part or diffusion coefficient (*D*) determined by the mobility of gas molecules through the membrane expressed as following:[7]

$$P = DS \qquad (2.17)$$

In addition, the values of *D*, *P* and *S* parameters can be determined by various methods. For example, time-lag method is used for calculating *D*, solubility coefficient (*S*) can also be obtained from eqn. 2.17. Furthermore, the units for permeability coefficient (*P*) widely accepted are Barrer and GPU, which 1 Barrer equals 10^{-10} cm^3 (STP) cm cm^{-2} $s^{-1}cmHg^{-1}$ and 1 GPU equals 1 Barrer/1 micron or 10^{-6} cm^3 (STP) cm^{-2} $s^{-1}cmHg^{-1}$

2.3.1 Membrane separation for H_2O removal

Struis and Stucki (2001) [23, 24] studied H-, Li-, K-Nafion membranes for separation of water from reacting gases in tubular membrane reactor and the permeability and selectivity properties of Nafion, a perfluorinated cation exchange polymer material, was determined at PSI. The permeation coefficients of the reactor gas components relating to the methanol synthesis were determined as a function of the temperature (40–200°C) at pressure (1 atm) and expressed as Fig. 2.11 [23].

จุฬาลงกรณ์มหาวิทยาลัย
Chulalongkorn University

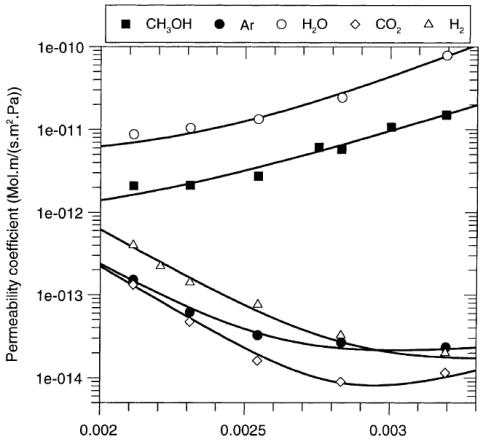

Fig. 2.11: Permeability coefficients (P) for various gases and vapours as a function of the absolute temperature [23].

The significant problem of using H-, Li- and K- Nafion membranes was the high permeation of other substances following Fig. 2.11. Consequently, Rohde et al. (2008) [38] developed hydroxy sodalite (H-SOD), which was a zeolite-like material membrane prepared by direct hydrothermal synthesis on alpha-Al_2O_3 supports. This membrane was an excellent candidate for small molecules separation due to excellent thermal and mechanical stability, high selectivity of water to hydrogen and low price [39]. Moreover, The H-SOD membrane was nearly 100% selective for removal water from H_2, CO, CO_2. Furthermore, Rohde et al. [38] also characterized about permeation properties of hydrogen. The hydrogen permeation across the H-SOD membrane was below the detection limit of the experimental equipment (approximately 10^{-12} mol/(sm^2Pa)) and did not significantly change over the temperature range (30-150 °C) and feed pressure range (0.1013-0.5013 MPa). From reasons mentioned above, the H-SOD membrane is appropriate alternative for this research. In addition, the water flux of H-SOD membrane relating to temperature was depicted in Fig. 2.12 as following:

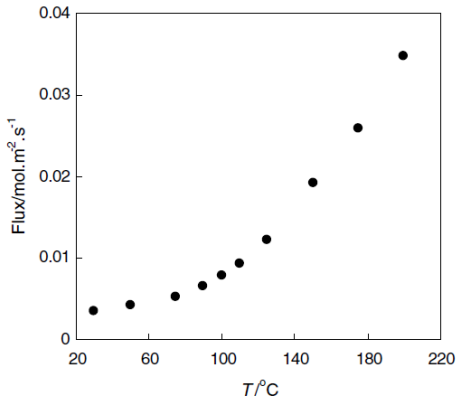

Fig. 2.12: Water flux as function of temperature (T: 30–200 °C); feed pressure P = 1.2 MPa, permeate pressure P = 1000 Pa.[38]

In terms of the permeation rate equation, it relates to partial pressure difference of water across the membrane, permeability, surface area and volume is obtained as following: [40]

$$J_{H_2O} = \frac{Q_{H_2O} A_S}{V_r}\left(P_{H_2O,in} - P_{H_2O,out}\right) \qquad (2.18)$$

where A_S is the surface area, Q_{H_2O} is permeance of water (1-10 x 10^{-7} $mols^{-1}m^{-2}Pa^{-1}$ at temperature of 250 °C [41]) and V_r is reactor volume, $P_{H_2O,in}$ and $P_{H_2O,out}$ are partial pressures of water in both sides of the membrane (reaction and permeation sides).

2.3.2 Membrane separation for CO_2 removal

For separation of carbon-dioxide gases from biogas, Matrimid® 5218, Kapton®, and p84 polyimides were used as CO_2 commercial selective membrane as shown in Fig. 2.13. Due to the poor thermal properties of polymer, the membrane separation was often operated at room temperature and atmosphere pressure. However, the high temperature and pressure are required in methanol synthesis. In this research, the membrane should have the properties below:

- High thermal stability at 200-300 °C operating temperature
- High selectivity of CO_2 to H_2, H_2O, CH_3OH, CO and high permeability
- High stability at difference of pressure at least 5-10 bar

Chen et al. [7] revealed inorganic membranes, which relate to zeolite, carbon, ceramic and metal such as copper, alumina, iron, nickel, palladium, platinum, vanadium, cobalt, niobium and so on, perform the high chemical and thermal stability. Therefore, the inorganic membrane is one of candidates for CO_2 selective membrane in methanol synthesis due to ability for operation at high temperature.

จุฬาลงกรณ์มหาวิทยาลัย
Chulalongkorn University

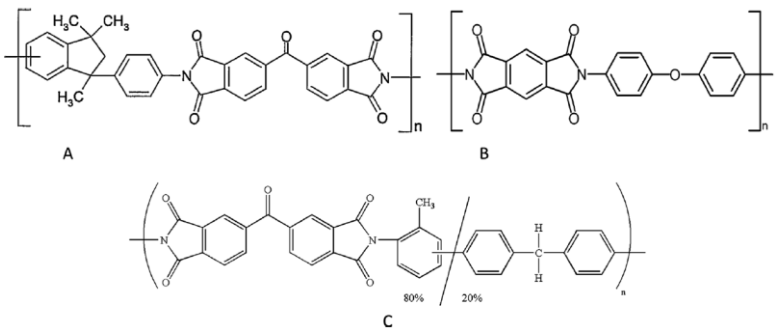

Fig. 2.13: Chemical structure of commercial polyimides: (a) Matrimid® 5218, (b) Kapton®, and (c) p84 [7]

However, the separation mechanism of inorganic membranes is controlled by CO_2 preferential adsorption which has low CO_2 selectivity at high temperatures (200-300 °C) [42] because H_2 can more absorb on the membrane surface than CO_2 in high temperature. To fix this problem, Osamu et al. [43] developed CO_2-facilitated transport membrane or cesium carbonate contained in polyvinyl alcohol-polyacrylic acid copolymer gel layer supported by PTFE porous membrane (Cs_2CO_3-PVA-PAA/PTFE) for CO_2 permeation. This membrane which is able to CO_2 permeability of about 1×10^{-4} mol m^{-2} s^{-1} kPa^{-1}at 200 °C can provide the high CO_2 ideal selectivity and thermal stability in high operating temperature. All of this results from Cs_2CO_3 acting as carbon dioxide carrier capable of transporting carbon dioxide or a permeable material from the high CO_2 concentration side to the interface at low CO_2 side. Moreover, the CO_2 Permeance (mol/(m^2 s kPa)) at different pressure at the feed side (kPa) are expressed in Fig. 2.14.

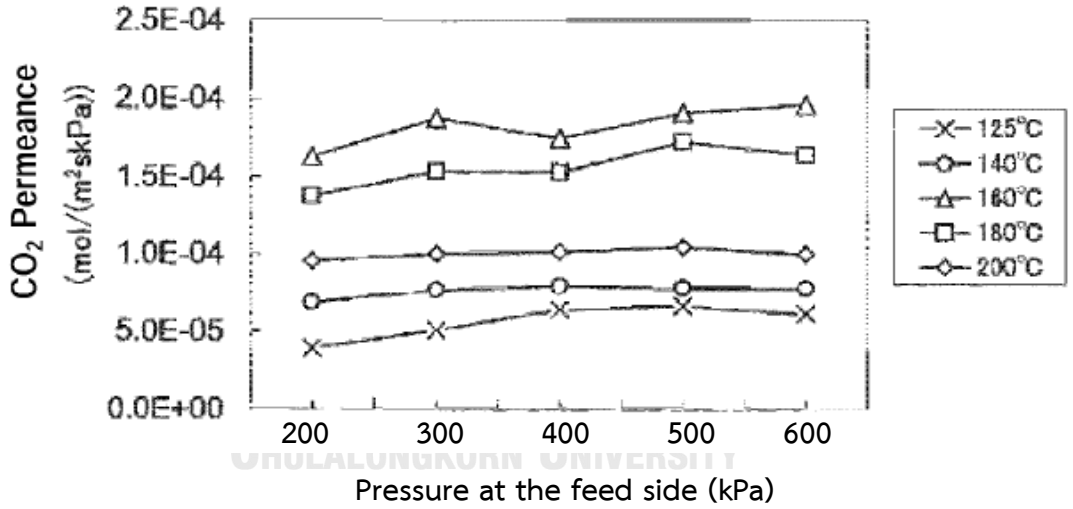

Fig. 2.14: CO_2 Permeance (mol/(m^2 s kPa)) at different pressure at the feed side (kPa) (Osamu et al., 2013 [43])

2.4 Computational fluid dynamics modeling

The computational fluid dynamics (CFD) is the essential equipment for scale-up and analysis and can represent the fluid flow, heat transfer, chemical and physical phenomena inside reactor or other tools. The CFD has been widely used in various applications such as aerodynamic of aircraft and vehicle, hydrodynamics of ships,

power plant, environmental engineering, chemical process engineering and biomedical engineering and so on. [44]

There are several numerical methods known as discretization techniques, vortex dynamic and direct numerical simulation (DNS), in which these techniques are provided in the solution of the CFD model equations. The discretization method including finite difference, based on Taylor's series, polynomial expansions, finite element, based on weighted residuals method, and finite volume, based on the control volume formulation has been widely used. Therefore, the codes provide a complete CFD analysis, they consist of three main elements: pre-processor, solver and post-processor as following Fig. 2.15.

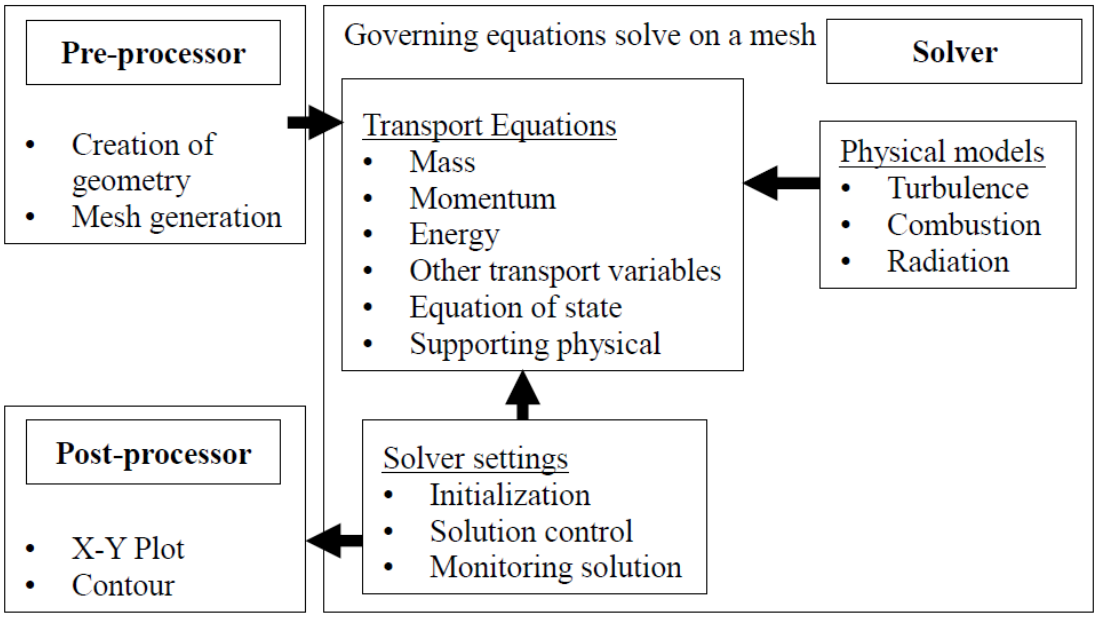

Fig. 2.15: The interconnectivity functions of the three main elements within a CFD analysis framework. (Tu et al., 2013)

The pre-processor is similar to input of system composing of creation of geometry, mesh or grid generation, specification of chemical and physical properties and definition of boundary conditions. The mesh generation is significant steps of CFD simulation after definition of the domain geometry because the number of cells into geometry domain affect to the accuracy of the computational fluid dynamics solution. Typically, increasing mesh resolution will enhance the accuracy of the CFD solution. Furthermore, there are many other factors influencing to the accuracy such as kind of

mesh, the sufficient techniques chosen to the physics of the problem. However, the accuracy of the CFD solution is absolutely limited by calculation turnover times and the computational costs. In solver section, the discretization method mentioned above is widely used for numerical solution and the transport equations, physical models and auxiliary equations have to be defined initially. Then, the steps of the solver can be mainly divided into three steps as following:

- Approximation of unknown variables
- Discretization into subsequent mathematical manipulation
- Solution of the algebraic equation

In the post processor, the results from computational fluid dynamics (CFD) solution can be depicted in different suitable ways to analyze the results such as contour, X-Y plot, streamline, arrow surface etc.

2.4.1 governing equations

The computational fluid dynamics models of this research involve mathematical models of chemical reactions, fluid flow, mass and heat transfer in both fluid and porous media phase. The fundamental governing equations are the conservation laws of mass, momentum, energy and species.

จุฬาลงกรณ์มหาวิทยาลัย
CHULALONGKORN UNIVERSITY

Conservation of mass:

The equation for conservation of mass also named as continuity equation can be written as following:

$$\frac{\partial \rho}{\partial t} + \nabla \cdot \left(\rho \vec{u} \right) = S_m \qquad (2.19)$$

This equation is the general form of the continuity equation where ρ is density (scalar), u is velocity of fluid (vector) and S_m is the mass added to continuous phase from the dispersed second phase, for instance due to vaporization of liquid droplets. Additionally, this equation can be valid for both incompressible as well as

compressible fluid flow. If the system operates under steady state condition, $\partial\rho/\partial t$ will be neglected.

Conservation of momentum:

The general form of equation of conservation of momentum or Newton's second law can be written as following eq. 2.20

$$\frac{\partial\left(\rho\vec{u}\right)}{\partial t}+\nabla\cdot\left(\rho\vec{u}\vec{u}\right)=-\nabla p-\nabla\cdot\left(\bar{\bar{\tau}}\right)+\rho\vec{g}+\vec{F} \qquad (2.20)$$

$$\frac{\rho D\vec{u}}{Dt}=-\nabla p-\nabla\cdot\left(\bar{\bar{\tau}}\right)+\rho\vec{g}+\vec{F} \qquad (2.21)$$

The equation (2.21) is substantial derivative form of equation of conservation of momentum (2.20) where p is the static pressure, $\bar{\bar{\tau}}$ is the shear stress, $\rho\vec{g}$ is term of gravitational body force and F is term of external body forces (vector) or other model-dependent source terms such as porous media.

The shear stress ($\bar{\bar{\tau}}$) is given by:

$$\bar{\bar{\tau}}=-\mu\left(\vec{\nabla}\vec{u}+\left(\nabla\vec{u}\right)^{T}\right)+\left(\frac{2}{3}\mu-\kappa\right)\left(\vec{\nabla}\cdot\vec{u}\right)\bar{\bar{\delta}} \qquad (2.22)$$

This equation above is a general form of Newton's law of viscosity where μ is the molecular viscosity, δ is the tensor unit and κ is dilatational viscosity which is equal to zero in gas phase.

Conservation of energy:

The general form of equation of conservation law of energy in substantial derivative is written as following:

$$\frac{\rho\hat{C}_{p}DT}{Dt}=Q_{sv}-\left(\vec{\nabla}\cdot\vec{q}\right)-\left(\bar{\bar{\tau}}:\vec{\nabla}\cdot\vec{u}\right)-\left(\frac{\partial\ln\rho}{\partial\ln T}\right)_{p}\frac{Dp}{Dt} \qquad (2.23)$$

where $\hat{C}_{p}$ and Q_{sv} are the specific heat capacity and the external heat sources, respectively.

$-\left(\vec{\nabla}\cdot\vec{q}\right)=k\nabla^2 T$ if the system is assumed to be an isotropic medium (Fourier's law of conduction).

$-\left(\overline{\overline{\tau}}:\vec{\nabla}\cdot\vec{u}\right)=\mu\Phi_V$ if the system is assumed to be a Newtonian fluid (viscous dissipation function).

$\left(\frac{\partial \ln\rho}{\partial \ln T}\right)_p$ =0 if the system is assumed to be an incompressible fluid.

Conservation of chemical species:

The general form of equation of conservation law of species is written as following:

$$\frac{\partial}{\partial t}\left(\rho\omega_i\right)+\nabla\cdot\left(\rho\vec{u}\omega_i\right)=-\nabla\cdot\vec{J_i}+R_i+S_i \qquad (2.24)$$

where ω_i is the local mass fraction of each species. $\vec{J_i}$, R_i and S_i are the mass diffusion flux, the net of rate of reaction and the rate of creation by addition form the dispersed phase plus any user-defined sources of each species, respectively. The mass diffusion flux (J_i) is given by:

$$\vec{J_i}=-\left(\rho D_i^F\nabla\omega_i+\rho\omega_i D_i^F\frac{\nabla M_w}{M_w}+D_i^T\frac{\nabla T}{T}\right) \qquad (2.25)$$

จุฬาลงกรณ์มหาวิทยาลัย
Chulalongkorn University

This equation 2.25 is a general form of Fick's law, which D_i^F is diffusion coefficient of each species, M_w is molecular weight and D_i^T is thermal diffusion coefficient. The diffusion coefficient (D_i^F) is calculated by mixture averaged diffusion model (eq. 2.26) and the binary diffusion coefficient (D_{AB}) is determined from fuller correlation (eq. 2.27)

The mixture averaged diffusion model can be written as following:

$$D_i^F=\frac{1-\omega_i}{\sum_{k\neq i}\frac{y_k}{D_{ik}}} \qquad (2.26)$$

The fuller correlation can be written as following:

$$D_{AB} = \frac{10^{-3} T^{1.75} \left(\frac{1}{M_A} + \frac{1}{M_B} \right)^{\frac{1}{2}}}{P \left[\left(\Sigma V_A \right)^{\frac{1}{3}} + \left(\Sigma V_B \right)^{\frac{1}{3}} \right]^2} \tag{2.27}$$

where y_k is mole fraction of each species, D_{ik}, D_{AB} are the binary diffusion coefficient of each species, P is given in atm, T is temperature in Kelvin (K), M_i is molecular weight in g/mol and ΣV_i is sum of the diffusion volume of component i which can be calculated by sum of atomic diffusion volumes in Fig. 2.16

Atomic and Structural Diffusion Volume Increments

C	16.5	(Cl)	19.5
H	1.98	(S)	17.0
O	5.48	Aromatic or heterocyclic rings	−20.2
(N)[a]	5.69		

Diffusion Volumes of Simple Molecules

H_2	7.07	CO_2	26.9
D_2	6.70	N_2O	35.9
He	2.88	NH_3	14.9
N_2	17.9	H_2O	12.7
O_2	16.6	(CCl_2F_2)	114.8
Air	20.1	(SF_6)	69.7
Ne	5.59	(Cl_2)	37.7
Ar	16.1	(Br_2)	67.2
Kr	22.8	(SO_2)	41.1
(Xe)	37.9		
CO	18.9		

[a]Parentheses indicate that the value is based on only a few data points.
Source: E. N. Fuller, P. D. Schettler, and J. C. Giddings, *Ind. Eng. Chem., 58*(5), 19 (1966).

Fig. 2.16: the values of atomic and simple molecular diffusion volumes [45]

Furthermore, for solid or porous media phase, the effective diffusion efficient can be calculated by:

$$D_{i,eff} = \frac{\varepsilon}{\tau} \left(\frac{1}{D_i^F} + \frac{1}{D_{i,KA}} \right)^{-1} \tag{2.28}$$

where ε and τ in eq. 2.28 are the porosity and the tortuosity of solid phase, respectively. The Knudsen diffusion coefficient ($D_{i,KA}$) was computed by:

$$D_{i,KA} = 4850 d_p \sqrt{\frac{T}{Mw_i}} \tag{2.29}$$

where d_p is the pore diameter of the solid phase. For the fluid flow in solid phase, the velocity in porous media can be calculated by Darcy's law as following:

$$\frac{\partial \varepsilon \rho}{\partial t} + \nabla \cdot \left(\rho \vec{u} \right) = S_m \tag{2.30}$$

$$\vec{u} = \frac{\kappa}{\mu} \nabla p \tag{2.31}$$

where κ is permeability of solid phase.

จุฬาลงกรณ์มหาวิทยาลัย
CHULALONGKORN UNIVERSITY

CHAPTER 3: LITERATURE REVIEWS

In order to develop the multifunctional reactor for simultaneous methanol production with biogas upgrading, we mainly focus on the design of the integrated reactor in micro scale with membrane separation for bio-methane (biogas upgrading) and methanol production. Therefore, these literatures can be divided into two parts; 1. microchannel reactor and 2. membrane reactor

3.1 Microchannel reactor

Microchannel reactor can be an interesting choice for various reactions due to its space and weight limitation, requirement of compact reactor and safe technology, in which methanol synthesis is one of those. Hence, the microchannel system for methanol synthesis has been proposed in several researches. Tonkovich et al. [46] developed methanol technologies for offshore floating production, storage and offloading plant (FPSO) due to the space limitation. It included syngas synthesis from methane steam reforming and methanol synthesis by using micro-devices, shown in Fig 3.1, which they called “isopotential microchannel reactor”. This microchannel reactor consists of reaction channels containing particulate catalyst and cross flow coolant channels. Tonkovich and Daly [47] achieved approximately 5 %CO conversion at 270°C and 51 atm. The isopotential microchannel reactor offers advantages over the fixed bed conventional reactor at low contact time (<300 ms), presented in Fig 3.1.

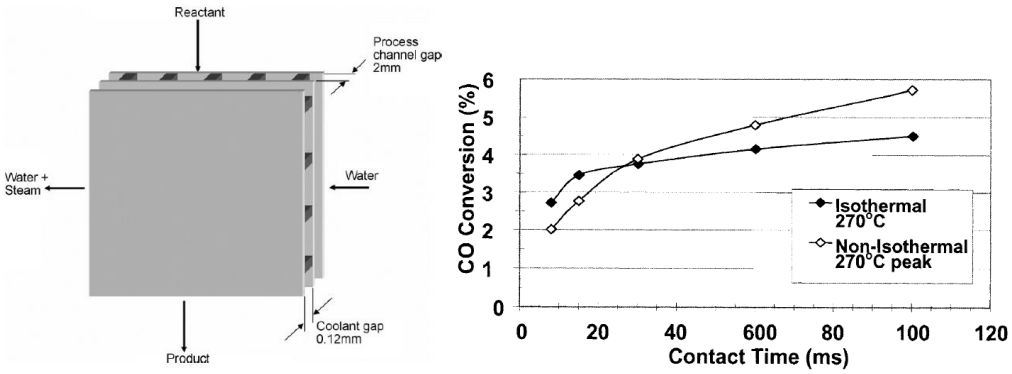

Fig. 3.1: Schematic of a microchannel methanol synthesis reactor [46] and CO conversion of this microchannel reactor and non-isothermal fixed bed reactor [47].

Then, an integrated micro packed bed reactor heat exchanger (IMPBRHE) was fabricated by the Institute of Micro Process Engineering (IMVT) at Karlsruhe Institute of Technology (KIT), formerly Forschungszentrum Karlsruhe, in Germany. The IMPBRHE module comprises eight reaction slits and each reaction slit is sandwiched by two cross flow oil channels acting to heat transfer. This microchannel reactor is made of stainless steel and carries out pressure up to 100 bar. The IMPBRHE module and schematic reaction slits and oil channels are shown in Fig 3.2 (a) and (b), respectively [19].

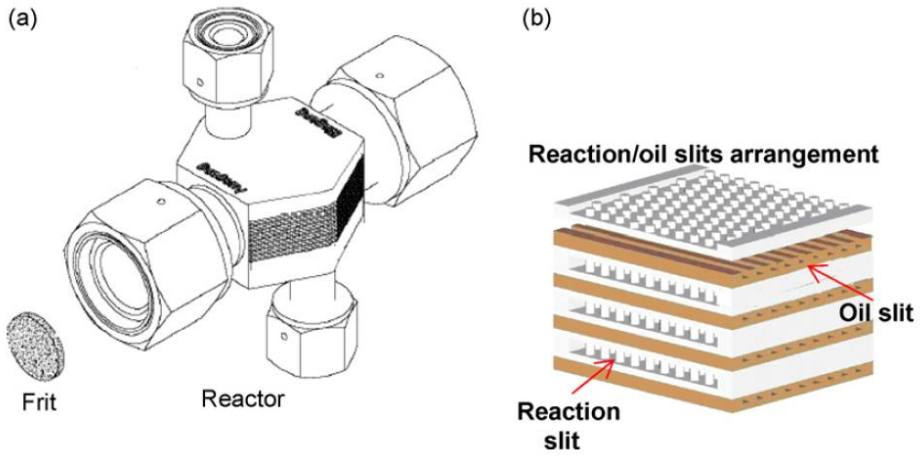

Fig. 3.2: (a) IMPBRHE module and (b) schematic reaction slits and oil channels arrangement [19]

The catalyst slits are made by etching 0.4 mm deep cylindrical pillar structures in which each pillar is hexagonally arranged in stainless steel foils. Hence, the two foils face to face give a 0.8 mm deep pillar structure. A SEM picture of catalyst slits is illustrated in Fig 3.3. Moreover, the reaction slits are 60 mm length with 8.0 mm x 0.8 mm cross section area. [19] From the outstanding characteristic mentioned earlier, the IMPBRHE has been studied in several researches. F.Hayer et al. [12, 48] studied the IMPBRHE in dimethyl ether synthesis. They compared the temperature profile along length of IMPBRHE with fixed bed reactor with the same operating condition. The simulated temperature profile by using COMSOL Multiphysics is performed, as shown in Fig. 3.4. While the temperature gradients of fixed bed reactor were up to 33°C, the temperature behavior in microchannel reactor was similar to isothermal condition due to high heat transfer from the high surface/volume ratios. For this reason, the highly exothermic reaction can be provided in microchannel reactor.

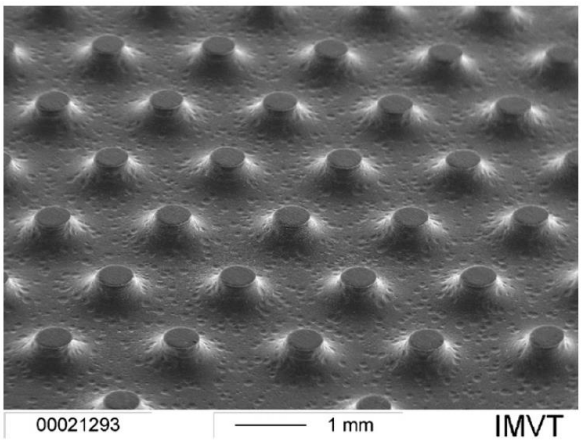

Fig. 3.3: SEM picture of the pillar arrangement inside one reaction slit. [19]

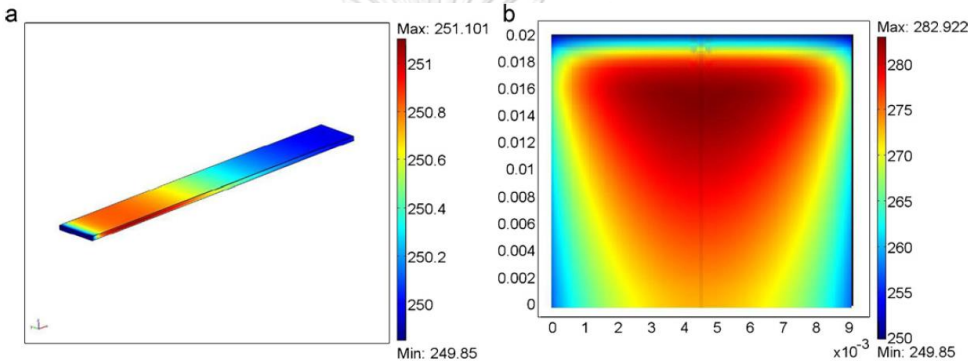

Fig. 3.4: temperature profile in (a) the microchannel reactor and (b) a laboratory fixed bed reactor the same DME synthesis operating conditions (T(wall/feed) = 250°C, 50 bar total pressure, H_2:CO = 1 and SV = 9000 Nml/gcat/h). [12]

Furthermore, Bakhtiary Davijany et al. (a) [19] investigated the (IMPBRHE) for compact methanol synthesis from syngas over Cu/ZnO/Al_2O_3 catalyst under industrial operating condition: temperature of 523 K and pressure of 80 bar. They found that the CO conversion from reaction experiments was near equilibrium conversion at contact time approximately 470 ms g/ml. Moreover, the pressure drop measurements and characteristics of velocity within the IMPBRHE were also investigated. According to the results in Fig 3.5, the different velocities at wall and middle flow path caused redistribution and mixing within reaction slits. In other words, rate of mass transfer could be improved by pillar structures. In addition, the results of pressure drop measurement and calculation by Ergun equation indicated an isobaric condition. The pressure in IMPBRHE reduced approximately 0-8 mbar from 80 bar at different superficial velocity. However, Bakhtiary Davijany et al. (b) [49] performed the possibility

of mass transfer limitations in IMPBRHE for methanol synthesis. Experiments were shown with three different particle size distributions (50-200 μm) at 215-270°C, 80 bar over Cu-based catalyst. The IMPBRHE was found to operate with internal or external diffusion limitations at particle sizes above 125 μm. Moreover, loading the particle size was often hard to obtain a well-defined particle size distribution. Hence, filling catalyst particles must be careful for avoiding flow maldistribution [50]. To avoid this problem, the wall-coated microchannel reactor has been studied. Phan et al. [50] said that the heat and mass transfer properties of wall-coated microchannel had a higher activity than powder packing. Therefore, a stack foil micro-reactor (SFMR) containing two catalyst foil coatings was proposed in this study. Phan et al. [50] studied Pd/CeO_2 and $Cu/ZnO/Al_2O_3$ catalysts for methanol synthesis under temperature of 300°C, pressure of 80 bar and H_2/CO ratio of 2.6. According to this experimental results, the Pd catalyst performed lower conversion than Cu catalyst at temperature below 255°C and Cu catalyst showed higher selectivity of methanol than Pd catalyst in the range of 95%. Therefore, Cu based catalyst has been widely used in catalytic processes of methanol synthesis.

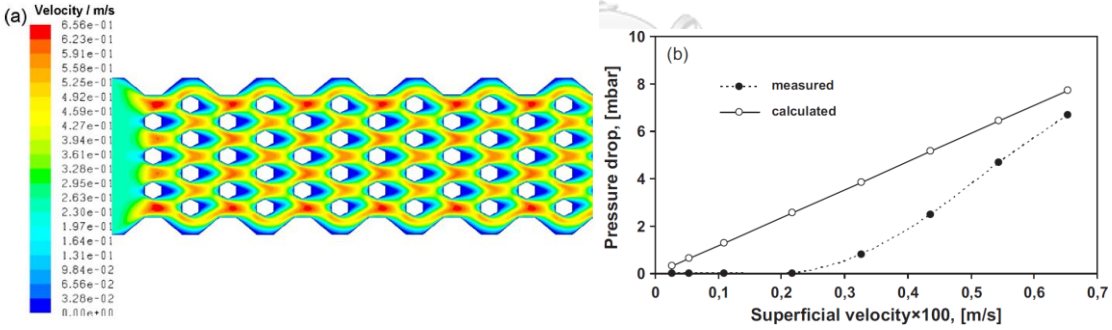

Fig. 3.5: (a) velocity contours in an empty reaction slits of IMPBRHE, (b) calculated and measured pressure drop over the IMPBRHE at 293 K, 80 bar [19]

3.2 membrane reactor

Due to the nature of CO_2, the methanol synthesis from CO_2 is strongly limited by the reaction equilibrium. Therefore, membrane reactor can be an interesting candidate because not only it can be applied with microchannel reactor, but it also improves the conversion of CO_2. According to Le Chatelier's principle: "When any

system at equilibrium is subjected to change in concentration, temperature, volume, or pressure, then the system readjusts itself to counteract (partially) the effect of the applied change and a new equilibrium is established."[51] For methanol synthesis, the water removal out of reaction zone by using membrane can shift the reaction equilibrium to forward side. Hence, there are many model of simulations for methanol synthesis in membrane reactor. Struis et al. [23, 24] simulated one dimensional pseudo homogeneous model of tubular membrane reactor for methanol synthesis by using Nafion membrane. The yield of single pass reactor (membrane reactor) improved to 40% under conditions (T = 200°C, P= 40 bar, GHSV = 5000 h^{-1}) and the additional costs of the materials could return in two production months. Then, Farsi et al. (a, b) [10, 21] simulated both steady state and dynamic heterogeneous one-dimensional mathematical model using alumina-silica membrane. They compared performance of the conventional reactor with the membrane reactor under temperature of 503 K and pressure of 76.98 bar which the schematic of these reactors were shown in Fig 3.6. They found that the methanol yield of both steady state and dynamic models increased compared to the conventional reactor. In steady state model (Farsi et al. (b) [21]), this membrane reactor could overcome the thermodynamic equilibrium limitations and improved the yield of methanol approximately 7% from traditional reactor. For dynamic model (Farsi et al. (a) [10]), not only this membrane reactor could provide the methanol production about 4.06% compared with the industrial methanol reactor during the production time, but it also enhanced the catalyst life time due to destruction matrix material by water and reduction of Cu surface tension, leading to sintering [10]. From the reasons mentioned above, combination of micro-channel reactor and membrane reactor or membrane micro-reactor (MMRs) are the interesting alternative for methanol synthesis due to high heat and mass transfer, high surface/volume ratio, enhanced CO_2 conversion, design flexibility and safety operation. [52]

จุฬาลงกรณ์มหาวิทยาลัย
Chulalongkorn University

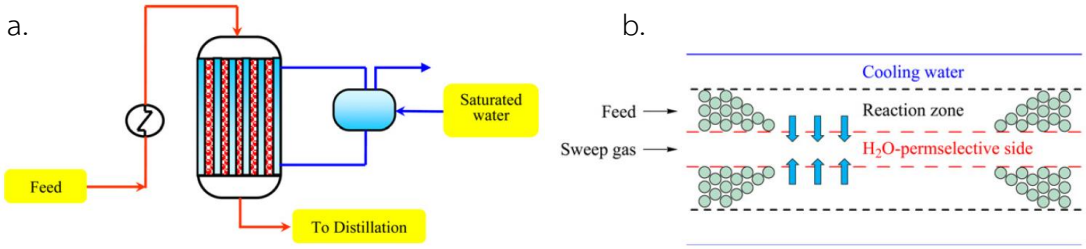

Fig. 3.6: (a) Schematic of conventional methanol reactor [21] and (b) an element of membrane reactor [10]

Furthermore, there are many researchers studying about dual-membrane reactor or different membrane reactor. In this system, the two substances required to be isolated can be separated through two different membranes. The dual membrane reactor can be flexibly applied in various researches for improving performance reactor or conversion, reducing purification cost and enhancing purity of product etc. Farsi et al. (c,d) [53, 54] simultaneously integrated Pd/Ag membrane tubes for addition of hydrogen to reaction zone and alumina-silica composite membrane tubes for water vapor removal from reaction zone. The diagram of this membrane reactor was depicted in Fig 3.7 (a). From these simulating results, the methanol yield of this configuration could be improved to 10.02% compared with conventional reactor at the same operating condition. On the other hand, Bakhtyari et al. [40] proposed the thermally coupled double membrane heat exchanger reactor, in which the removal of water vapor and hydrogen from reaction zone were achieved in this configuration. Therefore, the dual-membrane reactor offers the possibility for addition CO_2 to react with H_2 into the reaction zone and water removal from the reaction zone for this research. Moreover, it can also be applied in micro-scale.

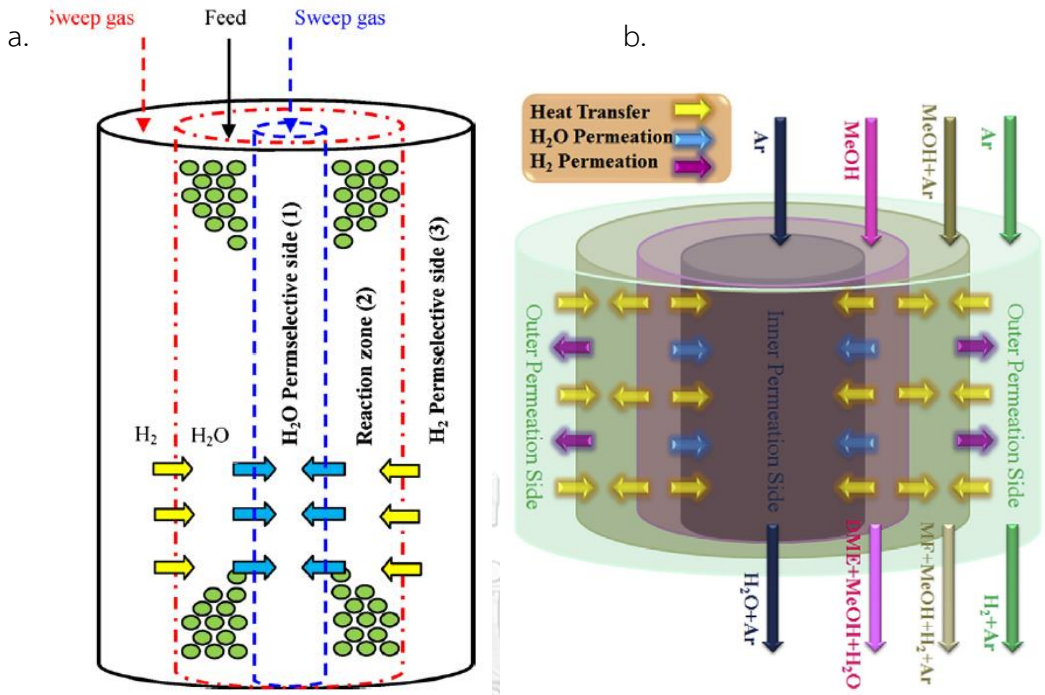

Fig. 3.7: (a) The proposed schematic for a membrane tubes and reaction side and (b) diagram of thermally coupled double membrane heat exchanger reactor[40]

In conclusion, both the microchannel reactor and the membrane reactor offer the possibility to use simultaneous methanol synthesis and biogas upgrading due to four main advantages: 1. High surface/volume ratio of microchannel can improve heat and mass transfer. 2. The wall-coated microchannel can avoid flow maldistribution and pressure drop can be neglected (isobaric condition). 3. The dual-membrane reactor shows the possibility for simultaneous addition CO_2 into reaction zone and water removal from reaction zone. 4. The yield of methanol can be increased significantly due to shifting the equilibrium to the forward side by using membrane to remove water in reaction zone. From all of the reasons mentioned above, the planar membrane wall-coated microchannel reactor is sufficiently potential for investigation in this research.

จุฬาลงกรณ์มหาวิทยาลัย
CHULALONGKORN UNIVERSITY

CHAPTER 4: SIMULATION AND DESIGN

In this chapter, the method for simulation and design of the planar membrane wall-coated microchannel reactor (MMR) and the triple pipe tubular membrane reactor (TMR) for simultaneous methanol production with biogas grading are explained. For solving the numerical solution, COMSOL Multiphysics version 5.3a was employed by finite element method in this research due to being potential device for representing the fluid flow, heat transfer, chemical and physical phenomena inside several chemical equipment. Furthermore, the Aspen Plus was conducted for thermodynamic model selection owing to potential in comparison the experimental data of vapour liquid equilibrium with various thermodynamic models.

4.1 Model description

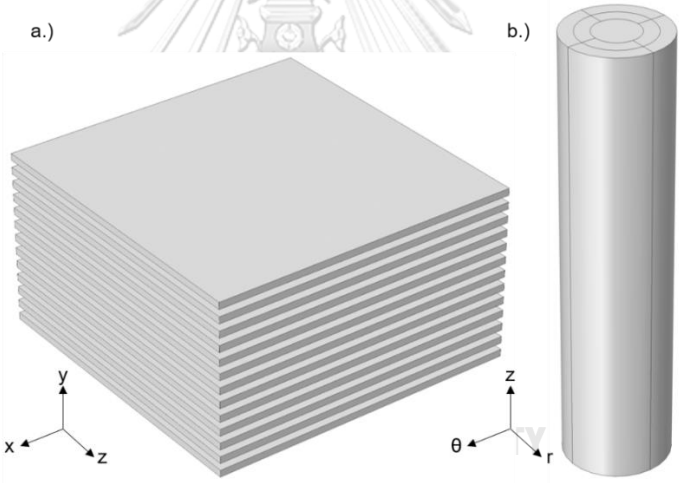

Fig. 4.1: (a) The proposed schematic of the planar membrane wall-coated microchannel reactor (MMR) and (b) the triple pipe tubular membrane reactor (TMR)

The schematic of the planar membrane wall-coated microchannel reactor (MMR) and the triple pipe tubular membrane reactor (TMR) are represented in Fig. 4.1a and Fig. 4.1b, respectively. The channels of both reactors can be separated into three channels; biogas channel (BC), reaction channel (RC) and sweep gas channel (SC). For the dimensions of MMR, all channels are in the same configuration and the dimensions of channel are 45 mm length with 1 mm × 45 mm (cross-sectional area) and are tabulated in detail in Table 4.1. For biogas channel of MMR, cesium carbonate

contained in polyvinyl alcohol-polyacrylic acid copolymer gel layer supported by PTFE porous membrane (Cs_2CO_3- PVA-PAA/PTFE) [43] which is the CO_2 selective membrane is coated on the surface wall of BC in order to separate the CO_2. For the reaction channel of MMR, the thin defect free hydroxy sodalite (H-SOD) membrane is specifically deposited on the channel wall of RC attaching with SC for water permeation. The $CuO/ZnO/Al_2O_3$ catalyst [34] is also coated over the surface wall of RC. On the side attaching SC, the catalyst is applied over the H-SOD membrane. For sweep gas channel of MMR, the nitrogen gas is fed in order to act as the carrier gas. For TMR, the length of this reactor is 150 mm. The radius of three layers from internal channel to external channel are 8, 11.23 and 13.68 mm as shown in table 4.1. The configurations of sweep gas and biogas channel are similar to the MMR. On the other hand, the catalyst in TMR is fixed in the bed of reaction channel with 0.5 bed porosity instead of coating on the surface walls like MMR. However, the H-SOD membrane is applied on the surface wall in RC attaching with SC as well. Moreover, the arrangement of biogas, reaction and sweep gas channel in both MMR and TMR are explained by Fig. 4.2.

Table 4.1: the dimensions of MMR and TMR

Dimensions	**Value (mm)**
Planar membrane microchannel reactor (MMR)	
Width of reactor	1
Length of reactor	45
Depth of reactor	45
Triple pipe tubular membrane reactor (TMR)	
Length of reactor	150
Inner radius	8
Middle radius	11.23
Outer radius	13.68

จุฬาลงกรณ์มหาวิทยาลัย
Chulalongkorn University

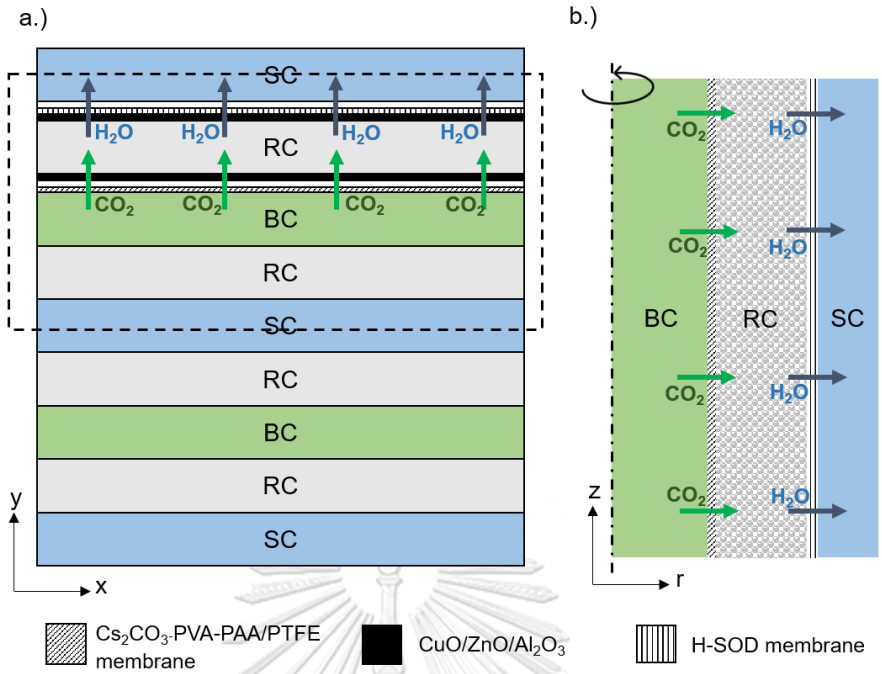

Fig. 4.2: Simulation configuration of a.) MMR and b.) TMR

In Fig. 4.2, the permeation through the membrane of carbon dioxide and water is also expressed. The biogas, hydrogen and nitrogen are fed into the biogas channel, reaction channel and sweep gas channel, respectively. After that, the CO_2 in biogas will be separated through Cs_2CO_3-PVA-PAA/PTFE membrane (CO_2 selective membrane) in order to react with hydrogen in RC to produce the methanol. The water produced in RC will diffuse through the H-SOD membrane (water selective membrane) to the SC in order to shift the reactions inside reaction zone to move forward.

For simulation, the simulation domains of both the planar membrane wall-coated microchannel reactor (MMR) and the triple pipe tubular membrane reactor (TMR) are expressed in Fig. 4.2a and 4.2b, respectively. For MMR, the two dimensional CFD model is used in simulation. The dash line box in Fig. 4.2a represents the repeat unit of this reactor consisting of a one biogas channel, the two reaction channels and sweep gas channels from surface walls attaching RC to the centreline of SC. In contrary, the two dimensional symmetrical CFD model is used in TMR model to represent cylindrical characteristics and domain study of TMR is presented in Fig. 4.2b. Furthermore, both MMR and TMR models are simulated under the same operating condition tabulated in table 4.2 in order to compare the effect of characteristics of

reactor on the reactor performance. For planar microchannel membrane reactor (MMR), the effect of parameters on reactor performance are also investigated. The parameters can be divided into two parts: operating parameters including inlet temperature, pressure, WHSV, mass flow ratio of BC to RC (inlet mass flow of BC) and mass flow ratio of SC:RC (inlet mass flow of SC) as well as design parameters involving channel width and reactor length. The studied ranges of each parameter are expressed in table 4.3

Table 4.2: the operating parameters of MMR and TMR

Parameters	**Value (unit)**
Inlet temperature	508.15 (K)
Pressure in RC, BC and SC	50, 50 and 1 (bar)
WHSV in RC	30 (h^{-1})
Mass flow ratio of BC:RC	0.75 (-)
Mass flow ratio of SC:RC	2 (-)
Density of catalyst	1775 (kg/m^3)
Catalyst porosity (TMR)	0.5 (-)
CO_2/CH_4 ratio in BC	1 (-)
H_2/N_2 ratio in RC	9 (-)

จุฬาลงกรณ์มหาวิทยาลัย
CHULALONGKORN UNIVERSITY

Table 4.3: studied ranges of each parameter for MMR case

Parameters	**Studied range**
Inlet temperature	473.15 – 573.15 (K)
Pressure in RC, BC	20 – 50 (bar)
WHSV in RC	15 – 200 (h^{-1})
Mass flow ratio of BC:RC	0.5 – 6 (-)
Mass flow ratio of SC:RC	0.5 – 6 (-)
Reactor length	30 – 90 (mm)
Reactor width	0.1 – 10 (mm)

4.2 Thermodynamics model selection

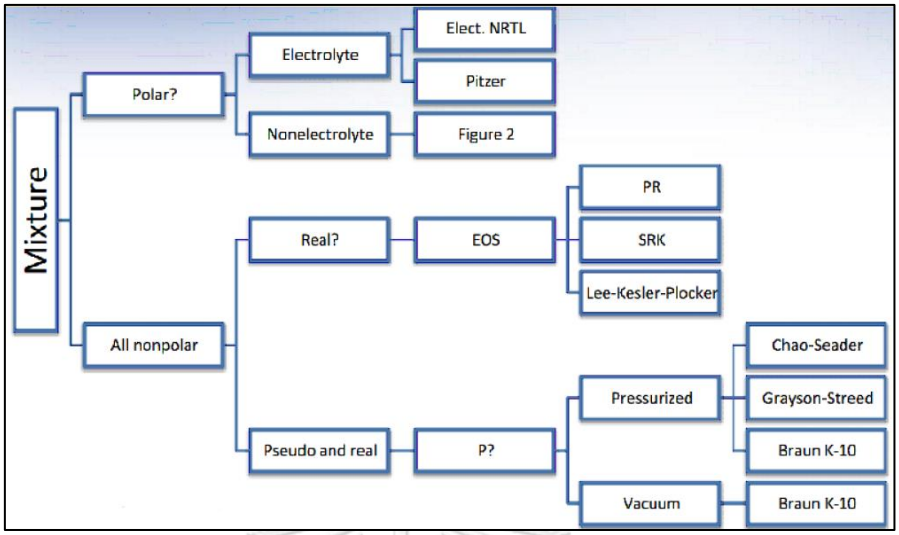

Fig. 4.3: Thermodynamics model selection Guideline of Eric Carlson (Obtained from Ali Kh. Al-matar, Chemical Engineering Department King Fahd University of Petroleum and Minerals, Dhahran, Sauidi Arabia)

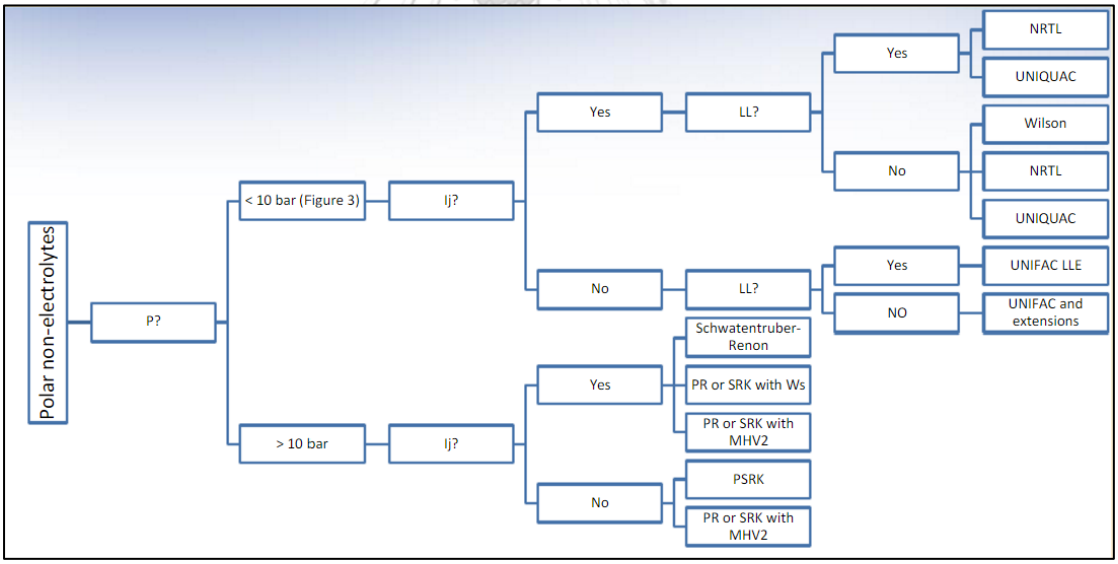

Fig. 4.4: Thermodynamics model selection Guideline: Polar non-electrolyte of Eric Carlson (Obtained from Ali Kh. Al-matar, Chemical Engineering Department King Fahd University of Petroleum and Minerals, Dhahran, Sauidi Arabia)

In order to predict the hydrocarbon gas behaviour in severe condition of methanol synthesis (200-300 ºC of temperature and high pressure approximately 50 bar), and unsuitability of the ideal gas law in this condition, the thermodynamics model selection guideline of Eric Carlson is considered as shown in Fig. 4.3 and 4.4. Due to

the methanol and water in our system being polar and non-electrolyte component, the selection guideline for polar non-electrolyte in Fig. 4.4 is also discussed from route in Fig. 4.3. From route in Fig. 4.4, it found that the equation of state (EOS) approaches such as Soave Redlich Kwong (SRK) model and Peng Robinson (PR) model can be the proper candidates for applying with this investigation instead of ideal gas law due to high pressure (>10 bar) system. Furthermore, consistency of EOS near the critical region can handle the mixture at high temperatures and high pressure. Therefore, the Soave Redlich Kwong (SRK) model is applied in this research.

4.3 Model assumptions and the equations

4.3.1 Model assumptions:

In this study, the transport phenomena in z direction of MMR was neglected due to no significant changes in this direction as same as the transport phenomena in θ direction of TMR. Therefore, the 2D model and the 2D symmetrical model were conducted for MMR and TMR, respectively. The flow regime of each channel was assumed to be laminar flow and steady state condition. The thickness of catalyst and membrane layers which applied from M. Tadbir and M.H. Akbari [55] and Rohde et al. [38] were neglected due to extremely thin at 100 and 2 μm, respectively. Hence, the mass and heat transfers in these areas were considered to be ideal. The Soave Redlich Kwong (SRK) thermodynamic model was used for predicting mixture fluid properties: mixture density, heat capacity, thermal conductivity and enthalpy flow. Reactions occurred on the surface of catalyst in RC. Finally, the operation was adiabatic (no heat loss out of reactors). All mentioned above can be summarized below:

- Steady state condition
- Laminar flow
- The transport phenomena in z direction is neglected in MMR case
- The transport phenomena in θ direction is neglected in TMR case
- The membrane and catalyst layers are neglected
- No heat loss out of these reactors

จุฬาลงกรณ์มหาวิทยาลัย
CHULALONGKORN UNIVERSITY

- Soave Redlich Kwong (SRK) thermodynamic model is applied
- The reactions occur at surface walls of RC in MMR case

4.3.2 Governing equations

The equation for conservation of mass or continuity equation at steady state condition is shown in Eq. 4.1

$$\nabla \cdot \left(\rho \vec{u} \right) = 0 \tag{4.1}$$

where ρ is density of gas mixture (scalar) and u is velocity of fluid (vector). The density of gas mixture can be calculated from Soave Redlich Kwong (SRK) model. For steady state condition, compressible fluid and laminar flow in fluid phase, the equation of conservation of momentum or Newton's second law is simplified as follows:

$$\rho\left(\vec{u}\cdot\nabla\right)\vec{u} = \nabla\cdot\left(-p\overline{\overline{\delta}} + \mu\left(\nabla\vec{u} + \left(\nabla\vec{u}\right)^{T}\right) - \frac{2}{3}\mu\left(\nabla\cdot\vec{u}\right)\overline{\overline{\delta}}\right) \tag{4.2}$$

where p is the static pressure, μ (the molecular viscosity) which can be determined based on molar average of species in the mixture is obtained from Data of Perry's Chemical Engineers' Handbook [27]. Moreover, δ is the tensor unit. The steady state equation of conservation law of energy for fluid flow can be written in Eq. 4.3

$$d_z \rho C_p \vec{u}\cdot\nabla T = \nabla\cdot\left(d_z k \nabla T\right) + d_z Q + Q_{vd} + Q_p + Q_{oop} \tag{4.3}$$

จุฬาลงกรณ์มหาวิทยาลัย
Chulalongkorn University

where $\hat{C}_p$ and d_z are the specific heat capacity and the thickness of channel, respectively. k is thermal conductivity of the mixture, Q is heat source term due to heat of reactions which occur only the wall surfaces in MMR case. Q_{vd}, Q_p and Q_{oop} are heat source from viscous dissipation, pressure work and out of plane, respectively. Therefore, Q_{vd}, Q_p and Q_{oop} can be neglected owing to heat source occurring only heat of reaction. The equation of conservation law of chemical species under steady state condition for this study can be written in Eq. 4.4

$$\rho\left(\vec{u}\cdot\nabla\right)\omega_i = -\nabla\cdot\vec{J_i} + R_i \tag{4.4}$$

where ω_i is the local mass fraction of each species. J_i and R_i are the mass diffusion flux and the net of rate of reaction on wall surfaces, respectively. The method for calculation of the diffusion flux (J_i) is explained in the chapter 2 which can be calculated from Eq. 2.25 and so on.

4.3.3 Auxiliary equations

In this study, the kinetic models of methanol synthesis were applied from Vandal & Chakib Bouallou [26] rearranged from Vanden Bussche and Froment [34]. The reactions consist of three main equilibrium reactions: CO hydrogenation (R1), CO_2 hydrogenation (R2) and reverse water gas shift (R3). These reactions were expressed as follows:

$CO + 2H_2 \leftrightarrow CH_3OH$ (2.1)

$CO_2 + 3H_2 \leftrightarrow CH_3OH + H_2O$ (2.2)

$CO_2 + H_2 \leftrightarrow CO + H_2O$ (2.3)

The corresponding reaction rates for reactions (2.2, 2.3) could be written as shown in chapter 2 and below.

Methanol synthesis:

$$r_{CH_3OH} = \frac{k_1 P_{CO_2} P_{H_2} - k_6 P_{H_2O} P_{CH_3OH} P_{H_2}^{-2}}{\left(1 + k_2 P_{H_2O} P_{H_2}^{-1} + k_3 P_{H_2}^{0.5} + k_4 P_{H_2O}\right)^3} \quad (2.13)$$

Reverse water-gas shift:

$$r_{RWGS} = \frac{k_5 P_{CO_2} - k_7 P_{H_2O} P_{CO} P_{H_2}^{-1}}{1 + k_2 P_{H_2O} P_{H_2}^{-1} + k_3 P_{H_2}^{0.5} + k_4 P_{H_2O}} \quad (2.14)$$

$$lnk_i = A_i + \frac{B_i}{T} \quad (2.15)$$

The permeation flux (N_i) of both water and CO_2 permeation as a function of permeability coefficient (ξ_i) and difference of partial pressure of species i can be calculated from Eq. 4.5

$$N_i = \xi_i \Delta p_i \quad (4.5)$$

จุฬาลงกรณ์มหาวิทยาลัย
Chulalongkorn University

In order to operate in temperature range of 200 – 300 °C, a thin defect hydroxyl sodalite (H-SOD) membrane produced from hydrothermal synthesis on a-Al_2O_3 supports could be able to water permeance (ξ_{H_2O}) in ranging $1x10^{-6} > \xi_{H_2O} > 1x10^{-7}$ mol m^{-2} s^{-1} Pa^{-1} [38]. For CO_2 selective membrane, Osamu et al. [43] developed CO_2-facilitated transport membrane or cesium carbonate contained in polyvinyl alcohol-polyacrylic acid copolymer gel layer supported by PTFE porous membrane (Cs_2CO_3-PVA-PAA/PTFE) for CO_2 permeation. This membrane which was able to CO_2 permeability of about 1×10^{-4} mol m^{-2} s^{-1} kPa^{-1}.

Moreover, the performance indicators for this investigation can be divided into three variables; the yield of methanol and the factor of CO_2 and water permeation (FP) which are expressed in Eq. 4.6, 4.7 and 4.8, respectively.

$$yield_{methanol} = \frac{F_{MeOH,RC}}{F_{CO_2,BC,inlet}} \times 100\% \quad (4.6)$$

$$FP_{CO_2} = \frac{F_{CO_2,BC,inlet} - F_{CO_2,BC,outlet}}{F_{CO_2,BC,inlet}} \times 100\% \quad (4.7)$$

$$FP_{H_2O} = \frac{F_{H_2O,SC,outlet}}{F_{H_2O,RC,outlet} + F_{H_2O,SC,outlet}} \times 100\% \quad (4.8)$$

จุฬาลงกรณ์มหาวิทยาลัย
Chulalongkorn University

4.4 Mesh geometry & boundary condition

As Fig. 4.6a and Fig. 4.6b, free triangular meshes were generated at 1.437×10^5 and 2.07×10^5 domain elements which were extremely finer at surface wall of each channel for MMR and TMR, respectively. The maximum element size of free triangular meshes was fixed at 0.03 mm. After setting mesh geometry, in order to ensure these meshes, the mesh analysis is also investigated. The free triangular meshes are varied at 2,142, 9,561, 27,496, 37,873, 74,479, 143,735 and 177,801 domain elements for MMR case under base case condition in table 4.2. In Fig. 4.7, the results perform that the yield of methanol is almost constant at 1.437×10^5 domain elements. Therefore, this point is used as mesh geometry for this investigation.

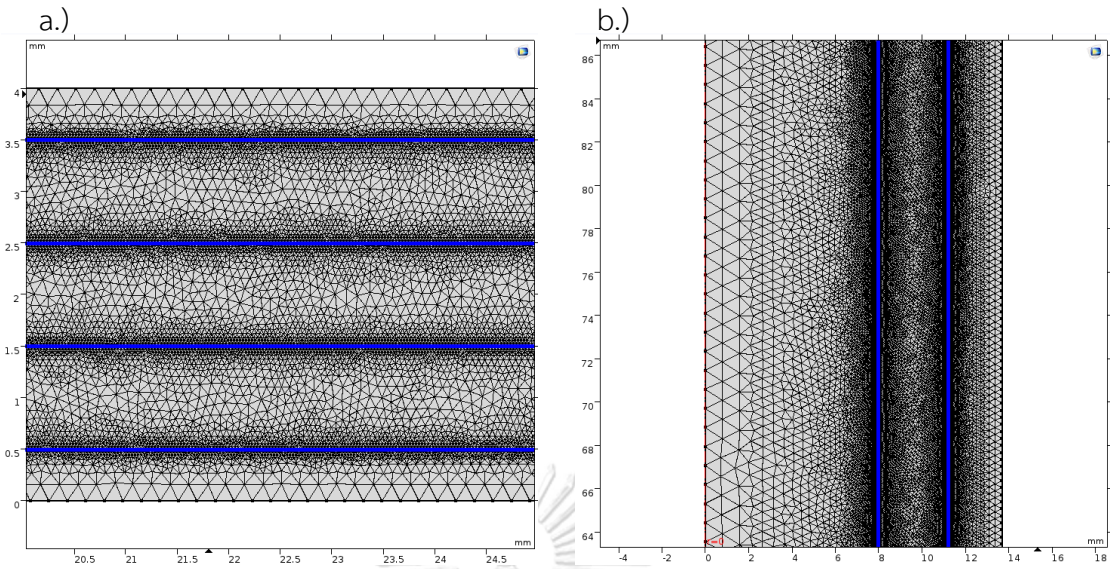

Fig. 4.5: the mesh geometry of a.) MMR and b.) TMR

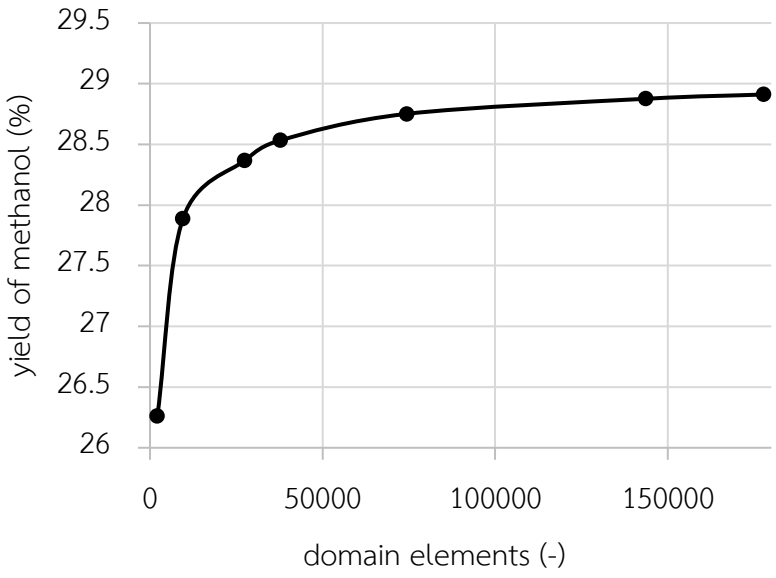

Fig. 4.6: the yield of methanol at different domain elements under based case.

For boundary condition as shown in Table 4.4, the inlet velocity, mass fraction and temperature were fixed at inlet of BC, RC and SC. On the other hand, the pressure of system and zero flux of mass fraction and temperature were set at the outlet. The velocity at wall surfaces of each channel was specified as functions of permeation flux and density. The CO_2 permeation flux was defined at the wall surfaces between RC and BC, whereas water permeation flux was indicated at the wall surfaces between RC

and SC. For surfaces inside RC, the net rate of reactions and heat source term from all reactions were specified. The symmetry condition was applied at the center line of SC or dashed lines in Fig. 4.2a for MMR. On the other hand, the center line of BC in Fig. 4.2b was symmetry condition.

Table 4.4: the boundary conditions

Boundary	Conditions
inlet	Velocity: $\vec{\boldsymbol{u}} = \vec{\boldsymbol{u}}_{\boldsymbol{0}}$ Composition: $\boldsymbol{\omega_i} = \boldsymbol{\omega_{i,0}}$ Temperature: $\boldsymbol{T} = \boldsymbol{T_0}$
outlet	Zero flux: $\frac{\partial \boldsymbol{T}}{\partial \boldsymbol{z}} = \frac{\partial \boldsymbol{\omega_i}}{\partial \boldsymbol{z}} = \boldsymbol{0}$ Pressure: $\boldsymbol{P} = \boldsymbol{P_0}$
surface wall of RC	Velocity: $\vec{\boldsymbol{u}}_{\boldsymbol{s}} = \frac{\boldsymbol{1}}{\boldsymbol{\rho}} \sum \boldsymbol{N_i}$ Mass source term: $\boldsymbol{R_i} = \sum_{\boldsymbol{j}} (\boldsymbol{r_j M_{w,i}})_{\boldsymbol{i}}$/ $\boldsymbol{N_{CO_2}} = \boldsymbol{N_{CO_2}}$ (attached BC)/ $\boldsymbol{N_{H_2O}} = -\boldsymbol{N_{H_2O}}$ (attached SC) Heat source term: $\boldsymbol{Q} = \boldsymbol{Q_R}$
surface wall of BC	Velocity: $\vec{\boldsymbol{u}}_{\boldsymbol{s}} = \frac{\boldsymbol{1}}{\boldsymbol{\rho}} \sum \boldsymbol{N_i}$ Mass source term: $\boldsymbol{N_{CO_2}} = -\boldsymbol{N_{CO_2}}$ Symmetry: $\frac{\partial \vec{\boldsymbol{u}}}{\partial \boldsymbol{z}} = \frac{\partial \boldsymbol{T}}{\partial \boldsymbol{z}} = \frac{\partial \boldsymbol{\omega_i}}{\partial \boldsymbol{z}} = \boldsymbol{0}$ (center line, TMR)
surface wall of SC	Velocity: $\vec{\boldsymbol{u}}_{\boldsymbol{s}} = \frac{\boldsymbol{1}}{\boldsymbol{\rho}} \sum \boldsymbol{N_i}$ (attached RC) $\vec{\boldsymbol{u}} = \boldsymbol{0}$ (outer surface, TMR) Mass source term: $\boldsymbol{N_{H_2O}} = \boldsymbol{N_{H_2O}}$ (attached RC) Symmetry: $\frac{\partial \vec{\boldsymbol{u}}}{\partial \boldsymbol{z}} = \frac{\partial \boldsymbol{T}}{\partial \boldsymbol{z}} = \frac{\partial \boldsymbol{\omega_i}}{\partial \boldsymbol{z}} = \boldsymbol{0}$ (center line, MMR)

CHAPTER 5: RESULTS AND DISCUSSION

In this chapter, the simulation results of reactors for simultaneous methanol production with biogas upgrading are provided. Furthermore, the proper operating condition and dimensions of a suitable reactor are determined. This chapter is divided into four parts; 1) The model validation, 2) The comparison of reactor performance of planar membrane microchannel reactor (MMR) and triple pipe tubular membrane reactor (TMR), 3) The operating parameters study of MMR and 4) The design parameters study of MMR.

5.1 The model validation

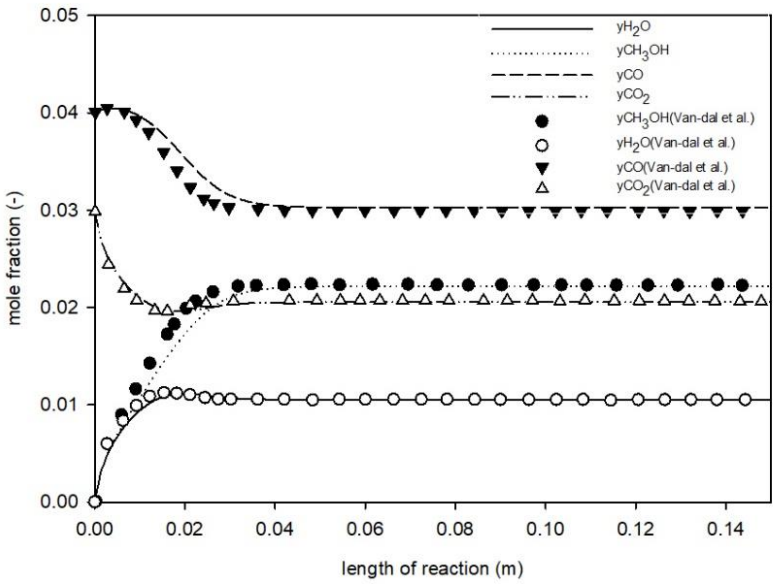

Fig. 5.1: The mole fraction profile comparison between this study and Van-dal et al. under condition in Appendix B.

The LHHW (Langmuir Hinshelwood Hougen Watson) kinetic model applied from Van-dal and Chakib Bouallou [26] was implemented on COMSOL Multiphysics 5.3a. The characteristics of reactor and operating conditions for simulation reported in Van-dal and Chakib Bouallou [26] are summarized in Tables A1-A3 in Appendix B. The adiabatic tubular stainless steel reactor model for methanol synthesis was simulated. In order to validate the CFD code, the mole fraction results from Van-dal and Chakib

Bouallou [26] were compared with those simulated using CFD model in the same reactor configuration. From results in Fig. 5.1, the computed curves of CH_3OH, H_2O, CO and CO_2 mole fractions could well resemble those of Van-dal and Chakib Bouallou [26]. From the results and the mass balance as well as atomic balance shown in Appendix C, the model accuracy was assured.

5.2 The comparison of reactor performance of TMR and MMR

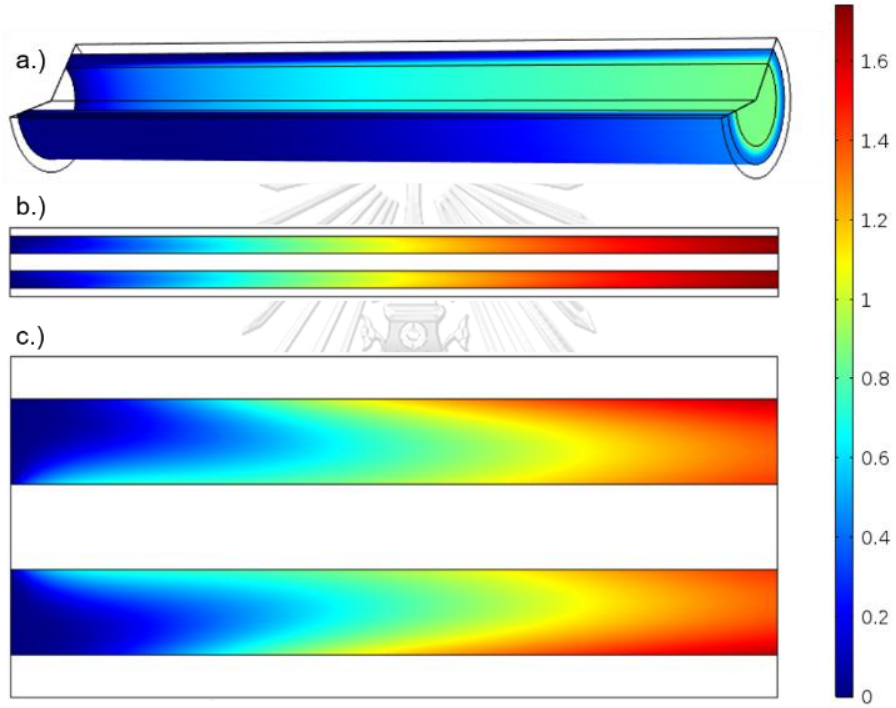

Fig. 5.2: The methanol mole fraction profile (in percentage) in reaction channel (RC) under based case study for a) TMR, b) MMR (width 1 mm) and c) MR (width 5 mm)

For this section, the tubular membrane reactor (TMR) and membrane wall-coated microchannel reactor (MMR) were simulated under base case tabulated in Table 4.2 using governing equations mentioned in the previous chapter (chapter 4) in order to compare their effect of reactor characteristics on reactor performance. For Figs. 5.2-5.4, the blue to red colour represents the low to high mole fraction area of each component. The methanol mole fraction profiles of both in RC are presented in Figs. 5.2a and 5.2b. For TMR, the highly cumulative methanol mole fraction area can be observed at surface wall of RC attaching BC due to poor radial dispersion affecting

to reaction area between CO_2 and H_2. On the other hand, the radial diffusion shows slight effect in the reaction channel in MMR due to high mass transfer from high surface to volume ratio [12]. From the computed results, the mole fractions of methanol at outlet are 0.017 and 0.006 for MMR and TMR, respectively. It can be summarized that the MMR provides the higher methanol.

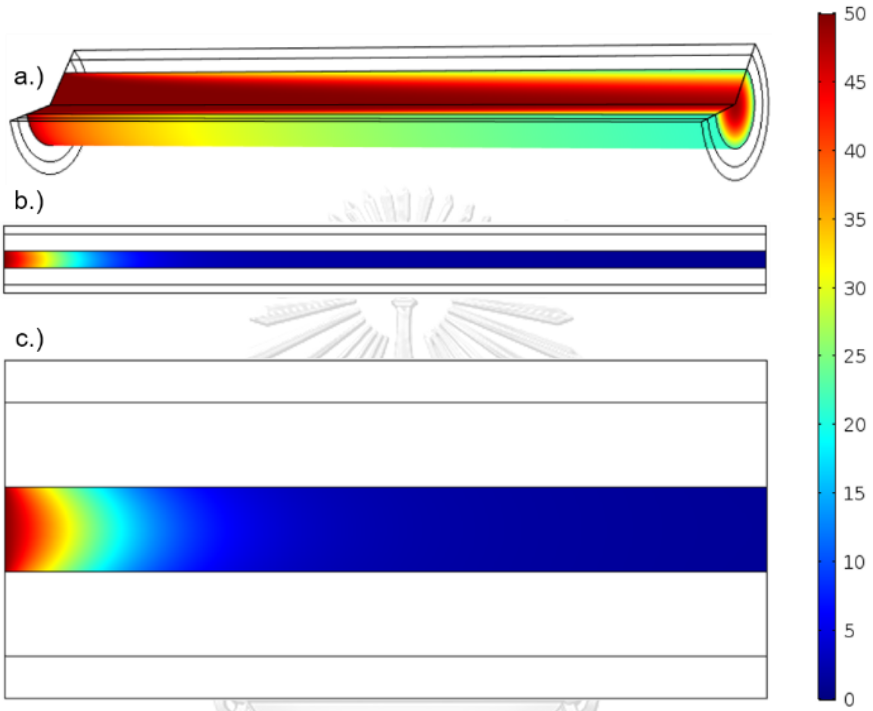

Fig. 5.3: The carbon dioxide mole fraction profile (in percentage) in biogas channel (BC) under based case study for a) TMR, b) MMR (width 1 mm) and c) MR (width 5 mm)

CHULALONGKORN UNIVERSITY

For the substance diffusing through the membrane, both CO_2 and H_2O mole fractions are shown in Figs. 5.3a, 5.3b, 5.4a and 5.4b, respectively. The accumulation of CO_2 appears in the center line of BC in TMR case (Fig. 5.3a) which provides 0.3532 of CO_2 mole fraction at outlet. On the contrary, CO_2 can smoothly transfer and does not have accumulative area in MMR case (Fig. 5.3b). Therefore, the CO_2 mole fraction at outlet of MMR can be reduced to 0.0087. As shown in Fig. 5.4a, water occurred from reaction (2.1-2.3) in RC is accumulated at surface area attaching BC because the water near SC side is selectively permeated via H-SOD membrane as well as the radial dispersion has also a strong impact on water accumulation. In contrast, the water near BC side in MMR case (Fig. 5.4b) is slightly accumulated when compared with TMR. For

temperature profile in TMR and MMR, these results are expressed in Figs. 5.5a and 5.5b, respectively. When considering the temperature profile in the axial direction, the temperature of MMR is more increased than TMR owing to high reaction rate of CO_2 hydrogenation which is an exothermic reaction. As shown in Fig. 5.6, the heat transfer to the other phases of TMR and MMR are expressed. It can be separated into three parts following the phases inside the reactor (BC, RC and SC). For TMR, The heat source of this reactor occurs from heat of reaction from the fixed bed inside RC especially area attaching BC. On the other hand, heat source of MMR is obtained from heat of reaction at the surface walls of RC. The heat of reaction inside RC of TMR transfers to biogas channel and sweep gas channel as same as the transference in MMR. From the results in Fig. 5.6, it was found that the heat transfer to the other phases (y direction) of MMR is more effective than heat transfer of TMR (r direction) because of high surface to volume ratio of MMR affecting to higher both heat and mass transfer. Therefore, the temperature profile of MMR is more uniform than TMR.

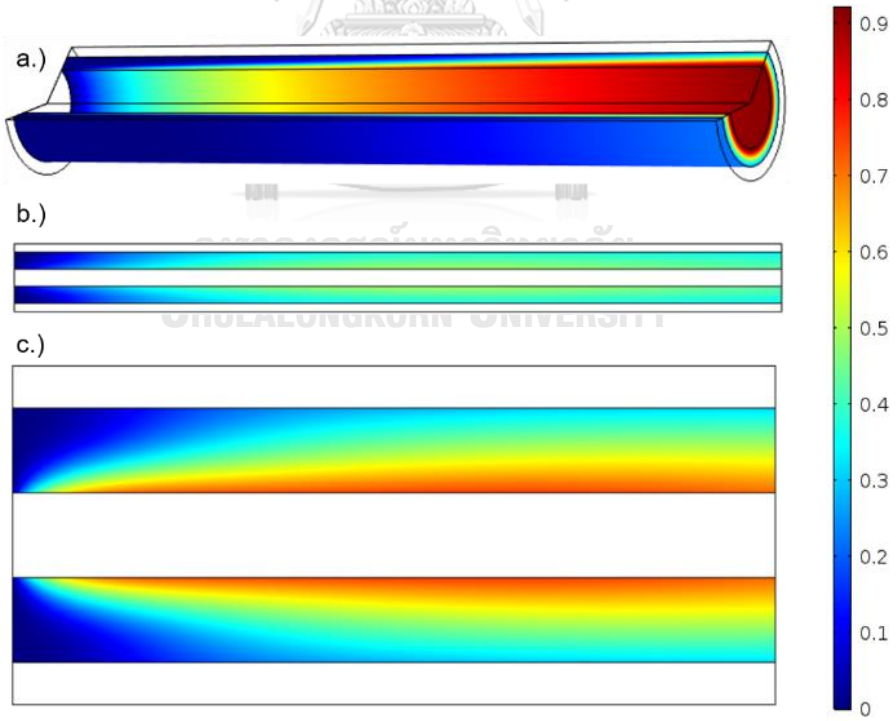

Fig. 5.4: The water mole fraction profile (in percentage) in reaction channel (RC) under based case study for a) TMR, b) MMR (width 1 mm) and c) MR (width 5 mm)

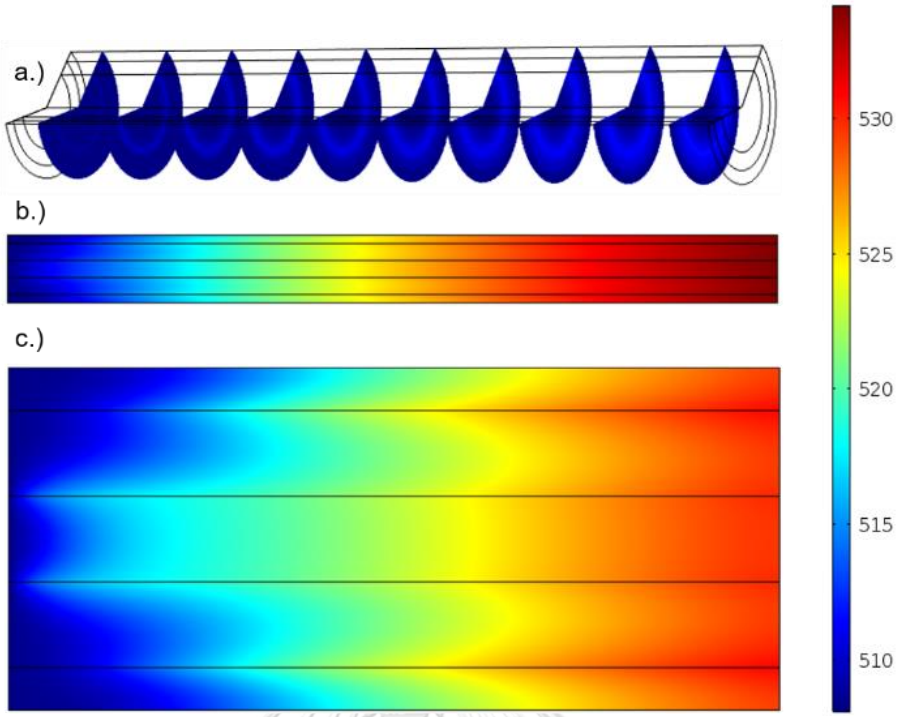

Fig. 5.5: The temperature profile (in Kelvin, K) under base case study for a) TMR, b) MMR (width 1 mm) and c) MR (width 5 mm)

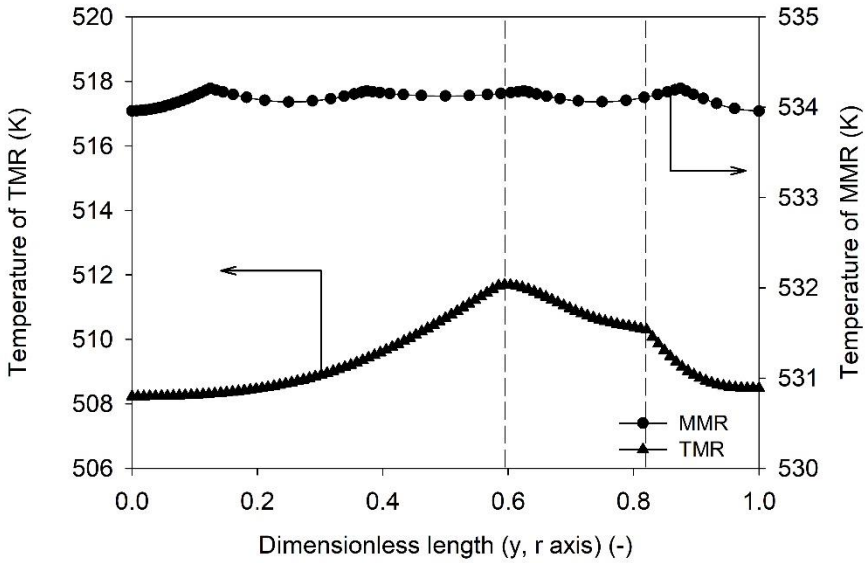

Fig. 5.6: The temperature profiles at outlet in y and r direction of MMR and TMR, respectively.

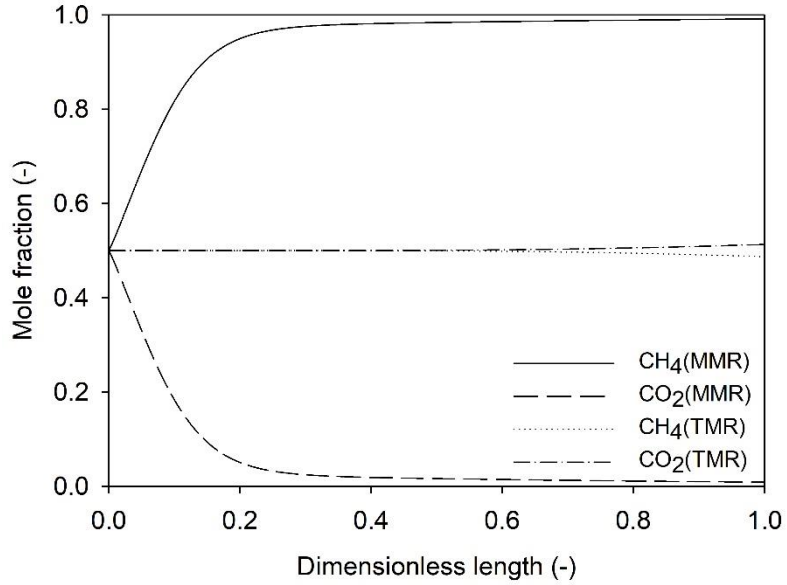

Fig. 5.7: The mole fraction profiles at the centerline of the biogas channel (BC) under base case

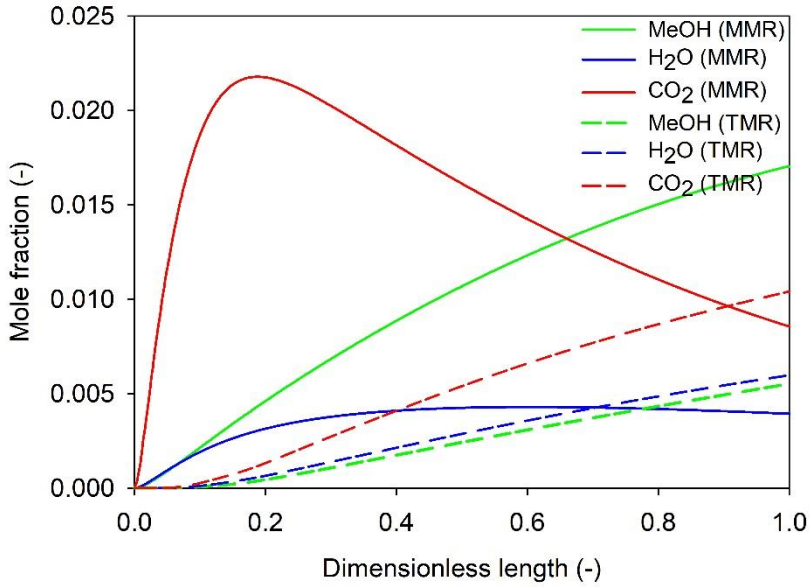

Fig. 5.8: The mole fraction profiles at the centerline of the reaction channel (RC) under base case

In Figs. 5.7 and 5.8, the mole fractions along the centerline of the biogas channel and the reaction channel are performed, respectively. According to Figs. 5.2-

5.4, the average CO_2 mole fraction at outlet of MMR can be reduced to 0.0087 and CH_4 mole fraction at outlet of MMR can be improved to 0.9913, whereas the accumulation of CO_2 at the centreline of biogas channel in TMR leads to suppression of CO_2 permeation out of BC. The average CO_2 and CH_4 mole fraction at outlet of TMR are 0.3995 and 0.6005, respectively. In Fig. 5.8, the effect of permeation of CO_2 and water on mole fraction profile can be observed. In MMR, the CO_2 mole fraction curve can be divided into two sections; addition of CO_2 from BC into RC, the reduction of CO_2 by the reactions (2.2-2.3). In contrast, the CO_2 mole fraction curve of TMR is in the period of addition of CO_2 from BC. When comparing water mole fraction of MMR with TMR, it was found that the mole fraction of water in MMR is less than TMR in spite of providing more methanol owing to no accumulation of water inside the reaction zone.

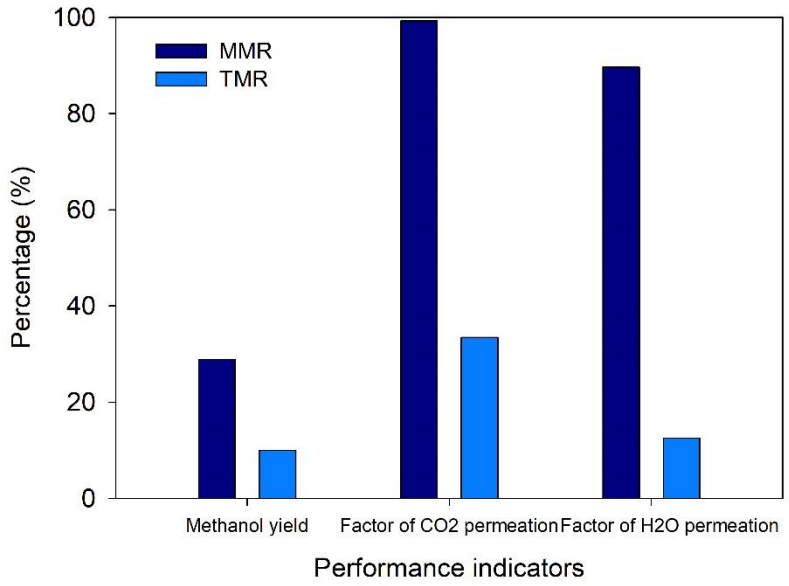

Fig. 5.9: Comparison of performance indicators between MMR and TMR under based case study

From summary diagram in Fig.5.9, the performance of reactor can be signified by three performance indicators; yield of methanol, factor of CO_2 and water permeation (FP). The methanol yield, FP_{CO2} and FP_{H2O} of MMR are 28.88, 99.24 and 89.64%, respectively, whereas those indicators of TMR are 9.96, 33.45 and 12.48, respectively. From these results, it can be summarized that MMR provides higher in

both methanol production rate and purity of methane in upgraded biogas than TMR because of the characteristics of reactor. It strongly affects the performance of reactor due to limitation of mass and heat transfer. Therefore, the designed reactors should avoid limitations of mass and heat transfer. Furthermore, the operating parameters and design parameters of MMR were studied by sensitivity analysis in order to find suitable design and proper condition in the next sections 5.3-5.4.

5.3 The operating parameters study

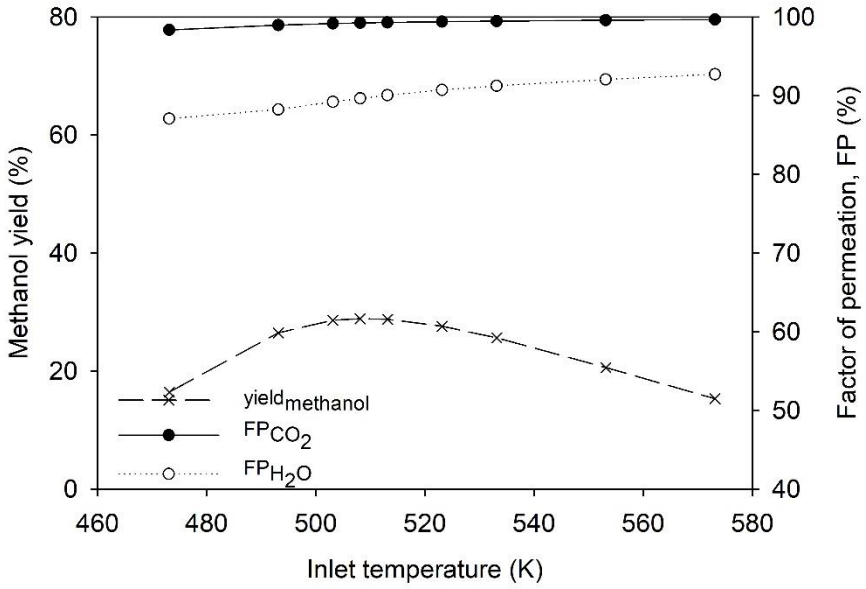

Fig. 5.10: Effect of temperature on methanol yield, and factor of CO_2 and water permeation (FP) at outlet under condition, P = 50 bar WHSV = 30 h^{-1} BC:RC ratio= 0.75 and SC:RC ratio = 2

In determining the effect of operating parameters, the inlet temperature, pressure, WHSV of RC, mass flow ratio of BC:RC and SC:RC were investigated in this study. In Fig. 5.10, the effect of inlet temperature on performance indicators at predetermined range (473.15-573.15 K) was investigated under base case study. Initially, increasing temperature in range (473.15-508.15 K) increases yield of methanol because of enhancement of rate of CO_2 hydrogenation reaction (Eq. 2.13). The inlet temperature directly affects rate of reaction due to kinetic control. Furthermore, it

indirectly affects CO_2 and water permeation flux because the higher rate of reaction can promote the driving force of CO_2 and water from reduction of CO_2 and increment of water in RC. Hence, the differences of partial pressure of CO_2 and water are improved according to Eq. 4.5. However, the excessive increment of inlet temperature can lead to the thermodynamic equilibrium of endothermic reaction. Consequently, the reverse water gas shift reaction (2.3) which is endothermic can be more promoted than CO_2 hydrogenation in range (508.15-573.15 K). Therefore, the yield of methanol in this range is reduced, nevertheless the CO_2 and water permeation flux are improved due to CO_2 still used by reverse water gas shift (2.3) and water occurred from reverse water gas shift reaction (2.3) as well. Hence, the FPs of CO_2 and water are still enhanced which can indicate to purity of methane in BC. Moreover, reduction of water in RC can reduce the complex of separation units for methanol production. From this results, the inlet temperature about 508.15 K which provides 28.88, 99.24 and 89.64% of methanol yield, FPs of CO_2 and water, respectively, is considered to be the proper parameter.

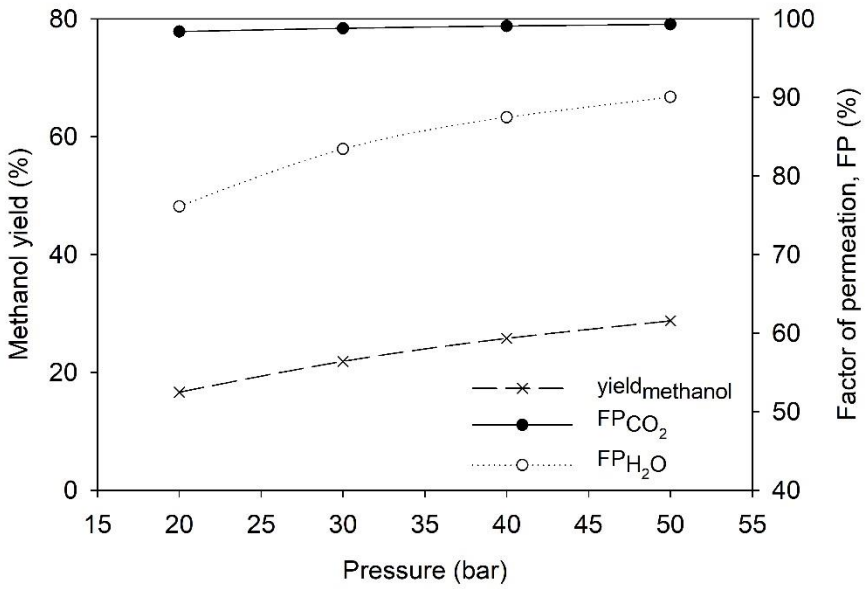

Fig. 5.11: Effect of pressure on methanol yield, and factor of CO_2 and water permeation (FP) at outlet under condition, T = 513.15 K WHSV = 30 h^{-1} BC:RC ratio = 0.75 and SC:RC ratio = 2

In Fig. 5.11, the effect of pressure on methanol yield, FP_{CO2} and FP_{H2O} at 20, 30, 40 and 50 bar was studied. From this graph, increasing pressure causes the enhancement of methanol yield, FP_{CO2} and FP_{H2O} Because of, the increased gaseous pressure leads to CO_2 hydrogenation (2.2) to move forward according to Le chatelier's principle. Moreover, the increasing pressure directly affects to water permeation flux due to the difference of water partial pressure between RC and SC improved. From this result, it can be summarized that high pressure at 50 bar which provides 28.75, 99.30 and 90.04% of methanol yield, FPs of CO_2 and water, respectively, is suitable with our system. However, increasing pressure leads to high energy consumption and more complicated system.

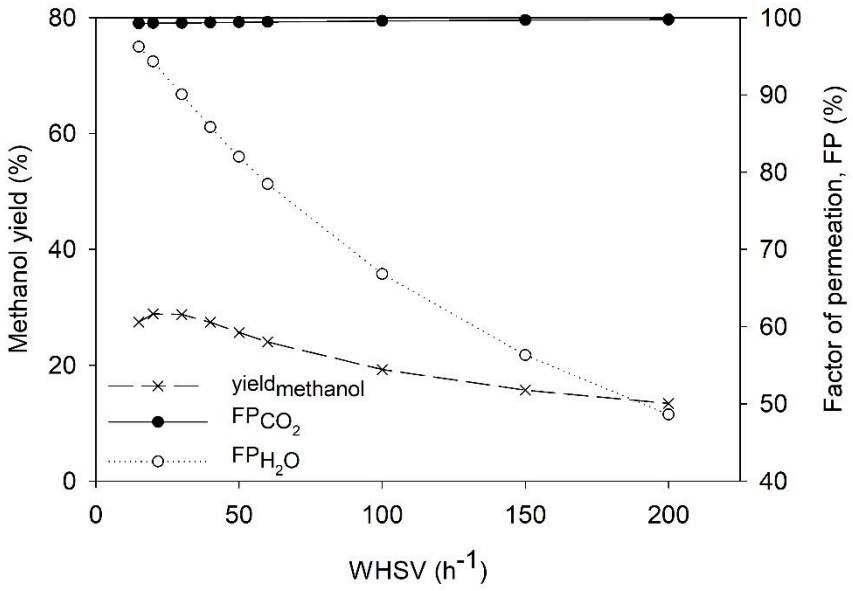

Fig. 5.12: Effect of WHSV on methanol yield, and factor of CO_2 and water permeation (FP) at outlet under condition, T = 513.15 K P = 50 bar m_b, m_p = 4.41×10^{-6} and 1.18×10^{-5} kg/s, respectively

The effect of WHSV on methanol yield, FP_{CO2} and FP_{H2O} in predetermined range (15-200 h^{-1}) at mass flow rate of BC and SC = 4.41×10^{-6} and 1.18×10^{-5} kg/s and the same catalyst loading is expressed in Fig. 5.12. From this graph, the increasing WHSV significantly depreciates permeation factor of water since the increment of gas flow rate in RC can improve convection term. As consequence, the CO_2 and water inside

RC are diluted and the water permeation flux is decreased because of the difference of water partial pressure weakened. On the other hand, the CO_2 permeation flux is improved from the enhancement of driving force. Moreover, increasing WHSV can makes contact time of reactants in RC reduce. As a result, both yield of methanol and water flux are significantly decreased. From this result, the maximum value of yield of methanol (28.84%) is depicted at WHSV 20 h^{-1}. Hence, this value can be considered as a suitable WHSV which provides 99.29 and 94.31% of FPs of CO_2 and water, respectively.

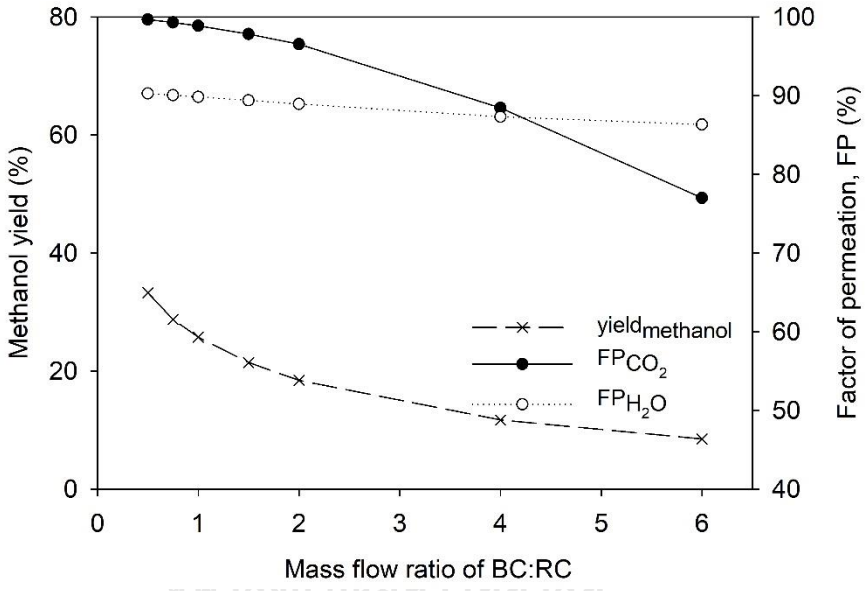

Fig. 5.13: Effect of mass flow ratio of BC to RC on methanol yield, and factor of CO_2 and water permeation (FP) at outlet under condition, T = 513.15 K P = 50 bar WHSV = 30 h^{-1} and SC:RC ratio = 2

As shown in Fig. 5.13, the effect of mass flow ratio of BC:RC in range of 0.5-6 on methanol yield and factor of CO_2 and water permeation was investigated. The mass flow rate of RC was fixed at WHSV 30 h^{-1}. As similar to the effect of WHSV, the enhancement of gas flow rate of biogas in BC strongly reduces residence time of reactants in the reactor. Therefore, the permeation factor of CO_2 and methanol yield are directly suppressed. Furthermore, the reduction of reaction rate (Eqs.2.13-2.14) indirectly leads to the abatement of water permeation flux due to low by-product

from reaction (2.1-2.3). Accordingly, it can be concluded that the low mass flow ratio of BC:RC at 0.5 is appropriate for our system which offers 33.28, 99.68, 90.28% of methanol yield, FPs of CO_2 and water, respectively.

In Fig. 5.14, the effect of mass flow ratio of SC to RC was studied in the same range of BC to RC ratio (0.5-6). From this result, it was found that the gas flow rate of sweep gas (N_2) in SC slightly leads to yield of methanol and CO_2 permeation factor. However, the increasing flow rate of SC still results in increment of the water permeation flux in initially by reason of improvement of driving force of water flux from increasing convection term of water in SC which makes it dilute. From this FP_{H2O} curve, the mass flow ratio of SC to RC at 4 is sufficient value for our system which provides 29.97, 99.32, and 91.93% of methanol yield, FPs of CO_2 and water, respectively.

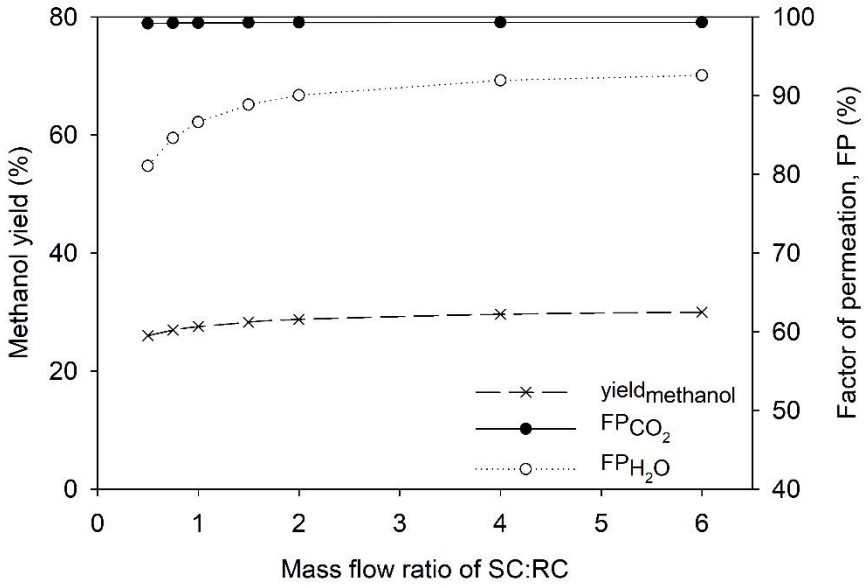

Fig. 5.14: Effect of mass flow ratio of BC to RC on methanol yield, and factor of CO_2 and water permeation (FP) at under condition, T = 513.15 K P = 50 bar WHSV = 30 h^{-1} and BC:RC ratio = 0.75

5.4 The design parameters study

To discuss the effects of design parameters, the length and width of MMR were studied in this investigation at 45 mm of depth of reactor and under base case study

tabulated in Table 4.2. In Fig. 5.15, the effect of length of reactor at 0.72 g of wall-coated catalyst was studied. Increasing length leads to higher contact surface area of both membrane and catalyst as well as contact time of reactants. Hence, the methanol yield and factor of CO_2 and water permeation are enhanced. As shown in Fig. 5.15, it can be summarized that the methanol yield, FPs of CO_2 and water are almost constant at reactor length of 75 mm which provide 31.32, 99.39 and 92.53%, respectively. Hence, this reactor length is appropriate for our system.

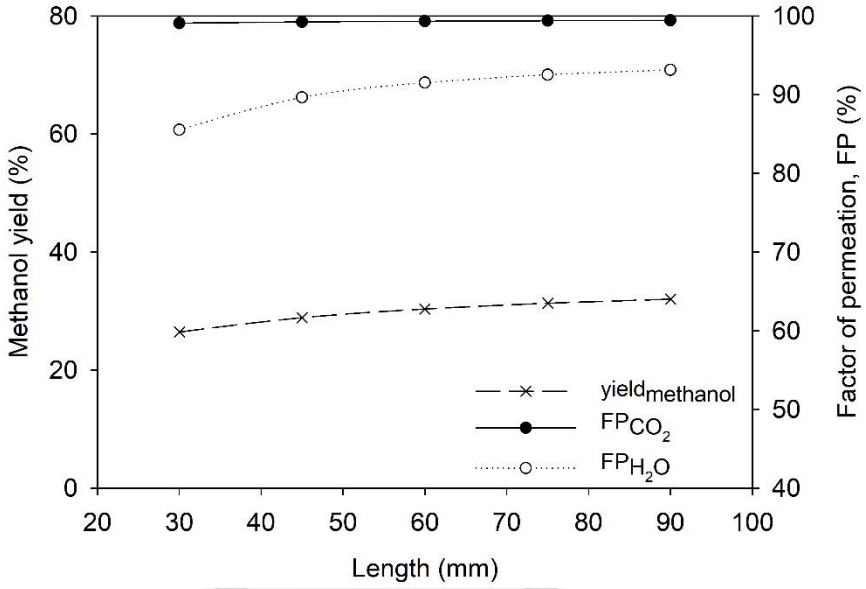

Fig. 5.15: Effect of length of reactor on methanol yield, and factor of CO_2 and water permeation (FP) at outlet under condition, T = 508.15 K P = 50 bar WHSV = 30 h^{-1} BC:RC ratio = 0.75 and SC:RC ratio = 2

จุฬาลงกรณ์มหาวิทยาลัย
Chulalongkorn University

To investigate the effect of reactor width, the length and depth of reactor are fixed at 45 mm under base case study shown in Table 4.2. The mole fraction profiles of methanol, CO_2, water and temperature profile of planar membrane wall-coated reactor at 5 mm of reactor width are depicted in Figs. 5.2c, 5.3c, 5.4c and 5.5c, respectively, in order to compare with micro-scale at 1 mm of width. From the methanol mole fraction profile in Fig. 5.2c, it was found that the area near SC can produce more methanol than the side attaching BC resulting from poor dispersion in y direction and the high permeation of water through membrane at area attaching SC.

This water permeation can overcome restriction of thermodynamic equilibrium of methanol synthesis [25] and move the reactions (R2-R3) forward. From CO_2 mole fraction profile in Fig. 5.3c, it can be observed that the increasing reactor width does not significantly change CO_2 permeation flux in BC. However, the accumulation of water at the area attaching with BC can be seen as shown by water mole fraction profile in Fig. 5.4c owing to poor dispersion in y-direction as same as methanol profile in Fig. 5.2c. When comparing the temperature profile of 5 mm reactor width (Fig. 5.5c) with 1 mm of width in Fig. 5.5b. It found that heat transfer in y direction of 5 mm width is less proficient than at width 1 mm.

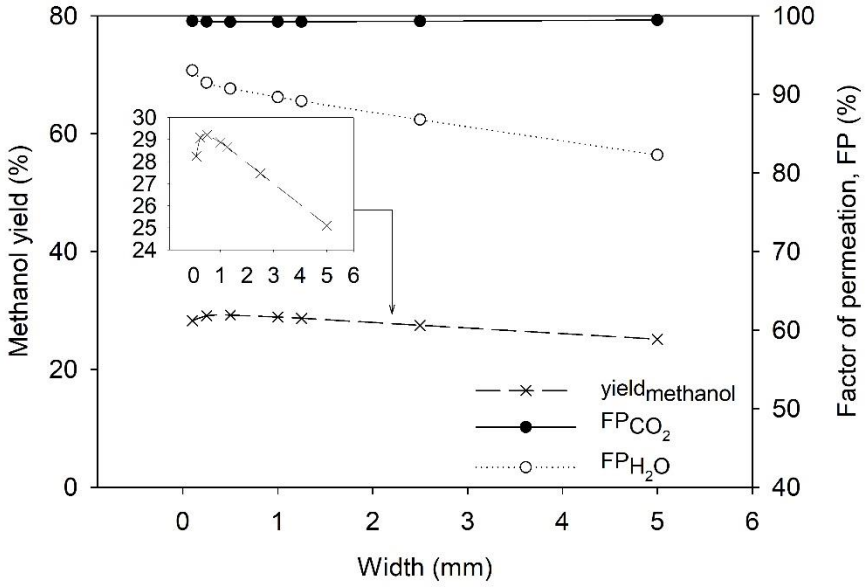

CHULALONGKORN UNIVERSITY

Fig. 5.16: Effect of width of reactor on methanol yield, and factor of CO_2 and water permeation (FP) at outlet under condition, T = 508.15 K P = 50 bar WHSV = 30 h^{-1} BC:RC ratio = 0.75 and SC:RC ratio = 2

From these dimension of reactors, the surface to volume ratio of MMR 1 mm and 5 mm of width can be calculated to 2000, 400 m^{-1}, respectively. The higher surface to volume of 1 mm width reactor which can provide better heat and mass transfer than the 5 mm width reactor shows the high performance. Thus, decreasing reactor width can improve the performance of reactor. However, the excessive reduction of reactor width would increase the gas velocity and decrease the contact time of

reactants. As a result, the yield of methanol is slightly reduced in initial stage as shown in Fig.5.16. Moreover, the maximum peak of methanol yield can be observed at 0.5 mm which have 29.07, 99.26 and 91.49% of the methanol yield, FPs of CO_2 and water, respectively. Thereby, the reactor width at 0.5 mm is considered as a suitable width. Finally, the optimal condition of all parameter studied is summarized in Table 5.1. From the studied ranges, the appropriate parameters consist of inlet temperature of 508.15 K, pressure of 50 bar, WHSV of 20 h^{-1}, BC:RC ratio of 0.5, SC:RC ratio of 4, length of 75 mm and width of 0.5 mm.

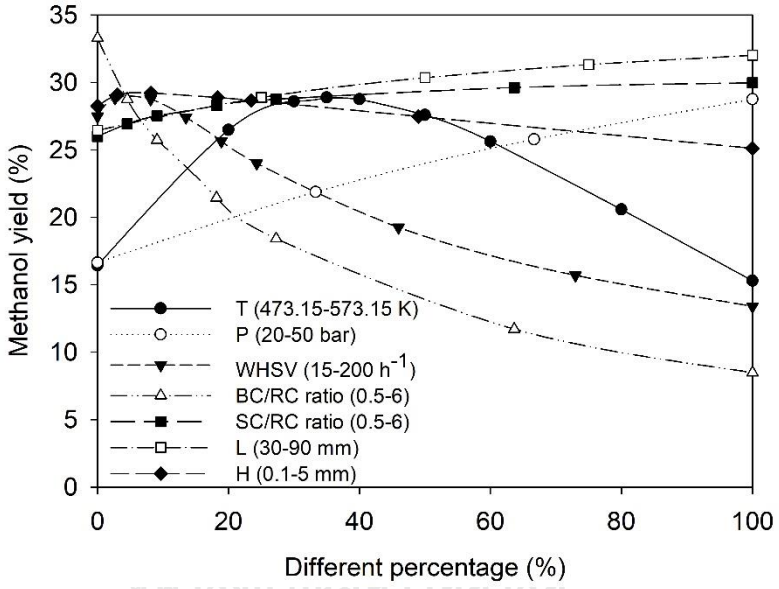

Fig. 5.17: The summary of methanol yield in each parameter for studied operating ranges

จุฬาลงกรณ์มหาวิทยาลัย
Chulalongkorn University

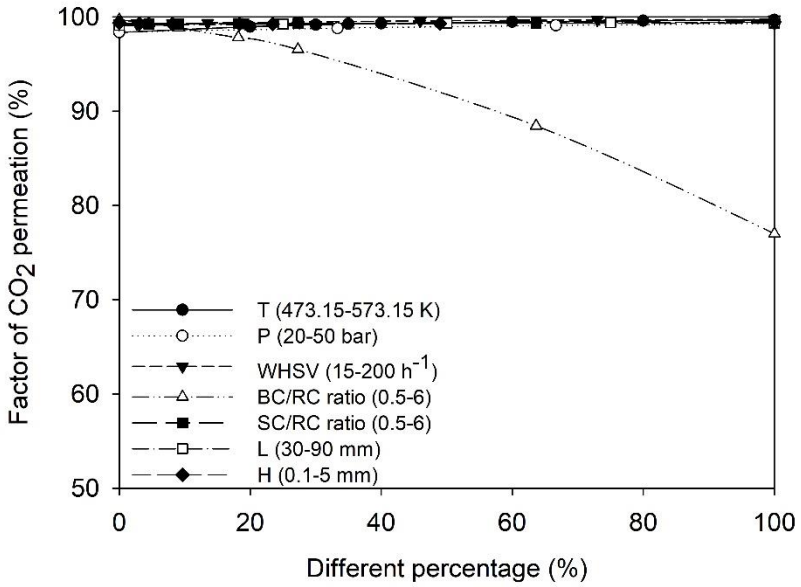

Fig. 5.18: The summary of the factor of CO_2 permeation (FP) in each parameter for studied operating ranges

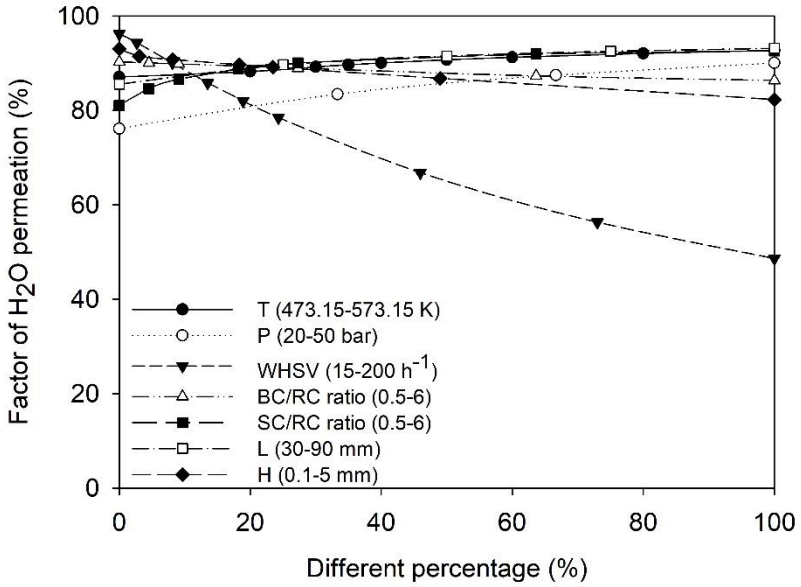

Fig. 5.19: The summary of the factor of H_2O permeation (FP) in each parameter for studied operating ranges

Table 5.1: the optimal parameters in studied ranges

Parameters	unit	Studied ranges	Optimal condition
Inlet temperature	K	473.15 – 573.15	508.15
Pressure in RC, BC	bar	20 – 50	50
WHSV in RC	h^{-1}	15 – 200	20
Mass flow ratio of BC:RC	-	0.5 – 6	0.5
Mass flow ratio of SC:RC	-	0.5 – 6	4
Reactor length	mm	30 – 90	75
Reactor width	mm	0.1 – 10	0.5

As shown in Figs. 5.17, 5.18 and 5.19, the effect of all parameters in studied operating and design ranges on methanol yield, FPs of CO_2 and water, respectively, were expressed. The all studied ranges are normalized in different percentage (%) from minimum point of each parameter in order to compare effect of these parameters on performance indicators. From result in Fig. 5.17, all operating and design parameters have influence on the yield of methanol, so the impact on methanol yield should be considered in manipulation of each parameter. The BC to RC mass flow ratio, WHSV, inlet temperature, pressure, reactor length, SC to RC ratio and reactor width can strongly affect to this variable, respectively. In Fig. 5.18, the mass flow ratio of BC to RC which is clearly observed extremely affects to factor of CO_2 permeation. From result in Fig. 5.19, it found that the WHSV in RC strongly results in factor of water permeation. From all results, it can be concluded that the mass flow ratio of BC to RC which strongly leads to both methanol yield and FP_{CO2} and WHSV are considered as significant parameters for selection of suitable parameter to our system.

จุฬาลงกรณ์มหาวิทยาลัย
Chulalongkorn University

CHAPTER 6: CONCLUSION AND RECOMMANDATIONS

6.1 Conclusion

To select a suitable reactor for simultaneous methanol production and biogas upgrading, the triple pipe tubular membrane reactor (TMR) and the planar membrane wall-coated microchannel reactor (MMR) were simulated via COMSOL Multiphysics 5.3a under base case study to compare their performances.

From CFD results, the MMR case offers higher the methanol yield, the factor of CO_2 and water permeation than TMR. Furthermore, the accumulation of methanol, CO_2 and water slightly appear in MMR, whereas these could be found in TMR case clearly. The heat transfer to the other phases (r direction) of TMR is also less effective than MMR. All of this is the result from high surface to volume ratio of MMR leading to high both heat and mass transfer as well as the enhancement of permeability of CO_2 and water. Therefore, the planar membrane wall-coated microchannel reactor (MMR) is an appropriate characteristic of reactor for simultaneous methanol production with biogas upgrading. The operating parameters and design parameters of this reactor were also investigated.

In the next section, the operating parameters including inlet temperature, pressure, WHSV, mass flow ratio of BC to RC and SC to RC as well as design parameters involving reactor length and width of MMR were studied in order to find the optimal condition and the suitable dimensions of the reactor. Based on these results, the increasing inlet temperature, pressure and SC to RC ratio are able to improve the reactor performance; however, the excessive increment of temperature will suppress the performance of MMR. On the other hand, the increment of WHSV and BC to RC ratio will reduce the reactor performance. For design parameters, the MMR should have the sufficient length in order to achieve the suitable contact time of reactants and adequate area for permeation and reactions. Whereas, the reactor width of MMR should be in micro-scale (<1mm) owing to its high surface to volume ratio providing high mass and heat transfer. However, the very narrow reactor width (< 0.5 mm for this studied range) will suppress the performance of reactor.

Moreover, the parameters significantly influencing on the performance of MMR are mass flow ratio of BC to RC (gas flow rate in BC) and WHSV in RC. Based on the studied ranges of parameters, the suitable parameters include inlet temperature of 508.15 K, pressure of 50 bar, WHSV of 20 h^{-1}, BC to RC ratio of 0.5, SC to RC ratio of 4, length of 75 mm and width of 0.5 mm. All of this is tabulated in Table 5.1.

Finally, the influence of all studied parameters can be used as a recommendation for the optimization of the condition of planar membrane wall-coated microchannel reactor (MMR) in future work.

6.2 Recommendations

1. To develop this model more, the transport phenomena of catalyst layers, the membranes and the porous media should be computed in CFD models.
2. This planar membrane wall-coated microchannel reactor was investigated by modelling simulation via COMSOL Multiphysics. In order to ensure the CFD results, the experiment for simultaneous methanol production with biogas upgrading should be studied.
3. This planar membrane wall-coated microchannel reactor is specifically designed at reaction and separation zones. Therefore, the design of feed flow distributer and product collector should be also deserved.
4. To improve the performance of reactor, the recycling line should be also integrated additionally. Therefore, the recycling system for simultaneous methanol production with biogas upgrading should be studied in the future work.
5. In order to combine this planar membrane wall-coated microchannel reactor with the methanol production to serve the biodiesel process and sodium methoxide production, this reactor should be scaled up to enhance the production rate of methanol.

จุฬาลงกรณ์มหาวิทยาลัย
Chulalongkorn University

REFERENCES

[1] L. Meher, D. Vidyasagar, and S. Naik, "Technical aspects of biodiesel production by transesterification—a review," *Renewable and Sustainable Energy Reviews,* vol. 10, no. 3, pp. 248-268, 2006.

[2] G. Vicente, M. Martinez, and J. Aracil, "Integrated biodiesel production: a comparison of different homogeneous catalysts systems," *Bioresour Technol,* vol. 92, no. 3, pp. 297-305, May 2004.

[3] D. Y. C. Leung, X. Wu, and M. K. H. Leung, "A review on biodiesel production using catalyzed transesterification," *Applied Energy,* vol. 87, no. 4, pp. 1083-1095, 2010.

[4] R. Johannes, "Metal alkoxides as catalysts for the biodiesel production," *Chemical Today,* vol. 26, pp. 26-28, 2008.

[5] K. Chanran, R. Nithya, K. Sankaran, A. Gopalan, and V. Ganesan, "Synthesis and characterization of sodium alkoxides," *Bull. Mater. Sci.,* vol. 29, pp. 173-179, 2006.

[6] J. F. O. Granjo and N. M. C. Oliveira, "Process Simulation and Techno-Economic Analysis of the Production of Sodium Methoxide," *Industrial & Engineering Chemistry Research,* vol. 55, no. 1, pp. 156-167, 2015.

[7] X. Y. Chen, H. Vinh-Thang, A. A. Ramirez, D. Rodrigue, and S. Kaliaguine, "Membrane gas separation technologies for biogas upgrading," *RSC Advances,* 10.1039/C5RA00666J vol. 5, no. 31, pp. 24399-24448, 2015.

[8] S. Basu, A. L. Khan, A. Cano-Odena, C. Liu, and I. F. Vankelecom, "Membrane-based technologies for biogas separations," *Chem Soc Rev,* vol. 39, no. 2, pp. 750-68, Feb 2010.

[9] H. Naims, "Economics of carbon dioxide capture and utilization-a supply and demand perspective," *Environ Sci Pollut Res Int,* vol. 23, no. 22, pp. 22226-22241, Nov 2016.

จุฬาลงกรณ์มหาวิทยาลัย
Chulalongkorn University

[10] M. Farsi and A. Jahanmiri, "Dynamic modeling of a H2O-permselective membrane reactor to enhance methanol synthesis from syngas considering catalyst deactivation," *Journal of Natural Gas Chemistry,* vol. 21, no. 4, pp. 407-414, 2012.

[11] I. Omae, "Recent developments in carbon dioxide utilization for the production of organic chemicals," *Coordination Chemistry Reviews,* vol. 256, no. 13, pp. 1384-1405, 2012/07/01/ 2012.

[12] F. Hayer, H. Bakhtiary-Davijany, R. Myrstad, A. Holmen, P. Pfeifer, and H. J. Venvik, "Synthesis of dimethyl ether from syngas in a microchannel reactor—Simulation and experimental study," *Chemical Engineering Journal,* vol. 167, no. 2–3, pp. 610-615, 3/1/ 2011.

[13] R. Myrstad, S. Eri, P. Pfeifer, E. Rytter, and A. Holmen, "Fischer–Tropsch synthesis in a microstructured reactor," *Catalysis Today,* vol. 147, pp. S301-S304, 2009.

[14] X. Ying, L. Zhang, H. Xu, Y. Ren, and J. Xuan, "An Experimental Study on a Microchannel Reactor for Fischer-tropsch Synthesis," *Energy Procedia,* vol. 61, pp. 1394-1397, 2014.

[15] T. Jiwanuruk, S. Putivisutisak, P. Ponpesh, P. Bumroongsakulsawat, T. Tagawa, H. Yamada, S. Assabumrungrat, "Effect of flow arrangement on micro membrane reforming for H_2 production from methane," *Chemical Engineering Journal,* vol. 293, pp. 319-326, 2016.

[16] N. Engelbrecht, S. Chiuta, R. C. Everson, H. W. J. P. Neomagus, and D. G. Bessarabov, "Experimentation and CFD modelling of a microchannel reactor for carbon dioxide methanation," *Chemical Engineering Journal,* vol. 313, pp. 847-857, 2017.

[17] H. Kreuder, T. Boeltken, M. Cholewa, J. Meier, P. Pfeifer, and R. Dittmeyer, "Heat storage by the dehydrogenation of methylcyclohexane – Experimental studies for the design of a microstructured membrane reactor," *International Journal of Hydrogen Energy,* vol. 41, no. 28, pp. 12082-12092, 2016.

[18] S. Yamamoto, T. Hanaoka, S. Hamakawa, K. Sato, and F. Mizukami, "Application of a microchannel to catalytic dehydrogenation of cyclohexane on Pd membrane," *Catalysis Today,* vol. 118, no. 1–2, pp. 2-6, 10/30/ 2006.

จุฬาลงกรณ์มหาวิทยาลัย
Chulalongkorn University

[19] H. Bakhtiary-Davijany, F. Hayer, X. Phan, R. Myrstad, H.J. Venvik, P. Pfeifer, A. Holmen, "Characteristics of an Integrated Micro Packed Bed Reactor-Heat Exchanger for methanol synthesis from syngas," *Chemical Engineering Journal,* vol. 167, no. 2–3, pp. 496-503, 3/1/ 2011.

[20] A. Karim, J. Bravo, D. Gorm, T. Conant, and A. Datye, "Comparison of wall-coated and packed-bed reactors for steam reforming of methanol," *Catalysis Today,* vol. 110, no. 1-2, pp. 86-91, 2005.

[21] M. Farsi and A. Jahanmiri, "Application of water vapor-permselective alumina–silica composite membrane in methanol synthesis process to enhance CO2 hydrogenation and catalyst life time," *Journal of Industrial and Engineering Chemistry,* vol. 18, no. 3, pp. 1088-1095, 5/25/ 2012.

[22] G. Barbieri, G. Marigliano, G. Golemme, and E. Drioli, "Simulation of CO2 hydrogenation with CH3OH removal in a zeolite membrane reactor," *Chemical Engineering Journal,* vol. 85, no. 1, pp. 53-59, 2002/01/15/ 2002.

[23] R. P. W. J. Struis and S. Stucki, "Verification of the membrane reactor concept for the methanol synthesis," *Applied Catalysis A: General,* vol. 216, no. 1–2, pp. 117-129, 8/1/ 2001.

[24] R. P. W. J. Struis, S. Stucki, and M. Wiedorn, "A membrane reactor for methanol synthesis," *Journal of Membrane Science,* vol. 113, no. 1, pp. 93-100, 1996/05/01/ 1996.

[25] F. Gallucci and A. Basile, "A theoretical analysis of methanol synthesis from CO2 and H2 in a ceramic membrane reactor," *International Journal of Hydrogen Energy,* vol. 32, no. 18, pp. 5050-5058, 2007.

[26] É. S. Van-Dal and C. Bouallou, "Design and simulation of a methanol production plant from CO2 hydrogenation," *Journal of Cleaner Production,* vol. 57, pp. 38-45, 10/15/ 2013.

[27] Perry's Chemical Engineers' Handbook*, eighth ed.*, 2008.

[28] M. Bayat, Z. Dehghani, and M. R. Rahimpour, "Membrane/sorption-enhanced methanol synthesis process: Dynamic simulation and optimization," *Journal of Industrial and Engineering Chemistry,* vol. 20, no. 5, pp. 3256-3269, 9/25/ 2014.

จุฬาลงกรณ์มหาวิทยาลัย
Chulalongkorn University

[29] D. Milani, R. Khalilpour, G. Zahedi, and A. Abbas, "A model-based analysis of CO2 utilization in methanol synthesis plant," *Journal of CO2 Utilization,* vol. 10, pp. 12-22, 2015.

[30] T. Arthur, "Control structure design for methanol process, Norwegian University of Science and Technology," 2010.

[31] T. Wurzel, "Lurgi MegaMethanol Technology –Delivering the building blocks for future fuel and monomer demand," *Air Liquide Engineering & Construction Methanol and Derivatives*.

[32] J. B. Hansen, "Methanol Production Technology: Todays and future Renewable Solutions," *Methanol Workshop, Lund University,* 2015.

[33] A. A. Kiss, J. J. Pragt, H. J. Vos, G. Bargeman, and M. T. de Groot, "Novel efficient process for methanol synthesis by CO2 hydrogenation," *Chemical Engineering Journal,* vol. 284, no. Supplement C, pp. 260-269, 2016/01/15/ 2016.

[34] K. M. Vanden Bussche and G. F. Froment, "A Steady-State Kinetic Model for Methanol Synthesis and the Water Gas," *Journal of Catalysis,* vol. 161, pp. 1-10, 1996.

[35] G. H. Graaf, H. Scholtens, E. J. Stamhuis, and A. A. C. M. Beenackers, "Intra-particle diffusion limitations in low-pressure methanol synthesis," *Chemical Engineering Science,* vol. 45, no. 4, pp. 773-783, 1990/01/01/ 1990.

[36] V. Vrbová and K. Ciahotný, "Upgrading Biogas to Biomethane Using Membrane Separation," *Energy & Fuels,* vol. 31, no. 9, pp. 9393-9401, 2017.

[37] "BIOMETHANE REGIONS, Introduction to the Production of Biomethane from Biogas," *Intelligent energy europe*.

[38] M. P. Rohde, G. Schaub, S. Khajavi, J. C. Jansen, and F. Kapteijn, "Fischer–Tropsch synthesis with in situ H2O removal – Directions of membrane development," *Microporous and Mesoporous Materials,* vol. 115, no. 1-2, pp. 123-136, 2008.

[39] F. Samimi, S. Kabiri, and M. R. Rahimpour, "The optimal operating conditions of a thermally double coupled, dual membrane reactor for simultaneous methanol synthesis, methanol dehydration and methyl cyclohexane dehydrogenation," *Journal of Natural Gas Science and Engineering,* vol. 19, pp. 175-189, 7// 2014.

[40] A. Bakhtyari, M. Parhoudeh, and M. R. Rahimpour, "Optimal conditions in converting methanol to dimethyl ether, methyl formate, and hydrogen utilizing a double membrane heat exchanger reactor," *Journal of Natural Gas Science and Engineering,* vol. 28, pp. 31-45, 1// 2016.

[41] M. D. Falco and M. Capocelli, "Direct Synthesis of Methanol and Dimethyl Ether From a CO2-Rich Feedstock: Thermodynamic Analysis and Selective Membrane Application," in *Direct Synthesis of Methanol and Dimethyl Ether*University "Campus Bio-Medico" of Rome, Rome, Italy, pp. 113-128.

[42] X. Dong and Y. S. Lin, "Catalyst-free ceramic-carbonate dual phase membrane reactor for hydrogen production from gasifier syngas," *Journal of Membrane Science,* vol. 520, pp. 907-913, 2016.

[43] O. Osamu, M. Teramoto, R. Yegani, H. Matsuyama, K. Hyogo, K. Shimada, K. Morimoto, "CO_2-facilitated transport membrane and method for producing the same," United States Patent US 8,377,170 B2, 2013.

[44] H. K. Versteeg, W. Malalasekera, "An introduction to computational fluid dynamics: the finite volume method," *Pearson Education,* 2007.

[45] E. N. Fuller, P. D. Schettler, and J. C. Giddings, "A new method for prediction of binary gas-phase diffusion coefficients," *Industrial and Engineering Chemistry,* vol. 58, no. 5, p. 19, 1966.

[46] A. Tonkovich, K. Jarosch, R. Arora, L. Silva, S. Perry, J. McDaniel, F. Daly, B. Litt, "Methanol production FPSO plant concept using multiple microchannel unit operations," *Chemical Engineering Journal,* vol. 135, pp. S2-S8, 2008.

[47] F. Daly and L. Tonkovich, "Enabling offshore production of methanol by use of an isopotential reactor," *Studies in Surface Science and Catalysis,* vol. 147, pp. 415-420, 2004.

[48] F. Hayer, H. Bakhtiary-Davijany, R. Myrstad, A. Holmen, P. Pfeifer, and H. J. Venvik, "Characteristics of integrated micro packed bed reactor-heat exchanger configurations in the direct synthesis of dimethyl ether," *Chemical Engineering and Processing: Process Intensification,* vol. 70, pp. 77-85, 2013.

[49] H. Bakhtiary-Davijany, D. Farbod, F. Hayer, X. Phan, R. Myrstad, H.J. Venvik, P. Pfeifer, A. Holmen, "Analysis of External and Internal Mass Transfer at Low

จุฬาลงกรณ์มหาวิทยาลัย
Chulalongkorn University

Reynolds Numbers in a Multiple-Slit Packed Bed Microstructured Reactor for Synthesis of Methanol from Syngas," *Industrial & Engineering Chemistry Research,* vol. 51, no. 42, pp. 13574-13579, 2012.

[50] P. Xuyen K., H. Bakhtiary-Davijany, R. Myrstad, J. Thormann, P. Pfeifer, H.J. Venvik, A. Holmen, "Preparation and Performance of a Catalyst-Coated Stacked Foil Microreactor for the Methanol Synthesis," *Ind. Eng. Chem. Res.,* vol. 49, pp. 10934-10941, 2010.

[51] Available: https://en.wikipedia.org/wiki/Le_Chatelier%27s_principle

[52] X. Tan and K. Li, "Membrane microreactors for catalytic reactions," *Journal of Chemical Technology & Biotechnology,* vol. 88, no. 10, pp. 1771-1779, 2013.

[53] M. Farsi and A. Jahanmiri, "Methanol production in an optimized dual-membrane fixed-bed reactor," *Chemical Engineering and Processing: Process Intensification,* vol. 50, no. 11–12, pp. 1177-1185, 11// 2011.

[54] M. Farsi and A. Jahanmiri, "Application of water vapor and hydrogen-permselective membranes in an industrial fixed-bed reactor for large scale methanol production," *Chemical Engineering Research and Design,* vol. 89, no. 12, pp. 2728-2735, 12// 2011.

[55] M. A. Tadbir and M. H. Akbari, "Methanol steam reforming in a planar wash coated microreactor integrated with a micro-combustor," *International Journal of Hydrogen Energy,* vol. 36, no. 20, pp. 12822-12832, 2011.

จุฬาลงกรณ์มหาวิทยาลัย
CHULALONGKORN UNIVERSITY

APPENDIX

จุฬาลงกรณ์มหาวิทยาลัย
Chulalongkorn University

APPENDIX A: Nomenclature

T	Temperature (K)
p	Pressure (Pa)
$\vec{u}$	Velocity (m s^{-1})
$\vec{u}_s$	Surface velocity (m s^{-1})
$M_{w,i}$	Molecular weight of species i (kg $kmol^{-1}$)
r_i	Rate of reaction j (mole m^{-2} s^{-1})
N_i	Permeation flux of species i (mole m^{-2} s^{-1})
R_i	Net rate of reaction of species i (kg m^{-3} s^{-1})
D_i^F	Mass diffusivity of species i in mixture (m^2 s^{-1})
D_i^T	Thermal diffusion coefficient of species i (kg m^{-1} s^{-1})
D_{ik}	Binary diffusivity in gas phase (m^2 s^{-1})
V_i	Diffusion volume of species i (-)
$\vec{J}_i$	Mass diffusion flux of species i (kg m^{-2} s^{-1})
P_i	Partial pressure of species i (Pa)
d_z	Thickness of channel (m)
C_p	Heat capacity of species i (J/kg/K)
k_i	Thermal conductivity of species i (W/m/K)
k	Kinetic parameter (-)
Q_i	Heat source term of reaction j (W m^{-2})
Q_{vd}	Heat source from viscous dissipation (W m^{-3})
Q_p	Heat source from pressure work (W m^{-3})
Q_{oop}	Heat source from out of plane (W m^{-3})
y_k	Mole fraction of species k (-)
F_i	Mole flow rate of species i (mole/s)
$\vec{g}$	Gravity constant (m s^{-2})
A_S	Surface area (m^2)
Q_{H_2O}	Permeance of water ($mols^{-1}m^{-2}Pa^{-1}$)
V_r	Reactor volume (m^3)

จุฬาลงกรณ์มหาวิทยาลัย
Chulalongkorn University

t	time (s)
S_m	Mass added to continuous phase from the dispersed second phase
$\vec{F}$	External body forces
$D_{i,eff}$	Effective diffusion efficient (m^2 s^{-1})
$D_{i,KA}$	Knudsen diffusion coefficient (m^2 s^{-1})
d_p	Pore diameter of the solid phase (m)

Greek symbol

ρ	Density (kg m^{-3})
μ	Dynamic viscosity (Pa s)
ω_i	Mass fraction of species i (-)
ξ_i	Permeability coefficient (mole m^{-2} s^{-1} Pa^{-1})
$\bar{\bar{\delta}}$	Tensor unit (-)
$\bar{\bar{\tau}}$	Shear stress
κ	Dilatational viscosity
ε	Porosity (-)
τ	Tortuosity (-)

Abbreviations

WHSV	Weight hourly space velocity (h^{-1})
RC	Reaction channel
BC	Biogas channel
SC	Sweep gas channel
MMR	Membrane micro-channel reactor
TMR	Tubular membrane reactor
MR	Membrane reactor
FP	Factor of permeation

จุฬาลงกรณ์มหาวิทยาลัย
Chulalongkorn University

APPENDIX B: Details of model validation

For methanol synthesis in this investigation, the kinetic model of Van-dal and Chakib Bouallou [26] with readjusted parameters from Vanden Bussche and Froment [34] was used and expressed in previous chapter (chapter 2). Therefore, in this Appendix, the kinetic model of Vanden Bussche and Froment [34] is shown in below where pressure are expressed in bar, temperature in K and reaction rate in $molkg^{-1}s^{-1}$

Methanol synthesis:

$$r_{CH_3OH} = \frac{k_1 P_{CO_2} P_{H_2} \left(1 - \frac{1}{K_{eq1}} \frac{P_{H_2O} P_{CH_3OH}}{P_{H_2}^3 P_{CO_2}} \right)}{\left(1 + k_2 P_{H_2O} P_{H_2}^{-1} + k_3 P_{H_2}^{0.5} + k_4 P_{H_2O} \right)^3} \quad \text{(A.1)}$$

Reverse water-gas shift:

$$r_{RWGS} = \frac{k_5 P_{CO_2} \left(1 - K_{eq2} \frac{P_{H_2O} P_{CO}}{P_{H_2} P_{CO_2}} \right)}{1 + k_2 P_{H_2O} P_{H_2}^{-1} + k_3 P_{H_2}^{0.5} + k_4 P_{H_2O}} \quad \text{(A.2)}$$

The kinetic constants following the Arrhenius law can be written in below

$$k_i = A_i \exp\left(\frac{B_i}{RT} \right) \quad \text{(A.3)}$$

จุฬาลงกรณ์มหาวิทยาลัย
Chulalongkorn University

$$\log_{10} K_{eq1} = \frac{3066}{T} - 10.592 \quad \text{(A.4)}$$

$$\log_{10} \frac{1}{K_{eq2}} = -\frac{2073}{T} + 2.029 \quad \text{(A.5)}$$

Table A1: The kinetic parameters of Vanden Bussche and Froment [34]

Kinetic parameters		**values**
k_1	A_1	1.07
	B_1	40,000
k_2	A_2	3453.38
	B_2	-
k_3	A_3	0.499

Kinetic parameters		values
	B_3	17,197
k_4	A_4	6.62×10^{-11}
	B_4	124,119
k_5	A_5	1.22×10^{10}
	B_5	-98,084

Table A2:Characteristics of reactor from Van-dal and Chakib Bouallou [26]

Parameters	Values
Tube diameter	0.016 (m)
Reactor length	0.15 (m)
Catalyst density	1775 (kg/m^3)
Fixed bed porosity	0.5 (-)
Mass catalyst	34.8 (g)
Pellet diameter	0.0005 (m)

Table A3:Operating condition from Van-dal and Chakib Bouallou [26]

Parameters	Values
Mass flow	2.8×10^{-5} (kg/s)
Pressure	50 (bar)
Temperature	220 (°C)
Feed composition (molar%)	
CO	4.00
H_2O	0.00
CH_3OH	0.00
H_2	82.00
CO_2	3.00
Ar	11.00

จุฬาลงกรณ์มหาวิทยาลัย
Chulalongkorn University

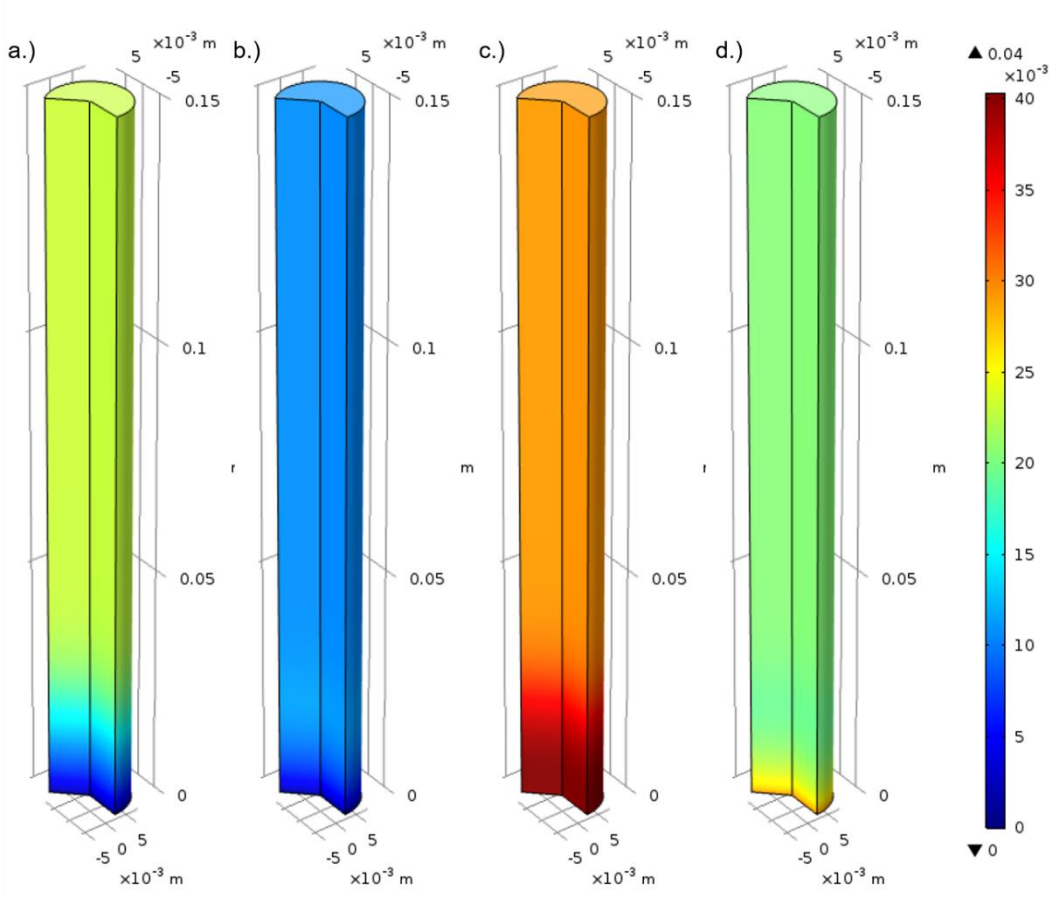

Fig. A1: The mole fraction profile (3D) for validating kinetic model of a.) Methanol, b.) Water, c.) Carbon monoxide and d.) Carbon dioxide.

As shown in Fig. A1, the mole fraction profile of methanol, water, carbon monoxide and carbon dioxide are expressed. The non-isothermal adiabatic tubular reactor (0.016 m of diameter and 0.15 m of reactor length) for methanol synthesis was repeated via COMSOL Multiphysics 5.3a under operating condition tabulated in table A3 above. The steady state condition, incompressible fluid and laminar flow region are assumed in this simulation. Moreover, the ideal gas law was used in this model. For the equations in simulation, the governing equations; continuity equation, conservation of momentum, mass species i and heat equations (Eq. 4.1-Eq. 4.4, respectively) and the kinetic model for methanol synthesis (Eq. 2.13-2.15) were applied in this CFD model. In order to validate the kinetic model for methanol synthesis, the average mole fractions at cross sectional area of each component are collected and plotted in Fig. 5.1 (chapter 5) to compare with data from previous research of Van-dal and Chakib Bouallou [26]

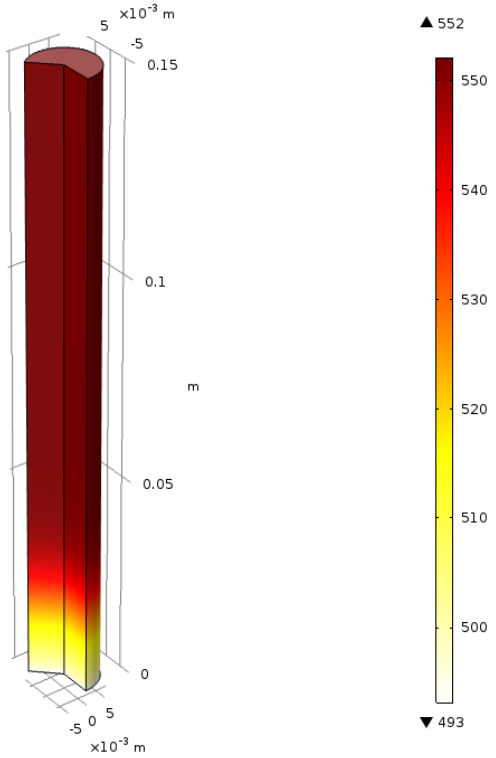

Fig. A2: The temperature profile (3D) for validation of kinetic model

The temperature profile of the non-isothermal adiabatic tubular reactor is presented in Fig. A2. It can observe that the temperature rises along with the length of the reactor due to overall heat of reactions being highly exothermic reaction. Hence, the temperature inside the reactor is increased to approximately 552 K.

จุฬาลงกรณ์มหาวิทยาลัย
Chulalongkorn University

APPENDIX C: Mass balance calculation

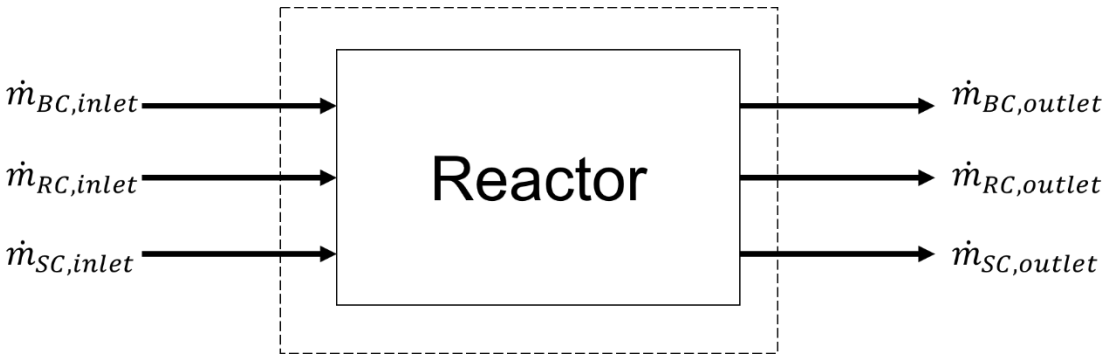

Fig. A3: Boundary for mass balance calculation

Table A4: The mass flow (kg/s) at the inlet and outlet of each channel (TMR)

Mass flow (kg/s)	Reaction Channel		Biogas Channel		Sweep gas Channel	
	Inlet	Outlet	Inlet	Outlet	Inlet	Outlet
CH_3OH	0	$8.62x10^{-6}$	0	0	0	0
H_2	$8.33x10^{-5}$	$8.15x10^{-5}$	0	0	0	0
H_2O	0	$4.95x10^{-6}$	0	0	0	$7.06x10^{-7}$
CO	0	$1.26x10^{-6}$	0	0	0	0
CO_2	0	$2.58x10^{-5}$	$1.18x10^{-4}$	$7.86x10^{-5}$	0	0
N_2	$1.30x10^{-4}$	$1.30x10^{-4}$	0	0	$4.13x10^{-4}$	$4.13x10^{-4}$
CH_4	0	0	$4.31x10^{-5}$	$4.31x10^{-5}$	0	0
Total	$2.13x10^{-4}$	$2.52x10^{-4}$	$1.61x10^{-4}$	$1.22x10^{-4}$	$4.13x10^{-4}$	$4.14x10^{-4}$

Table A5: The mole flow (mol/s) at the inlet and outlet of each channel (TMR)

Mole flow (mol/s)	Reaction Channel		Biogas Channel		Sweep gas Channel	
	Inlet	Outlet	Inlet	Outlet	Inlet	Outlet
CH_3OH	0	$2.69x10^{-4}$	0	0	0	0
H_2	$4.16x10^{-2}$	$4.08x10^{-2}$	0	0	0	0
H_2O	0	$2.75x10^{-4}$	0	0	0	$3.92x10^{-5}$
CO	0	$4.4\ x10^{-5}$	0	0	0	0
CO_2	0	$5.85x10^{-4}$	$2.68x10^{-3}$	$1.79x10^{-3}$	0	0
N_2	$4.63x10^{-3}$	$4.62x10^{-3}$	0	0	$1.48x10^{-2}$	$1.48x10^{-2}$
CH_4	0	0	$2.68x10^{-3}$	$2.68x10^{-3}$	0	0
Total	$4.63x10^{-2}$	$4.66x10^{-2}$	$5.37x10^{-3}$	$4.47x10^{-3}$	$1.48x10^{-2}$	$1.48x10^{-2}$

จุฬาลงกรณ์มหาวิทยาลัย
Chulalongkorn University

The example for mass balance calculation is shown in this section. In Fig. A3, the inlets around defined boundary of reactor include the inlets of biogas channel, reaction channel and sweep gas channel as same as the outlets. As shown in Table A4, this mass flow at both inlet and outlet of each channel is obtained from triple pipe tubular membrane reactor (TMR) model under the condition tabulated in Table 4.2. The total mass flows of each channel are computed by summary of mass flow each component.

To ensure the CFD model, the overall mass balance is calculated as shown in Table A6. From this result, it found that the total inlet flow is equivalent to the total outlet. Therefore, the overall mass transfer in this reactor is balance. Furthermore, the atomic balance for this reactor is also studied in order to assure this model. The mole flow of each atom can calculate from the number of atoms in the streams multiplied by their mole flow rate. From result in Table A7, it found that the atomic flow of C, H, O and N in inlet and outlet are equivalent. From all mentioned above, it can be summarized that the models in this simulation are reliable.

Table A6: The total mass flow (kg/s) at the inlet and outlet

Position	Mass flow (kg/s)
Total Inlet	7.87×10^{-4}
Total Outlet	7.87×10^{-4}

Table A7: Atomic balance of the TMR reactor

Atom	Position	mole flow (mol/s)
C	Inlet	5.368×10^{-3}
	Outlet	5.370×10^{-3}
H	Inlet	9.401×10^{-2}
	Outlet	9.399×10^{-2}
O	Inlet	5.368×10^{-3}
	Outlet	5.371×10^{-3}
N	Inlet	3.877×10^{-2}
	Outlet	3.877×10^{-2}

จุฬาลงกรณ์มหาวิทยาลัย
Chulalongkorn University

VITA

Mr. Khunnawat Ountaksinkul was born on April 1st, 1994 in Bangkok, Thailand. He graduated elementary school and high school from Assumption College in 2012. He received his Bachelor's Degree in Department of Chemical Engineering, Faculty of Engineering, Kasetsart University in 2016. At that time, he had the opportunity to do an internship program at Siam Michelin Co.,Ltd, Chonburi in position of Quality Operations (QO) Engineer. Afterwards, he decided to study Master's degree in Department of Chemical Engineering, Faculty of Engineering, Chulalongkorn University under supervision of Prof. Suttichai Assabumrungrat, Ph.D. and his co-advisor Paravee Vas-Umnuay, Ph.D. During master's degree, he received the tuition fees and fund for the international journal publication from Department of Chemical Engineering, Chulalongkorn University.

จุฬาลงกรณ์มหาวิทยาลัย
CHULALONGKORN UNIVERSITY

จุฬาลงกรณ์มหาวิทยาลัย
Chulalongkorn University